THE INTESTINAL-CELL MONOLAYER OF THE DOG (*CANIS FAMILIARIS*) AND MALPIGHIAN TUBULES OF *AEDES AEGYPTI*: POWERFUL *IN VITRO* MODELS FOR STUDYING EPITHELIAL TRANSPORT

A Dissertation

Presented to the Faculty of the Graduate School

of Cornell University

In Partial Fulfillment of the Requirements for the Degree of

Doctor of Philosophy

by

Xinghe Weng

May 2007

THE INTESTINAL-CELL MONOLAYER OF THE DOG (*CANIS FAMILIARIS*) AND MALPIGHIAN TUBULES OF *AEDES AEGYPTI*: POWERFUL *IN VITRO* MODELS FOR STUDYING EPITHELIAL TRANSPORT

Xinghe Weng, Ph.D.

Cornell University 2007

Homeostasis of the internal environment of vertebrates and invertebrates is maintained by a collection of organs involving the gastrointestinal system, the renal system and the pulmonary system, whose surfaces facing the external world are covered by a layer of highly polarized epithelial cells as the barrier and sites for substance exchange between body and the external world. As most studies on epithelial transport are done in animal cell- or tissue-models, this dissertation is set to address questions on two *in vitro* epithelial models: monolayers of cultured epithelial cells and Malpighian tubules of insects.

In the field of epithelial transport across mammalian small intestines, most of the cell monolayers that have been used in the past are abnormal: they are either derived from cancerous cells or poorly differentiated compared to normal tissues. By strictly controlling cultural conditions, we successfully developed an epithelial cell culture derived from normal dog jejune with full differentiation, which can form cell monolayers with remarkable resemblance to the normal small intestinal epithelia in morphology, expression of the junctional proteins and membrane transporter, and electrophysiological properties. Furthermore, different channels can be induced when the cell monolayer is treated with different hormones and agents, suggesting its wide application in basic and applied research studies.

Malpighian tubule of the yellow fever mosquitoes *Aedes aegypti* has been the epithelial transport model in our lab for more than twenty years. The V-type H^+ ATPase is thought to provide driving force for transepithelial electrolyte and fluid secretion in Malpighian tubules. Here we immunohisochemcially localized the proton pumps to the apical membranes of the mitochondria-rich principal cells of the Malpighian tubules, and measured enzymatic activities of the V-type H^+ ATPase as 50~60% of the total ATPase activities. In comparison the activities of the Na^+/K^+ ATPase were almost undetectable.

To understand the functions of Malpighian tubules, we also modeled the tubule into equivalent electrical circuits. However in our previous studies, the model was incomplete, as contribution of gap junction resistance between Malpighian tubule cells to the circuit has never been revealed. In this dissertation, we accurately measured the electrical resistance of gap junctions in a single cell by circuit analysis and rectified the values of all the electrical elements in our previous model. The equivalent electrical circuit has for the first time become complete. The results also show that gap junctions in *Aedes* Malpighian tubules are impermeable to the fluorescent dye Lucifer yellow CH, sensitive to the metabolic inhibitor dinitrophenol, while not so sensitive to elevated intracellular $[Ca^{2+}]$.

BIOGRAPHICAL SKETCH

Xinghe Weng was born in 1975 in Jiande county, Zhejiang province, China. After birth he lived with his grandmother in a beautiful little village for two years and joined his parents at the age of 4. Xinghe went to elementary school when he was five, taught by his mother who was a teacher in that school then. In 1991, Xinghe passed the National College Entrance Exam (NCEE) in China and got accepted by Peking University (PKU) in Beijing. In 1995 Xinghe started working on his B.S. thesis in an electrophysiological lab run by professor Zengquan Zhou in PKU and later became one of his graduate students. After Xinghe got his Master degree in 2000, he temporarily worked in an IT company as a webpage designer for about half a year until the January of 2001, when he flew to the USA and began to study in Dr. Beyenbach's lab in the department of Biomedical Sciences. Xinghe passed his A exam in the April of 2004.

To Mentors and Friends

AKNOWLEDGEMENTS

My deep gratitude will first go to my doctoral advisor, Dr. Klaus W. Beyenbach, and I would like to say that it has been my great pleasure and honor to work with him in the past six years. I would like to thank him for his every encouragement on my little progresses, his tremendous patience on my mistakes, his trust, and the freedom that he gave me in research while at the same time with the clearest directions when I was lost in my awkward experimental designs. All these will become my treasurable experiences when I look back in the future as an independent researcher. I am also fortunate enough to have a wonderful PhD committee that includes Dr. Andrea Quaroni, Dr. Mark S. Roberson, and Dr. Anthony P. Bretscher, who are always supportive during my study in Cornell. I remember whenever I had a problem in experiments with molecular biology, Dr. Quaroni and Dr. Roberson are always there to help and I have been using both of their labs as if they were my own labs for quite a long time. And I am also grateful to Dr. Roberson for his countless help as the DGS in our field.

There are many thanks to many others. There has been so much great advice and help from the former and current members of Beyenbach lab, Dr. Peter Piermarini and Dr. Ming-Jiun Yu, from whom I learned so much as one can learn for his peers; Daniel Wu, Andrew Fox, Atsuko Yamahiro, Stephen Schepel and Austin Blum et al, great pals. Members in Roberson lab helped me with the project on K channel cloning, and I received great help from Patricia Fisher and Mary Lou Norman in my immunohistochemial study in the V-type H^+ ATPase. During my six years of stay in Cornell, I've also made so many good friends in life that it is not possible to list all their names in this short acknowledgement, but what I want to say to them is that your

friendship has made my past six years one of the happiest periods of time in my life.

Finally I am grateful to my dearest parents, whose unconditional support to me has been one of the sources of all my strength and wisdom in life.

TABLE OF CONTENTS

LIST OF TABLES

LIST OF FIGURES

LIST OF ABBREVIATIONS

BCIP	5-bromo-4-chloro-3-indolyl phosphate p-toluidine
BL	basolateral
BSA	bovine serum albumin
CFTR	cystic fibrosis transmembrane conductance regulator
CTE	crude tubule extracts
db-cAMP	dibutyryl cyclic AMP
DIEC	dog intestinal epithelial cells
DNP	dinitrophenol
EIPA	5-(N-ethyl-n-isopropyl)-amiloride
ENaC	epithelial Na^+ channel
GJ	gap junction
HIAR	heat-induced-antigen-retrieval
IEC	intestinal epithelial cell line
IRK	inwardly rectifying K channel
LKVIII	leucokinin VIII
LU	lumen
MDCK	Madin Darley canine kidney cells
MNP	mosquito natriuretic peptide
NBDCI	4-chloro-7-nitrobenzo-2-oxa-1,3-diazol
NBT	nitro blue tetrazolium
NHE	Na^+/H^+ exchanger
NJ	non-junctional
PC	principal cell
PMSF	phenylmethylsulfonyl fluoride

SGLT1	Na/D-glucose cotransporter
SJ	septate junction
TEP	transepithelial potential
TJ	tight junction

CHAPTER ONE

INTRODUCTION

1. Models for the study of transepithelial transport.

The necessity to maintain and regulate extracellular fluid volume and composition is one of the greatest challenges faced by both vertebrates and invertebrates. The requirement of homeostasis is fulfilled by a diverse collection of organ systems, which selectively absorb from, or excrete into, the external environment the necessary amounts of non-electrolytes (sugars, amino acids, water) and electrolytes (sodium, potassium, chloride, bicarbonate etc). A feature shared by all of these organs is that their surfaces facing the external world are lined by a layer of closely packed epithelial cells, which are tightly joined to each other by a variety of intercellular junctions. The cell layer is given additional structural rigidity by a glycoprotein matrix namely the basement membrane. This configuration of a layer of packed cells attached to a basement membrane is the basic structural characteristic of an epithelium.

As the barrier and the site for substance exchange between the body and the external world, epithelial cells differentiate with sharp structural, biochemical and physiological asymmetry. A typical epithelial cell consists of two distinct membrane domains (apical and basolateral) that define three compartments (apical, basolateral and cellular). The transport systems located in the apical membranes are essentially different from those present in the basolateral membranes. The movement of a substance across such a barrier is limited to two pathways: paracellular (across the junctional complex and lateral intercellular space) and transcellular (across the apical and basolateral cell membranes).

In the field of epithelial transport, the primary goals are to: (*i*) establish the direction (absorption or secretion) and magnitude of the net transfer of solutes and water, and (*ii*) identify the mechanisms responsible for the control and regulation of

the transport processes. Since 1958 -- when the original model for transepithelial Na^+ transport on frog skin was established (66), a number of biological models have been developed to investigate the process of transepithelial transport (3, 11, 66, 71). Generally, these models can be divided into 4 major categories: 1) *in vivo* models where experiments are performed in live animals; 2) excised epithelial tissue models such as the frog skin and the excised rat intestinal epithelia; 3) confluent cell monolayer formed by cultured epithelial cells or cell lines; 4) *in vitro* models where experiments are performed on small epithelial tubules out side of the animal, such as isolated renal tubules of vertebrates and Malpighian tubules of insects.

A number of elegant experimental approaches have been developed to study ion transport *in vivo*. For example, the overall intestinal permeability is usually characterized with *in vivo* perfusion (71). In the double-balloon intestinal perfusion, a segment of human small intestine is separated by two intraluminal occluding balloons, and perfused with drugs or agents of interest; the absorption rate and intestinal permeability are determined from the disappearance rate of a compound from the perfusate (72). As an *in vivo* experiment, the human jejunal perfusion provides direct information on the intestinal transport. However it lacks the viability of mimicking the intact behavior of transmucosal transport (56). For example, many other processes besides transepithelial absorption are involved in the disappearance of compounds in the intestinal lumen, such as the binding of compounds to cells surfaces, and degradation of compounds by the cell surface enzymes, both of which can not be easily distinguished by the methods of human jejunal perfusion (71)

While the crucial step in understanding the transport function of an epithelium is to identify, characterize and localize specific transport proteins responsible for the

overall properties of the tissue, the choice of experimental methods used to accomplish these goals depends upon the structure and properties of the epithelium of interest. The studies on excised epithelium of animals include sheets of "planar" epithelia or large tubes and sacs that can be opened to yield flat sheets, such as small and large intestine (49, 125), gall bladder (83), urinary bladder (25), skin (66) and trachea (120). Compared with the *in vivo* studies, these flat-epithelial models provide several advantages. For example, the flat-epithelial models are easier to manipulate, and experiments are usually performed in Ussing chambers where composition of the solutions on both sides of the epithelial tissue can be conveniently controlled. Furthermore, since the flat epithelia are separated from animal body, regulation of the transepithelial transports can be tested without the influence of internal regulators, such as the endocrine system and central nervous systems. The disadvantage of this model is also obvious, as other epithelia that form small tubes, ducts or acini (e.g. renal tubule, pancreatic acinar and ductal cells, salivary acinar and ductal cells, sweat gland, etc.) will not be amenable to study as flat sheets.

One approach to studying epithelial tissues that form tubes, ducts, or acini is to form confluent monolayers of their cells in culture and study them as planar epithelia. The disruption of tissue architecture to isolate cells allows the formation of a sheet of transporting epithelium. While both the *in vivo* model and the excised epithelial tissue model have the problem that transport of substances has to go through layers of cells other than a single epithelium, the approach with epithelial cell monolayer completely eliminated this problem, amenable to a variety of electrophysiological, molecular and optical methods. Moreover, using genetic manipulation of cell populations or by selecting clonal cell populations it is possible to modulate the level of expression of specific transport proteins, allowing more detailed mechanistic analysis.

Another approach to studying non-flat epithelia is to investigate them directly by highly specialized techniques such as microperfusion. The primary and continuous cell cultures provide useful models, yet one must be aware that these cells may not retain all the normal physiological or biochemical properties of differentiated epithelial cells. In 1966, Burg et al invented the *in vitro* microperfusion system to study transepithelial transport in rabbit renal tubules (15). In this technique, segments of a single rabbit nephron are isolated and bathed in Ringer solutions, while the tubule lumen is perfused with micropipettes on both ends, so that the luminal and peritubular environments of the tubule can be selectively and specifically controlled (15).

Later on this technique was adopted to investigate transepithelial transport in insect Malpighian (renal) tubules (12). There are several great advantages for the Malpighian tubules to be the epithelial transport model. First, as renal tubules, Malpighian tubules lie almost freely in the haemolymph of an insect and each tubule consists entirely of a single layer of epithelial cells. Second, the predominant epithelial cell type (principal cells) are very large in size, which is convenient for electrophysiological studies. Third, Malpighian tubules of hematophagous insects have evolved some of the most active and efficient transepithelial transport mechanisms among the animal kingdom. Fourth, genetic manipulations of insects such as fruit flies provide powerful tools to identify and localize transport systems in the Malpighian tubules. As a matter of fact, after nearly 30 years of investigation, the Malpighian tubules have become one of the best studied transepithelial transport models. In our lab, the Malpighian tubules of the yellow fever mosquitoes *Aedes aegypti*, have been extensively investigated by a collection of techniques including *in vitro* microperfusion, the Ramsay fluid secretion assay, microelectrode recording and

voltage clamping, electron probe analysis of secreted fluid, ion-selective microelectrode measurements and cell coupling analysis etc. In the remainder of this chapter, after a brief introduction on monolayers of cultured epithelial cells, I will focus on the Malpighian tubule model with a review on the transport systems that have been identified and characterized in insects including *Drosophila melanogaster*, *Aedes aegypti*, and *Rhodnius prolixus*.

2. Monolayers of cultured epithelial cells.

The technique of cell and tissue culture was started as early as the beginning of the twentieth century for the studies of cell growth and behavior in the absence of other influences (34). Techniques of culturing epithelial cells were developed many years later and it was not until the late 70's that epithelial cell monolayers were used to study the mechanisms of transpeithelial transports (34). Culture of epithelium has traditionally been fraught with problems related to overgrowth of stromal cells such as fibroblast. To reduce such contamination, various physical separation methods and selective culture techniques have been developed over the years. A general consensus has been reached that the culture conditions have to be favorable and selective for epithelial survival in order for realistic studies to be performed in epithelial cell biology. When seeded on top of permeable supports, cultured epithelial cells can grow to form cell-monolayer resembling the *in vivo* epithelial cell layer. In 1976, Misfeldt et al grew MDCK cells on porous membrane filters, showing its easy handling and adaptability to the standard techniques of epithelial transport study (82). An additional bonus of the cell monolayer in permeable supports is that many epithelia differentiate more on a porous surface than on a solid surface such as standard tissue culture plastic (48, 116).

Two types of epithelial cell culture have been extensively used for studies of epithelial cell function: primary cell culture and continuous cell lines. Primary cell culture is a culture started from cells, tissues, or organs taken directly from organisms, therefore a primary culture may be regarded as such until it is subcultured for the first time. Each subculturing, i.e. re-suspension and plating of the cells, is referred to as a passage. A continuous cell line was defined as one which has an essentially infinite life span, usually originated from cancerous cells. Both primary and continuous cell cultures offer the previously stated advantages of precise control of growth conditions and provide a preparation with a simple structure, i.e. an epithelium without underlying connective tissue or smooth muscle layers. Some disadvantages of primary culture are that: 1) cell growth usually ceases after a few divisions; and 2) the cells can demonstrate phenotypic instability, i.e. the disappearance of physical, biochemical or physiological properties of interest after the cells are placed in culture. In contrast, continuous cell lines, particularly subclonal cell lines, are homogeneous and the supply of cells is essentially unlimited as one can grow as many cells as needed. Such cell lines also enable investigator to compare cellular functions in different stages of growth (i.e. actively dividing or growth-arrested stages) and to identify mutants that are defective in particular functions (107). That's probably the reason why nowadays most of the monolayers used, for example in the field of intestinal transport, are immortal cell lines such as Caco-2 and HT-29, derived from human colonic carcinoma cells (3). Caco-2 cell monolayers, the most widely used model at present, were first developed by Hidalgo et al in 1989 (56). Since then many studies on intestinal transport have been done on the monolayers of Caco-2 cells, successfully predicting transport properties of various drugs and agents (3).

Nonetheless, there are important limitations in using continuous cell lines. First, the cells are grown from minced organs and their precise origin is usually unknown. Moreover, some cell lines have abnormal numbers of chromosomes and cells clearly can differ with respect to their stage of differentiation (for example Caco-2 cells have a hypertetraploid karyotype and the chromosome number even varies among individual cells (107)). Another limitation to using continuous cell lines is the potential difference in gene expression in physiology between the continuous cell lines *in vitro* and the native tissue *in vivo*. For example even with the same concentrations of compounds applied, the effective permeability values of carrier-mediated transport of Caco-2 monolayers are much lower than natural human jejunum (3). Consistently, the expression of these transport machinery in Caco-2 is reported to be variable and generally lower than *in vivo* (58).

3. The Malpighian tubules of insects.

3.1. Transepithelial transport across the Malpighan tubules.

Insects Malpighian tubules are blind-ended renal tubes with the open ends connected to their digestive guts. In vertebrates with glomerular kidneys, renal tubules receive the non-selectively filtered plasma from glomeruli, reabsorb most of the solutes and water back into the interstitial compartment which eventually return to the circulatory system. Composition of plasma is therefore controlled by regulating the reabsorption and secretion processes along the renal tubules. In insects, lacking the muscular heart and the closed circulatory system to generate the high hydrostatic pressure, the haemolymph or circulatory fluid is actively secreted, instead of being filtered into the Malpighian tubule lumen (10, 12). It's not surprising that the fluid secretion rate of the Malpighian tubules is very high, especially in those blood-feeding insects such as mosquitoes, since the habits of gorging (meals up to 10 times the body

weight) and flying will call for potent mechanisms of urine excretion to reduce flight payloads. As an example, the Malpighian tubules of the blood-feeding hemipteran *Rhodnius prolixus* have the highest epithelial transport rate ever known (90).

The morphology and cell composition of Malpighian tubules vary among insect species. There are five Malpighian tubules in the yellow fever mosquito *Aedes aegypti*, while the fruit fly *Drosophila manlanogaster* has four. In fruit flies and mosquitoes, Malpighian tubules are composed by two different types of epithelial cells. The large-sized principal cells are the ones with majority population. Eighty six percent of the Malpighian tubule cells in *Aedes aegypti* are principal cells (109). Stellate cells are much smaller in size, sporadically spreading between the principal cells (109). In comparison, the Malpighian tubules of *Rhodnius prolixus* consist only of the principal cells (76). Despite these differences, functional organization of cells along these tubules is quite similar. Generally speaking, cells in the blind end, conventionally referred as the distal or upper end, of all these Malpighian tubules perform fluid secretion, while the proximal or lower end of the Malpighian tubules seems to be the site for fluid reabsorption (88, 89, 108). Both secretion and absorption processes in the Malpighian tubules are actively regulated by the insect hormone system (17).

Ion transport responsible for fluid secretion in the distal Malpighian tubules was thought to be rather well understood. Essentially, the significant steps were seen as

(1) Active transport sited in the apical microvilli of the plasma membrane generates huge electrochemical ionic gradient across the apical membranes of Malpighian tubules;

(2) The entry of sodium, potassium and chloride ions from the haemolymph into the cell through channels or transporters sited in the basolateral membranes, at relative rates characteristic of the particular insect and of the state of stimulation of the tubule;

(3) An accompanying movement of ions, usually of the counter ions of those taking the trancellular pathway, into the lumen down their electrochemical gradient through extracellular pathways.

Steps 1 and 2 are conventionally referred as the transcellular transport pathway. In the Malpighian tubules, transcellular transport pathway can be dominated by either cations such as Na^+ and K^+ or anions such as Cl^-. This active transport of cations or anions across the cell will result in a voltage difference across the epithelium, namely the transpithelial potential (TEP), positive for cation secretion and negative for anion secretion. The movement of counter ions through the intercellular space, namely the paracellular pathway, as a result preserves the electrical neutrality of solutions in all compartments that are separated by epithelial cells. Apparently, TEP becomes the main driving force for this passive transport of ions.

In the early days, step 1 was thought to be accomplished by a common cation pump, which can directly pump Na^+ and K^+ out of the apical membranes in the expense of ATP (77). Since 1990's people began to realize that the cation pump was actually a combination of the V-type H^+ ATPase and the functionally coupled H^+/cation exchangers (51, 126). The ratio of Na^+ to K^+ in the secreted fluid was thought to be dictated by the entry step 2 (78). Insects vary greatly in this respect, some tubules producing almost exclusively a KC1 solution and others secreting KCl

with NaCl (14, 53, 74). Mechanisms of these transports will be discussed in detail in the following sections based on the three steps mentioned above.

3.2. Transport systems in the apical membranes.

3.2.1. The V-type H^+ ATPase. The V-type H^+ ATPase is a huge protein complex composed by many subunits. It mainly consists of two functional domains, a cytoplasmic V_1 complex and a membrane-integrated V_0 complex. The V_1 complex is the site for ATP binding and hydrolysis. It is composed of eight different subunits (A–H). The V_0 complex is composed of five different subunits, designated a–d, that collectively function as the proton translocation pathway (126). Before the critical role of the V-type H^+ ATPase was discovered in transepithelial transport, the first transepithelial transport model proposed by H. Ussing in 1950's favored the Na^+/K^+ ATPase as the main energizer in that model, which is known as the "Na^+/K^+ ATPase paradigm" (66). In this paradigm, Na^+/K^+ ATPase, which is always located in the basolateral membrane of epithelia cells, generates remarkable concentration difference for K^+ and Na^+ across the cell membrane by bringing K^+ in and pumping Na^+ out of the cell. The electrochemical gradient of Na^+ and K^+ are utilized to drive numerous transport processes across the epithelia. The V-type H^+ ATPase was first discovered in plant vacuoles, where it gets the "v" letter in its name (84). Later on, the V-type H^+ ATPase was found in more and more epithelial tissues, especially in invertebrates, indicating their important role in the transport processes in those species. After years of research on the V-type H^+ ATPase, Harvey and Wieczorek proposed the "V-type H^+ ATPase paradigm" for the transepithelial transport as an alternative for the "Na^+/K^+ ATPase paradigm" (126). In brief, the new paradigm states that proton pumps located in the apical membrane of epithelial cells develop huge H^+ gradient and voltage gradient across the apical membrane by actively pumping H^+ out of the cell,

which in turn are utilized to drive secondary transport systems such as ion exchangers or cotransporters located in either apical or basolateral membranes.

In insects Malpighian tubules, the presence of the V-type H^+ ATPase has been confirmed by varieties of approaches (40, 42, 73, 104, 115, 124), and it is clear now that transepithelial transport in the Malpighian tubules of most insects follows this paradigm (126). Central role of the V-type H^+ ATPase in secretion by the Malpighian tubules has been proved in many insects. In *Aedes* Malpighian tubules, the specific inhibitor of the V-type H^+-ATPases, bafilomycin A_1, reduced rates of transepithelial fluid secretion with an IC_{50} of approximately 5 μM (14). And nearly all the electrophysiological variables of the Malpighian tubule were affected (14). Bafilomycin A_1 decreased the virtual short-circuit current vIsc, suggesting inhibition of the electrogenic transcellular transport, which was confirmed by the increase in both the electrical resistance across the whole epithelium and across the apical membrane.

In *Aedes*, the genes encoding the A and c subunits of the V-type H^+ ATPase were isolated as early in 1998 from the Malpighian tubules of the 4^{th} instar larvae by Gill et al (42). For the protein expression, in 2003 by using several antibodies against the V-type H^+-ATPase of *Manduca Sexta*, we confirmed its presence in Malpighian tubules of adult *Aedes aegypti* (124). As expected, immunostaining results identified the V-type H^+ ATPase at the apical membrane of the mitochondrion-rich brush border of principal cells while the stellate cells lack of it. Measurements of ATPase activity revealed that bafilomycin-sensitive and NO_3--sensitive ATPase activity accounted for 50-60% of total ATPase activity in the crude extracts of Malpighian tubules.

However, it's also worth noting that although the V-type H^+ ATPase is located in the apical membrane of the principal cells, in the microperfusion experiments, bafilomycin A_1 had no effect when applied from the tubule lumen. Therefore bafilomycin A_1 must take a cytoplasmic route to reach its blocking site. This is actually consistent with studies showing that bafilomycin blocks the proton channel of the V-type H^+ ATPase by binding to the 100 kD subunit a of the V_0 complex (135), which is a transmembrane protein with a large amino terminal soluble domain exposed in the cytoplasm (33). Subunit a also appears to play an important role in assembly of the V-type H^+ ATPase complex (70).

In the Malpighian tubules of fifth-instar larvae of *Rhodnius prolixus*, fluid secretion by tubules is much slowed by the V-type H^+ ATPase inhibitor 4-chloro-7-nitrobenzo-2-oxa-1,3-diazol (NBDCI) (78). In adult Malpighian tubules, bafilomycin A_1 also inhibited tubule fluid secretion rate by 49%, indicating an important role of this ATPase in tubular secretion (47). Again, the action of bafilomycin A_1 was only effective from the bath side as in the case of *Aedes* Malpighiant tubules, pointing to the relative impermeability of the apical membrane to bafilomycin A_1 in both insects (47).

The Malpighian tubules of the fruit fly *Drosophila melanogaster* are also energized by the V-type H^+ ATPase (19, 24). Fifty micromolar bafilomycin completely abolished fluid secretion by the Malpighian tubules either unstimulated or stimulated by the thoracic-ganglion extracts (24). As in *Aedes*, the V-type H^+ ATPase in *Drosophila* Malpghian tubules were also confined to apical membranes of the mitochondria-rich principal cells, suggesting its role in active transport processes (19, 26, 115). Mutation in the gene encoding the B subunit of the V-type H^+ ATPase

caused larval lethality (19), which could be rescued by transformation of flies with a wild type vha55:GFP fusion, confirming that the lethal phenotype described for these alleles was due to defects in V-type H^+ ATPase function (26).

3.2.2 *The Cation/H^+ exchanger.* In the Malpighian tubules of these insects, protons pumped out by the V-type H^+ ATPase into the extracellular microenvironment of the brush border are thought to return to the cell in exchange for Na^+ and K^+. In *Aedes*, inhibition of these antiporters has been shown to impair the secreting function of the tubules (96). In 2002, Hart et al identified two NHE genes from the Malpighian tubules of *Aedes aegypti*, encoding proteins of 678 and 1,179 amino acids, respectively (50). When comparing the primary sequences of these two proteins, the two clones show 98% identity to each other while the 1,179 aa protein has an extensive C-terminus that is absent in the 678 aa protein (50). Immunohistochemical study by the Gill group showed that expression of the 1,179 aa protein, named as NHE3, was detected in the apical membranes in the median Malpighian tubules, however in other sections of the Malpighian tubules NHE3 was predominantly localized to the basal membrane suggesting its function in mediating Na entry into the cell and the maintenance of intracellular pH (106). In 2007, Gill lab isolated and identified nhe8 gene from the cDNA library of *Aedes aegypti* (64). Results show that NHE8 is a single antiporter accepting both K^+ and Na^+ ions that is sensitive to amiloride, and it is exclusively located in the apical membranes of the principal cells of *Aedes* Malpighian tubules.

In the secretory segment of *Rhodnius* Malpighian tubules, evidence for the presence of NHE in the apical membranes is rather indirect. Results of measuring intracellular and luminal ion activities as well as membrane potential, thereof the

calculations of electrochemical gradients for Cl^-, Na^+, K^+ and H^+ across the apical membrane were consistent with the presumable presence of Na^+/H^+ and/or K^+/H^+ exchangers in the apical membrane (61). In 2004 Gutierrez found that amiloride at a concentration of 0.4 mM, in the lumen, but not in the bath, strongly inhibited the secretion rate of the Malpighian tubules (47).

In *Drosophila* Malpighian tubules, using a low-stringency homology searching, three members of the NHE family (DmNHE1, DmNHE2 and DmNHE3) were identified in the genomic sequence of the fruit fly (41). Expression patterns of these genes revealed their presence in the head, body and Malpighian tubules and at all developmental stages, indicating their extensive roles in insect physiology (41). In particular, gene nhe1 is significantly enriched in the Malpighian tubules as shown by the microarray work by Wang et al in 2004 (122). The localization of these Na^+/H^+ exchangers in the *Drosophila* Malpighian tubules is still unclear.

Besides its location in the Malpighian tubule, the stoichiometry of the cation-H^+ exchanger is also of particular importance in understanding its function in transcellular transport. If the antiport is electrically neutral, exchanging one H^+ ion for one Na^+ or K^+ ion, voltage is not a driving force. Therefore, only the net concentration difference of H^+ and Na^+ (or K^+) across the plasma membrane determines the direction and magnitude of the exchange transport. If the antiporter exchanges two H^+ ions for each Na^+ (or K^+) ion (98), as suggested for the goblet cells of the *Manduca sexta* midgut (5), then voltage is an additional driving force. In this case, an apical membrane voltage of 120 mV (cell-negative) is able to drive Na^+ and K^+ into the tubule lumen against a 100-fold concentration difference. Up to present, the molecular identity of the exchanger has yet to be elucidated. In *Aedes* Malpighian tubules, the NHE8

proteins, when reconstituted into proteolipsomes, seem to undergo an electrical neutral exchange of Na^+ and K^+ for H^+, however its physiological kinetics *in vivo* still remains uncertain (64).

3.2.3 Cl^- channel. In 1984, O'Donnell and Maddrell reported the occurrence of lumen-negative TEPs in *Rhodnius prolixus* Malpighian tubules by the Ramsey technique, in which electrodes are positioned in bathing and secreted fluid droplets for tubules isolated under paraffin oil (91). Later this lumen-negative TEP was confirmed by other techniques including luminal cannulation and microelectrode impalement (62). Lumen-negative TEPs strongly suggest that the Malpighian tubules of *Rhodnius prolixus* undergo active anion secretion through their transcellular pathway, which is in contrast to the more common finding of lumen-positive transepithelial voltages in secreting Malpighian tubules of *Drosophila* (87), *Onymacris* (86), *Formica* (136) and *Aedes* (2). Indeed, in *Rhodnius* Malpighian tubules a putative Cl^- channel was thought to be located in the apical membrane, next to the V-type H^+ ATPase, since the electrochemical potential for Cl^- is consistent with the passive movement of Cl^- from cell to lumen through Cl^- channels (61). The presence of a putative Cl^- channel next to the proton pump may also help to explain the low apical membrane potential of *Rhodnius* Malpighian tubules (+30 mV) in contrast with the much higher lumen positive V_a in *Aedes* and *Drosophila* Malpighian tubules, which are 110 and 100 mV, respectively (2, 87). Activation of this apical membrane Cl channel by the diuretic hormone serotonin is thought to cause the hyperpolarization of the transepithelial membrane voltage (91).

3.3. Transport systems in the basolateral membranes.

When Malpighian tubules undergo constant secretion or reabsorption, no matter whether they are stimulated or not, in steady state the cytoplasmic compositions of the epithelial cells should be relatively constant. In other words, the amount of Na^+, K^+ and Cl^- that is pumped out of the cell into tubule lumen across the apical membranes must equal those entering the cell from the haemolymph through the basolateral membranes. Several major channels and transport systems located in the basolateral membrane are responsible for this process, including K channel, Cl channel, the electroneutral $Na^+/K^+/2Cl^-$ cotransporter, amiloride sensitive Na^+/H^+ exchanger, Na^+/K^+ ATPase, the Na^+ dependent Cl^-/HCO_3^- exchanger, and the hormone-activated putative Na^+ and Ca^{2+} channels.

Among these transport systems, of particular interest are the ion-selective channels and electrogenic pumps. Since these transporters allow the movement of electrical currents, their functions will be directly reflected in variables such as the membrane voltages and resistances that can be conveniently measured by electrophysiological methods. From this perspective, the transport across the Malpighian tubules can be modeled by the equivalent electrical circuit as shown in Figure 1.1. In Fig. 1.1, the active transport pathway, taken by Na^+ and K^+ or Cl^- through principal cells, consists of electromotive forces (E) and the resistance (R) of the basolateral (bl) and apical (a) membranes. A shunt pathway for Cl^- or Na^+, K^+ consists of the single resistance, R_{sh}, located outside the principal cells. Transcellular and paracellular pathways are electrically coupled such that cationic current through principal cells equals anionic current through the shunt. Apparently, the potential difference in apical (V_a) or basolateral membranes (V_{bl}) is determined by both the electromotive forces and the voltage changes caused by currents passing through the membrane resistance. It's

Figure 1.1. Electrical model of transepithelial ion secretion through principal cells and the paracellular pathway of the Malpighian tubules. The electromotive force measured across the apical membrane (E_a) reflects the activity of the V-type H^+-ATPase located in the microvillus apical membrane. E, electromotive force; R, resistance; V, voltage difference; a, apical; bl, basolateral; sh, shunt.

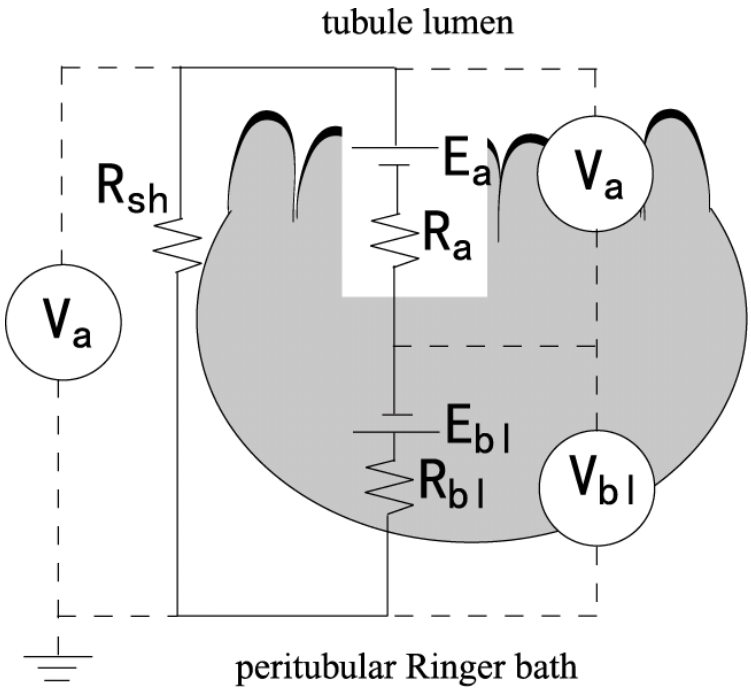
tubule lumen
R_{sh}
E_a
V_a
R_a
V_a
E_{bl}
R_{bl}
V_{bl}
peritubular Ringer bath

worth noting that fig. 1.1 shows the general scheme of electrogenic transport across the Malpighian tubules, while in different insect species, the arrangement of electromotive forces and membrane resistance can be quite different. For example, in *Drosophila* and *Aedes* Malpighian tubules, the basolateral membrane voltage is largely determined by the positive current passing across the membrane that is carried largely by K^+. In contrast, many evidences show that V_{bl} of the Malpighian tubules of *Rhodnius prolixus* is developed by the electrodiffusion of K^+ ions across the basolateral membrane. We'll discuss them in detail in the following sections.

3.3.1. K channel: In *Aedes* Malpighian tubules, positive current passing across the basolateral membrane is carried largely by K^+ ions, which is the major mechanism for K^+ entering the cell from the hemolymph (13, 80, 113, 128). In the presence of the K channel blocker Ba^{2+}, transepithelial fluid secretion significantly decreased from 0.84 to 0.37 nl/min and the K^+ concentration in secreted fluid decreased from 119.0 to 54.3 mM with no change in the Cl^- concentration. Rates of transepithelial Na^+ secretion significantly decreased, too (113). Consistently, the transepithelial resistance (R_t) was increased from 6.4 to 6.9 kΩcm (113). By the method of two-electrode voltage clamp (TEVC), measures of the input resistance R_{pc} together with membrane fractional resistance yielded estimates of the conductance of the basolateral membrane K^+ channels as 0.94 μS/tubule (13). Estimates of transference numbers yielded the basolateral membrane Na^+ conductance of 0.24 μS, leaving 0.30 μS (20%) of g_{bl} unaccounted (13).

The role of basolateral membrane K channels as an important entry pathway for K^+ into the cell is also supported by the hyperpolarization of the V_{bl} caused by Ba^{2+} (113). According to Fig. 1.1, when basolateral membrane K channels are blocked by

Ba^{2+}, the loop current of the equivalent electrical circuit is reduced, then the transepithelial potential will also decrease since it is the product of the loop current with the shunt resistance. Therefore V_{bl} value will approach to the apical membrane voltage V_a, appearing as a process of hyperpolarization. The hyperpolarization of V_{bl} caused by Ba^{2+} is strongly in contrast with the depolarizing effect of Ba^{2+} on resting membrane potentials in mammalian nerve or muscle cells. In nerve or muscle cells, membrane potentials, defined by Goldman equation, are caused by the electrodiffustion of conductive ions such as K^+ and Na^+ across the membrane. In normal conditions, K channels dominate the membrane conductance therefore the membrane potential is mainly dictated by the electrochemical gradient of K^+ ions across the membrane. When K channels are blocked by Ba^{2+} in those cells, the contribution of Na^+ conductance will increase, consequently bringing membrane potential towards the Nernst equilibrium potential of Na ions, i.e., depolarizing the membrane. In *Aedes* Malpighian tubules, the effect of Ba^{2+} on V_{bl} suggests that V_{bl} is not determined by the electrodiffusion of K^+ ions across the basolateral membrane, instead it is the net entry of K contributing to the value of V_{bl}.

The molecular identity of this K channel in *Aedes* Malpighian tubules is not clarified yet. Based on the sequences of *Drosophila* inwardly rectifying K channel (irks), in 2004 we did a BLAST search in the unfinished gene indices of *Aedes aegypti*. We discovered two TC sequences, TC15470 and TC16638, potentially encoding the inwardly rectifying K channels in the mosquito, whose complete amino acid sequences were confirmed in the newly updated *Aedes* genomic sequence database in PubMed in June 2006 by conceptual translation of their respective cDNAs. By the method of rtPCR, in 2004 we identified the expression of these two genes in the total RNA extractions of *Aedes* Malpighian tubules (data not published).

Nevertheless, since dissection of Malpighian tubules cannot practically remove tracheal cells attached to the tubules completely, rtPCR results did not exclude the possibility that the expression of these two genes were from *Aedes* tracheal cells, as in the case of *Aedes* aquaporin genes (27). To confirm the expression of irk genes in the Malpighian tubule cells of *Aedes aegypti*, experiments by the methods of *in situ* hybridization and immunohistochemstry will be necessary.

In *Drosophila* Malpighian tubules, addition of the K^+ channel blocker Ba^{2+} also significantly hyperpolarized the basolateral membrane voltage V_{bl} (60). The antidiabetic sulphonylureas, another selective inhibitors of inward rectifier K channels, completely inhibited fluid secretion by the Malpighian tubules, in which the effects of glibenclamide simulated that of the K^+-free bath solution (28). However measurements of $[K^+]_i$ show that $[K^+]_i$ is at near its electrochemical equilibrium with the bath $[K^+]$ across the basolateral membrane of resting *Drosophila* tubule, while in fact the electrochemical gradient is a little (9 mV) outward (60). Furthermore, addition of 6 mM Ba^{2+} to the bath solution had no effect on $[K^+]_i$ (60). It has been suggested that IRKs play only a minor role in basal secretion: their rectification properties imply that they are unlikely to let much K^+ out, down its electrochemical gradient. However, when the tubule is maximally stimulated, and the apical electrogenic V-type H^+ ATPase is driving more K^+ exit across the apical membrane, basolateral IRKs allow K^+ entry to support the activated apical membrane. Consistent with this, all the sulphonylureas showed a marked effect on stimulated, rather than basal, fluid secretion (28).

Three cDNAs encoding inwardly rectifying potassium (Kir) channels have been isolated from *Drosophila melanogaster*. The protein sequences of *Drosophila* IRK1

and IRKII are moderately (<44%) and IRKIII sequence is weakly (<27%) identical to human IRK channel subunits. Heterologous expression of wild type dIRKI and dIRKII in *Drosophila* S2 cells readily evoked typical inwardly rectifying K^+ currents, which were weakly sensitive to Ba^{2+} (23). Whole mount *in situ* hybridizations revealed dIRKII and dIRKIII are expressed in the embryonic hindgut and in Malpighian tubules, respectively, suggesting their roles in the entire osmoregulatory system of the developing fly (23). In the adult fly Malpighian tubules, microarray analysis by Wang et al identified that the three genes are extremely abundant and enriched compared to their expression in the rest of the body (122). The result was subsequently confirmed by quantitative RT-PCR of irk genes in the Malpighian tubules (28). All three irks localized to principal cells of the main segment (and ir and irk3 to the lower tubule) by *in situ* hybridization, suggesting roles both in primary secretion and reabsorption (28).

In contrast, in the secretory segment of *Rhodnius* Malpighian tubules, K channels seem to be more involved in the development of V_{bl} by electrodiffusion, instead of being a major pathway for K entry. Addition of 6 mM Ba^{2+} had no effect on the fluid secretion rate of *Rhodnius prolixus* Malpighian tubules stimulated with 1 μM serotonin (59). Consistently, the treatment of Ba^{2+} caused V_{bl} to depolarize (59).

3.3.2. $Na^+/K^+/2Cl^-$ cotransporter. In the Malpighian tubules of *Aedes aegypti*, the bumetanide-sensive $Na^+/K^+/2Cl^-$ cotransporter is another major pathway for Na^+, K^+ and Cl^- entering the principal cell. Bumetanide at 100 μM significantly decreased transepithelial K^+ secretion with no effect on transepithelial fluid secretion and the electrical resistance, consistent with the inhibition of electroneutral $Na^+/K^+/2Cl^-$ cotransport (55). Transepithelial Na^+ secretion significantly increased because other

Na^+ entry pathways remained active. Bumetanide plus Ba^{2+} completely inhibited transepithelial electrolyte and fluid secretion, with fast and slow kinetics reflecting the Ba^{2+} block of basolateral membrane K channels and the inhibition of $Na^+/K^+/2Cl^-$ cotransporter, respectively (113). The single and combined effects of Ba^{2+} and bumetanide demonstrated that K^+ channels and $Na^+/K^+/2Cl^-$ cotransporter are the primary mechanisms for bringing K^+ into cells. Furthermore it also suggests that the mechanisms of transepithelial K^+ and Na^+ secretion are coupled in *Aedes* Malpighian tubules such that complete block of K^+ secretion renders the epithelium unable to secrete Na^+.

In *Drosophila* Malpighian tubules, bumetanide lowered the secretion rate by 50 % in unstimulated tubules, which appear to be due to the reduction of K secretion (74). In contrast, Na^+ flux was not affected significantly (74), probably being due to the fact that normal Na^+ secretion has already been very low (60). In normal conditions, *Drosophila* Malpighian tubules secretes fluid highly enriched with K ions, the composition of Na is rather low, suggesting the transcellular pathway is more selective for K transport (74). It is thought that the basolateral membrane Na^+/K^+ ATPase recycles most of the Na^+ entry into the cell (we'll discuss it in next section). Indeed, when the *Drosophila* Malpighian tubules were first exposed to 0.1 mM ouabain for 30 minutes, bumetanide reduced Na^+ flux by 29% besides the reduction of K^+ flux (60).

In the serotonin-stimulated *Rhodniu* Malpighian tubules, fluid secretion was severely reduced by furosemide and bumetanide. In saline containing 0.1 mM furosemide, secretion rates dropped to 21% of their values in control saline (91). The effect of bumetanide was even more powerful (47, 91), during which both Na^+ and K^+ secretion were reduced by 69% and 87 %, respectively (59). The basis for the

inhibition of secretion was suggested by the dramatic effect of furosemide on the apical membrane voltage of the Malpighian tubule cells. Under the presence of 0.1 mM furosemide, the apical membrane voltage underwent a dramatic hyperpolarization from -50 to -116 mV (91). Accordingly, the transepithelial voltage changed from –30 mV (lumen negative) in control saline, to 50 mV (lumen positive) in saline containing furosemide (91). These changes were similar to the effects of chloride-free saline, suggesting that furosemide inhibited chloride entry into the cells. Indeed, a later study showed that intracellular Cl^- activity declined to 23% of its control value when the tubules were exposed to bumetanide (59). With the dramatic drop in intracellular Cl^- concentration, exit of Cl^- ions through apical membrane Cl channels should be restricted; therefore the huge voltage gradient developed by the V-type H^+ ATPase across the apical membrane is preserved. A small depolarization in the basolateral membrane voltage were also recorded during the effect bumatenide (91), which is similar as the effects in *Aedes* Malpighian tubules (55). The reason for this depolarization is unclear; it is probably an indirect effect that stems from decreased intracellular K^+ or Cl^- concentrations caused by the inhibition of the $Na^+/K^+/2Cl^-$ cotransporter.

3.3.3. Na^+/K^+ ATPase. The Na^+/K^+ ATPase is ubiquitously expressed in almost all kinds of animal cells. In epithelial cells, the Na^+/K^+ ATPase is always located in the basolateral membranes. However, the role of the Na^+/K^+ ATPase in the transepithelial secretion by different insects Malpighian tubules varies greatly. As it is well known that for every ATP hydrolyzed, the Na^+/K^+ ATPase pumps 3 Na^+ out of the cell and brings 2 K^+ into the cytoplasm, which keeps the cytosolic Na^+ level low and K^+ level high. From this perspective, the Na^+/K^+ ATPase located in the basolateral membranes of the Malpighian tubule cells may contribute the secretion of

K^+ ions through the cell, while on the other hand it definitely reduce the transcellular Na^+ transport from hemolymph to tubule lumen. Therefore, for insects that secrete urine with high Na^+ concentration, such as *Aedes aegypti*, it would be conceivable that the Na^+/K^+ ATPase may only play an indirect role in the urine secretion. Consistently, we observed no immediate effects of 1 mM ouabain on the transepithelial voltage and resistance of isolated *Aedes* Malpighian tubules (127). And the partial inhibition (approximately 50%) on transepithelial fluid secretion by ouabain was only observed after more than 30 min of ouabain treatment (55). In addition, the enzyme activities assay detected no significant ouabain- or vanadate-sensitive Na^+/K^+-ATPase activity in the protein extracts of *Aedes* Malpighian tubules (124). The low Na^+/K^+ ATPase activity is probably due to the low expression level of this enzyme in the tubules. As it is shown by the immunohistochemistry work by Gill et al, that to localize the Na^+/K^+-ATPase in the Malpighian tubule sections, the required titration of the primary antibody has to be remarkably high (1:20) (106).

In contrast, in *Drosophila* Malpighian tubules, the Na^+/K^+ ATPase seems to play a more significant role in tubular section. In normal conditions, *Drosophila* Malpighian tubules secrete urine with high K^+ concentration, while the urine Na^+ concentration is fairly low. As for the transport processes across the basolateral membrane, this could mean that the Na^+ entering cells through transporters such as the $Na^+/K^+/2Cl^-$ cotransporter are mostly recycled into the bath medium, such as by the Na^+/K^+ ATPase. Indeed, when the Na^+/K^+ ATPase are inhibited by ouabain, the Na^+ concentration of the urine in unstimulated *Drosophila* Malpighian tubules increased by 50–73 % (74). Fluid secretion rates also increased slightly (by 10–19 %), but significantly, when ouabain was added to the bath (74). Furthermore, unlike in *Aedes*

Malpighian tubules, immunocytochemical evidence showed that Na^+/K^+ ATPase is abundantly expressed in *Drosophila* Malpighian tubule (68).

The Malpighian tubules of *Rhodnius prolixus* in rest condition also secrete urine enriched with K^+ as in *Drosophila* Malpighian tubules. Similarly, ouabain increases the fluid secretion in isolated and unstimulated Malpighian tubules (79, 85, 93), which is consistent with the hypothesis that the basolateral membrane Na^+/K^+ ATPase recycles Na^+ back to the hemolymph from the cytoplasm. Serotonin, a diuretic hormone released by *Rhodnius* during blood meals dramatically increases the urine flow rate to 1000 times, while the urine Na^+ concentration is elevated remarkably (77). Of particular interest is that serotonin inhibits the Na^+/K^+ ATPase activity in Malpighian tubule cells of *Rhodnius prolixus* (46). Since the first step in the rapid excretion phase during blood meals is the elimination of urine enriched in NaCl and water, the inhibition of Na^+ recycling due to inhibition of the Na^+/K^+ ATPase activity would be an important component in this phase. Like in *Drosophila* Malpighian tubules, the inhibition of the Na^+/K^+ ATPase could lead to intracellular accumulation of Na^+ and, consequently, to an increase of Na^+ secretion through the apical membranes.

3.3.4. Cl^- channel. Similar to the function of Na^+/K^+ ATPase during the secretion by Malpighian tubules, Cl channels located in the basolateral membranes of the principal cells could be also responsible for the recycling of Cl^- ions, thus contribute to regulation of the compositions of fluid secretion. This is of particular importance in the Malpighian tubules of *Aedes aegypti* and *Drosophila melanogaster*, since in those tubules, the active transcellular transport pathway is dominated by the passage of cations, while most Cl^- ions take the passive transport pathway through the

intercellular spaces (133) or the stellate cells (92). Consequently, the Cl^- ions that are brought into the principal cells by the Cl^- carriers such as the $Na^+/K^+/2Cl^-$ cotransporter and the Na^+ dependent Cl^-/HCO_3^- exchanger have to be recycled back into the hemolymph across the basolateral membrane.

Measurements of Cl^- gradients across the basolateral membrane of *Drosophila* Malpighiant tubules showed that passive movement of Cl^- is favored from cell to bath (60). Specifically, addition of Ba^{2+} unmasked a basolateral Cl^- conductance that is smaller than that for K^+ (60). In *Rhodnius* Malpighian tubules, calculated Cl^- electrochemical potential also favors passive movement of Cl^- out of the cell across the basolateral membranes in both unstimulated and serotonin-stimulated conditions (59), while microelectrode studies in stimulated upper Malpighian tubules showed that ~25% of the total basolateral electrical permeability was due to Cl, which could be reduced by the Cl channel blocker DPC (47). Furthermore, bath DPC increased transepithelial secretion by 39%, suggesting the presence of a net return of Cl^- from cell to hemolymph and its inhibition would tend to increase $[Cl^-]$ within the cell, thus favoring net transepithelial Cl secretion (47).

3.3.5 Other transport systems. There are some other transport systems located in the basolateral membranes of the Malpighian tubules. They may or may not directly contribute to the transepithelial transport of ions across the Malpighian tubules, yet are definitely important in maintaining the normal functions of the Malpighian tubules and in the transport regulations of insect hormones. For example, in *Aedes* Malpighian tubules under control conditions, the Na channel blocker amiloride has no effects on transepithelial voltage and resistance (54). However when the tubules were pretreated with secretagogue db-cAMP (0.1 mM), which significantly depolarized V_{bl} and

increase g_{bl}, the effects were reversed by amiloride (13), suggesting the activation of Na^+ conductance during the effects of cAMP. The effects of amiloride are immediate — within seconds — consistent with the block of an epithelial Na^+ channel (ENaC) or a hypothetical electrogenic Na-carrier (11, 97, 110). Interestingly, cAMP has also been proved to be the second messenger of mosquito natriuretic peptide (MNP) released during blood meal (97). As we discussed previously, blood meal for hematophagous insects calls for rapid elimination of the excessive water and solutes especially Na^+, the activation of Na^+ conductance in the basolateral membrane by MNP is therefore not surprising at all.

Another example is the nifedipine-sensitive Ca channel in *Aedes* Malpighian tubules activated during the effects of the diuretic hormone leucokinin. The leucokinins were first isolated from the heads of cockroaches for their ability to stimulate the contraction of the hindgut (57). While their diuretic properties were first found in the Malpighian tubules of *Aedes aegytpi* in our lab (52), since then the leucokinins have been recognized as one of the most potent diuretic hormones in insects (17). The analysis of fluid secreted by *Aedes* Malpighian tubules in the presence of leucokinin-VIII revealed nonselective increases in both NaCl and KCl secretion, which was later proved to be due to a dramatic increase in paracellular Cl conductance (12). Besides that, leucokinin also significantly hyperpolarized V_{bl} and decreased the fractional resistance of the basolateral membrane (fR_{bl}) (134). The Ca channel blocker nifedipine reversed the effects of leucokinin-VIII on those variables, while under control conditions, it had no significant effects (134). Therefore the activation of a Ca channel in the basolateral membrane during leucokinin effects is strongly implicated.

Unlike the hormone activated Na and Ca channels, the NHE in the basolateral membranes of *Aedes* Malpighian tubules is active in normal conditions and could contribute to the tubular secretion of Na (113). Rates of fluid secretion by individual Malpighian tubules were inhibited by 78% of control in the presence of 100 μM 5-(N-ethyl-n-isopropyl)-amiloride (EIPA), a specific inhibitor of Na^+/H^+ exchange (96), however this reduction of fluid secretion could also be due to the inhibition of NHE in the apical membranes (96). Another important role for the basolateral membrane NHE is to regulate the intracellular pH of principal cells. Bathing the Malpighian tubules in 0 mM extracellular Na^+ or in the presence of 100 μM EIPA reduced the steady-state intracellular pH by 0.5 pH units. On the other hand, when principal cells were acid-loaded by using the NH_4Cl pulse technique, the rates of recovery of intracellular pH depended on the presence of extracellular Na^+, and it could also be inhibited by 100 μM EIPA (96). Besides the Na^+/H^+ exchanger, the Na^+ dependent Cl^-/HCO_3^- exchanger identified in *Drosophila* by Romero lab may also be an important pH_i regulator in the Malpighian tubules (112).

3.4. Paracellular transport pathway.

3.4.1 Paracellular pathway: tight junction and septate junction. The electrogenic, active transport of ions through the transcellular pathway forms electrical current, either positive or negative flowing from haemolymph into the Malpighian tubule lumen. This transcellular current must return to the haemolymph side to complete the electrical circuit, so that the electroneutrality of the solutions on both sides of the epithelium can be preserved, in spite of high rates of transepithelial salt and water flow. This is usually accomplished by the movement of counter ions through the extracellular space, i.e. the paracellular pathway, in the same direction of transcellular currents. The resistance of paracellular transport pathway is defined by the tight

junction (in vertebrates) or septate junction (in invertebrates) structures connecting the epithelial cells.

Compared with transcellular transport, paracellular transport generally differs in two ways: first, it is exclusively passive, driven by electroosmotic gradients produced by transcellular transport. Second, as the transmembrane channels, paracellular pathway also shows permselectivity over charges, however it does not rectify, i.e. it shows identical selectivity and conductance in both the mucosal and serosal directions (105). In comparison with transmembrane channels, paracellular pores are larger and thus less discriminating in size and charge (21, 117). The permeability differences between alkali-metal cations is only a few fold, in contrast to the thousand fold differences for cation channels of the plasma membrane. This low discrimination for similarly charged but differently sized cations is consistent with a relatively large pore size (105).

Up to now, most of our knowledge about paracellular permeability has been based on the studies of the tight junctions in vertebrate epithelial cells. In invertebrates where the tight junctions are absent, septate junction emerges as the functional counter part for the tight junction. Tight junctions (TJs) are the most apical component of the junctional complex in vertebrates and are defined as focal contacts between the plasma membranes of adjacent cells in ultrathin section electron microscopy (29, 111). The tight junction is characterized by the presence of 'kissing points' in electron micrographs: that is, the plasma membranes of two epithelial cells approach each other so closely that the intercellular space — typically 15–20 nm wide — is not apparent and the membranes appear to fuse. In contrast, septate junctions are located just basally to the adherens junction or may be the only belt-forming junction in some

epithelia, and no kissing points are seen (118). Instead, septate junctions show a ladder-like structure in ultrathin sections with steps ('septa') connecting adjacent plasma membranes across a 15-nm-wide intercellular space (118). Both tight junction and septate juncion encircle the cell pole and form the physical basis for the paracellular diffusion barrier. The reason invertebrates have SJs rather than TJs as occluding junctions is unknown. It's suggested that several septa reduce the net diffusion of solutes by increasing the diffusional distance rather than being an intrinsic impermeability of the material of the junction (67). After all, both tight junctions and septate junctions have also been proved to have functions in addition to permissive paracellular transport. For example, binding to the enterotoxin of *Clostridium perfringens*, the tight junction proteins claudin-3 and claudin-4 are thought to participate in triggering the diarrhea of the Clostridium infection (9, 65). And the septate junctions in *Drosophila* mediate apical secretion of the lumenal matrix-associated protein Verm, which is required to control tracheal tube size (123).

3.4.2 Tight junction proteins. For a long period of time, the molecular composition of tight junctions remained unclear. The fundamental breakthrough in understanding the barrier structure came in 1998 when the first claudins, isolated by S. Tsukita's group in Japan, were shown to reconstitute strands when expressed in claudin-null fibroblasts (36) and to be cell-to-cell adhesion molecules (39). Another transmembrane strand protein, called occludin (38), was discovered before claudins, but its function remains obscure. Claudin genes are found across a wide range of metazoa. Mammals have at least 24 (118). The puffer fish *Fugu* presently holds the record, with 56 claudin genes (75).

Claudins are tetraspan proteins ranging from 20 to 25 kDa and are recognized by the so-called WGLWCC motif in their first extracellular loop. Evidence showed that claudins are the structural and functional basis of the permeability of tight junctions. When expressed in low-resistance MDCK type II cells, claudin-1 (81), -4 (121), -8 (63, 131), -14 (8), and –15 (18) dramatically increases transepithelial resistance. In contrast, expression of claudin-2 in high-resistance MDCK type I monolayers decreased resistance (37). One can speculate that each claudin has a unique conductance and that their ensemble in each epithelium determines the overall conductance. In the case of claudin-4, -8, and -14, reduced conductance results from selective discrimination against cations (8, 121, 131). Low-conductance characteristics of claudin-4 and -8 are consistent with their expression in the distal renal tubule segments and those of claudin-14 with its expression in the inner ear, in both cases maintaining high cation gradients by limiting paracellular electrodiffusion. Some claudins, like claudin-1 in mammals, are rather ubiquitously expressed; others are highly restricted to specific cell types (45, 114) or certain periods of development (119).

In 2002, Colegio et al demonstrated that replacing some specific negative residues with positive ones in the first extracellular loop of claudin-15 converts it from a cation-selective to an anion-selective pore (18). Collectivity, these results suggest that fixed charges on the extracellular loops of claudins line the aqueous pores and electrostatically influence passage of soluble ions. This idea is further supported by the phenotype resulting from human mutations in claudin-16 (paracellin-1). Expression of claudin-16 is highly restricted to the junction of the thick ascending limb in the loop of Henle, coinciding with a region where paracellular cation reabsorption occurs down an electrical gradient (114). Homozygous individuals show

urinary Mg^{2+} and Ca^{2+} wasting due to a defect in paracellular cation reabsorption in this segment (114). Permeation through the shunt of *Aedes* Malpighian tubules has been assessed by measuring transepithelial halide diffusion potentials in perfused Malpighian tubules, after first inhibiting active transport with dinitrophenol (132). Diffusion potentials revealed Eisenman selectivity sequence I ($I^->Br^->Cl^->F^-$) which is the halide mobility sequence in free solution (132).

3.4.3 Septate junction proteins. Compared with tight junction, septate junctions have quite different protein compositions. Claudins seem to be quite conservative as the molecular components. In *Drosophila*, six claudin sequences are reported (7, 130). Two of these, Megatrachea (7) and Sinuous (130), have been located to the barrier-forming septate junctions in the tracheal tubes. By genetic screening of *Drosophila* mutants, many other septate junction proteins are also identified, yet most of them do not show any structural similarities with those in tight junctions (reviewed in (129)). Of particular interest is the unexpected role of the Na^+/K^+ ATPase as the structural component of the *Drosophila* septate junction, which is independent of its pump activities (94). Besides *Drosophila*, Tsukita and colleagues have identified five claudin-like proteins in *C. elegans* and have shown them to be necessary for controlling paracellular permeability across the gut (4).

4. Intercellular communications between epithelial cells through gap junctions.

4.1 Epithelial gap junction and its functions.

In 1959 when the direct cell-to-cell electrical coupling was first discovered in crayfish neurons (35), people didn't realize that this was due to one of the most fundamental protein structures in the cell membrane. Now we know that gap junctions, the intercellular membrane channels, are ubiquitously expressed in nearly

all cells in muticellular organisms throughout the animal kingdom (20, 95). The gap junction channels in excitable cells such as neurons and muscle cells have been extensively investigated during the past decades, since intercellular electrical communication is crucial for their functions (44). The channels permit rapid intercellular exchange of ions, and so they are used by neurons to avoid synaptic delays in escape responses when milliseconds dictate survival, and between neurons and other excitable cells (e.g. myocardiocytes) to entrain synchronous activity. In comparison, studies on gap junctions of epithelial cells are not as many probably due to the fact that the research on epithelial cells has been mainly focused on the vectorial transport of water and solutes between the interstitial compartment and the external world. Nonetheless, it has already been confirmed that gap junctions are responsible for the quick spreading of some cell-activating second messengers such as Ca^{2+}, IP_3, and cAMP etc between neighboring epithelial cells, resulting in a syncium of epithelial cells when the cells are responding to the regulating hormones. Zimmermann and Walz reported that a low dose of 5-HT (1-10 nM) not only could evoke periodic Ca^{2+} spikes in local cells, but also is capable of eliciting repetitive intercellular Ca^{2+} waves among neighboring cells that can be 400 μM away from the origin (137). And this spreading of Ca^{2+} waves could be prevented by the gap junction blocker octanol (137). Gap junctions have also been reported for direct involvement in the transepithelial transports of ions. The ciliary epithelium is composed of two cell layers, an outer pigmented layer (PE cell) whose basal surface lies adjacent to the stroma of the ciliary processes and an inner nonpigmented cell layer (NPE cell) whose basolatera1 membrane faces the posterior and vitreal spaces of the vertebrate eye (22). This epithelium secretes the aqueous humor, an approximately isotonic solution where Na and either Cl or HCO_3 seem to be the primary secreted ions (16). NaCl can be taken up by the PE cells from the stroma by

the $Na^+/K^+/2Cl^-$ cotransporter and parallel Na^+/H^+ and $C1^-/HCO_3^-$ exchanger, and pass through gap junctions to the NPE cells, thereafter Cl^- exit the cell through the Cl channels located in the NPE cell membranes (22).

4.2 Gap junction proteins

To understand the functional role of gap junctions in our epithelial transport models, one has to be aware that there are two distinct gap junction protein families, connexins and innexins, depending on which animal the model is from, vertebrates or invertebrates. Proteins from both families can form intercellular channels in membranes with average calculated pore sizes around 1~3 nm, while invertebrates tend to possess bigger channels (69). And each gap junction channel is composed by two hemi-channels located in the two opposing cell membranes of neighboring cells. The hemi-channel in turn is composed by six subunits of integral membrane proteins (20, 95). Yet, the integral proteins from these two families have almost completely different amino acid sequences (100, 102).

After the function of gap junctions was recognized in the early 1950s, the molecular basis of this structure remained unclear until in the middle of 1970s when connexin was first isolated and identified from mouse hepatocytes preparations (43). Connexins span the bilayer four times, and have both amino and carboxyl termini at the cytoplasmic side of the membrane, forming two extracellular loops and a cytoplasmic loop (44). M3 is believed to provide the channel lining structure, probably in conjunction with some part of M1 (44).

To be noted that connexins only exist in vertebrates. In invertebrates, the counter part of connexin is innexin, which have the similar transmembrane structures

(spanning 4 times across the membrane with 2 extracellular loops and 1 intracellular loop etc) (101). However it has taken scientists almost half a century to realize that the molecular basis of gap junction in invertebrates are so different in their primary sequences from vertebrates. For more than 2 decades since connexin was identified, people had tried to find the invertebrate connexins, yet all of them had failed (95). For example, with biochemical approaches Finbow et al isolated an 18 kD protein from *Nephrops norvegicus* that localized to the gap junctions (30), yet later on it's shown to be identical to the c subunit in the transmembrane V_0 complex of the V-type H^+ ATPase (31, 32). People also used degenerate primers designed to the conserved regions of connexins, to search the homologous peptides in invertebrates. All the attempts were consistently unsuccessful (99). It turned out later when the complete genomic sequences of *C. elegans* and *D. malanogaster* were released, that no homologous of connexin genes could be found (1, 6). The enigma of invertebrate gap junction component protein was finally solved by genetic research in *Drosophila* and *C. elegans* (100) . Since 1980s, evidence for a gene family to be involved in the intercellular communications between the fly neurons or the neuron-muscle coupler in the worms has accumulated steadily (100). And the identity of these proteins as the gap junction components was confirmed by Phelan et al in 1998 (103). While expressed heterogously in *Xenopus* oocytes, the *Drosophila* ShakingB proteins successfully formed intercellular channels with gap junction characteristics, unambiguously demonstrating its functional role in the forming of insect gap junctions (103).

5. Reference

1. **Adams MD, Celniker SE, Holt RA, Evans CA, Gocayne JD, Amanatides PG, Scherer SE, Li PW, Hoskins RA, Galle RF, George RA, Lewis SE, Richards S, Ashburner M, Henderson SN, et al.** The genome sequence of Drosophila melanogaster. *Science* 287: 2185-2195, 2000.

2. **Aneshansley DJ, Marler CE, and Beyenbach KW.** Transepithelial voltage measurements in isolated Malpighian tubules of *Aedes aegypti*. *J Insect Physiol* 35: 41-52, 1988.

3. **Artursson P, Palm K, and Luthman K.** Caco-2 monolayers in experimental and theoretical predictions of drug transport. *Adv Drug Deliv Rev* 46: 27-43, 2001.

4. **Asano A, Asano K, Sasaki H, Furuse M, and Tsukita S.** Claudins in Caenorhabditis elegans: their distribution and barrier function in the epithelium. *Curr Biol* 13: 1042-1046, 2003.

5. **Azuma M, Harvey WR, and Wieczorek H.** Stoichiometry of K+/H+ antiport helps to explain extracellular pH 11 in a model epithelium. *FEBS Lett* 361: 153-156, 1995.

6. **Bargmann CI.** Neurobiology of the Caenorhabditis elegans genome. *Science* 282: 2028-2033, 1998.

7. **Behr M, Riedel D, and Schuh R.** The claudin-like megatrachea is essential in septate junctions for the epithelial barrier function in Drosophila. *Dev Cell* 5: 611-620, 2003.

8. **Ben-Yosef T, Belyantseva IA, Saunders TL, Hughes ED, Kawamoto K, Van Itallie CM, Beyer LA, Halsey K, Gardner DJ, Wilcox ER, Rasmussen J, Anderson JM, Dolan DF, Forge A, Raphael Y, et al.** Claudin 14 knockout mice, a model for autosomal recessive deafness DFNB29, are deaf due to cochlear hair cell degeneration. *Hum Mol Genet* 12: 2049-2061, 2003.

9. **Berkes J, Viswanathan VK, Savkovic SD, and Hecht G.** Intestinal epithelial responses to enteric pathogens: effects on the tight junction barrier, ion transport, and inflammation. *Gut* 52: 439-451, 2003.

10. **Beyenbach KW.** Kidneys sans glomeruli. *Am J Physiol Renal Physiol* 286: F811-827, 2004.

11. **Beyenbach KW.** Mechanism and regulation of electrolyte transport in Malpighian tubules. *J Insect Physiol* 41: 197-207, 1995.

12. **Beyenbach KW.** Transport mechanisms of diuresis in Malpighian tubules of insects. *J Exp Biol* 206: 3845-3856, 2003.

13. **Beyenbach KW and Masia R.** Membrane conductances of principal cells in Malpighian tubules of Aedes aegypti. *J Insect Physiol* 48: 375-386, 2002.

14. **Beyenbach KW, Pannabecker TL, and Nagel W.** Central role of the apical membrane H+-ATPase in electrogenesis and epithelial transport in Malpighian tubules. *J Exp Biol* 203: 1459-1468, 2000.

15. **Burg M, Grantham J, Abramow M, and Orloff J.** Preparation and study of fragments of single rabbit nephrons. *Am J Physiol* 210: 1293-1298, 1966.

16. **Caprioli J.** The ciliary epithelia and aqueous humor. In: *Adzer's Physiology of the Eye: Clinical Application* (8th ed.), edited by Moses RA and Hart WM. St. Louis, MO: Mosby, 1987, p. 204-222.

17. **Coast G, Orchard I, Phillips J, and Schooley D.** Insect diuretic and antidiuretic hormones. *Advances in Insect Physiology* 29: 279-409, 2002.

18. **Colegio OR, Van Itallie CM, McCrea HJ, Rahner C, and Anderson JM.** Claudins create charge-selective channels in the paracellular pathway between epithelial cells. *Am J Physiol Cell Physiol* 283: C142-147, 2002.

19. **Davies SA, Goodwin SF, Kelly DC, Wang Z, Sozen MA, Kaiser K, and Dow JA.** Analysis and inactivation of vha55, the gene encoding the vacuolar ATPase

B-subunit in Drosophila melanogaster reveals a larval lethal phenotype. *J Biol Chem* 271: 30677-30684, 1996.

20. **De Mello WC.** In: *Cell-to-cell communication*. New York: Plenum Press, 1987.

21. **Diamond JM.** Channels in epithelial cell membranes and junctions. *Fed Proc* 37: 2639-2644, 1978.

22. **Do CW and Civan MM.** Basis of chloride transport in ciliary epithelium. *J Membr Biol* 200: 1-13, 2004.

23. **Doring F, Wischmeyer E, Kuhnlein RP, Jackle H, and Karschin A.** Inwardly rectifying K+ (Kir) channels in Drosophila. A crucial role of cellular milieu factors Kir channel function. *J Biol Chem* 277: 25554-25561, 2002.

24. **Dow JA, Maddrell SH, Gortz A, Skaer NJ, Brogan S, and Kaiser K.** The malpighian tubules of Drosophila melanogaster: a novel phenotype for studies of fluid secretion and its control. *J Exp Biol* 197: 421-428, 1994.

25. **Drewa T, Mlodzik-Danielewicz N, Tyrakowski T, Wolski Z, Pokrywka L, Kaczorowski P, and Krawczyk A.** The influence of ambroxol and capsaicin on the isolated rabbit bladder wall. *Acta Pol Pharm* 62: 399-403, 2005.

26. **Du J, Kean L, Allan AK, Southall TD, Davies SA, McInerny CJ, and Dow JA.** The SzA mutations of the B subunit of the Drosophila vacuolar H+ ATPase identify conserved residues essential for function in fly and yeast. *J Cell Sci* 119: 2542-2551, 2006.

27. **Duchesne L, Hubert JF, Verbavatz JM, Thomas D, and Pietrantonio PV.** Mosquito (Aedes aegypti) aquaporin, present in tracheolar cells, transports water, not glycerol, and forms orthogonal arrays in Xenopus oocyte membranes. *Eur J Biochem* 270: 422-429, 2003.

28. **Evans JM, Allan AK, Davies SA, and Dow JA.** Sulphonylurea sensitivity and enriched expression implicate inward rectifier K+ channels in Drosophila melanogaster renal function. *J Exp Biol* 208: 3771-3783, 2005.

29. **Farquhar MG and Palade GE.** Junctional complexes in various epithelia. *J Cell Biol* 17: 375-412, 1963.

30. **Finbow ME, Buultjens TE, Lane NJ, Shuttleworth J, and Pitts JD.** Isolation and characterisation of arthropod gap junctions. *Embo J* 3: 2271-2278, 1984.

31. **Finbow ME, Eliopoulos EE, Jackson PJ, Keen JN, Meagher L, Thompson P, Jones P, and Findlay JB.** Structure of a 16 kDa integral membrane protein that has identity to the putative proton channel of the vacuolar H(+)-ATPase. *Protein Eng* 5: 7-15, 1992.

32. **Finbow ME, Goodwin SF, Meagher L, Lane NJ, Keen J, Findlay JB, and Kaiser K.** Evidence that the 16 kDa proteolipid (subunit c) of the vacuolar H(+)-ATPase and ductin from gap junctions are the same polypeptide in Drosophila and Manduca: molecular cloning of the Vha16k gene from Drosophila. *J Cell Sci* 107 (Pt 7): 1817-1824, 1994.

33. **Forgac M.** Structure, function and regulation of the vacuolar (H+)-ATPases. *FEBS Lett* 440: 258-263, 1998.

34. **Freshney RI.** Culture of epithelial cells. New York: Wiley-Liss, 1992.

35. **Furshpan EJ and Potter DD.** Transmission at the giant motor synapses of the crayfish. *J Physiol* 145: 289-325, 1959.

36. **Furuse M, Fujita K, Hiiragi T, Fujimoto K, and Tsukita S.** Claudin-1 and -2: novel integral membrane proteins localizing at tight junctions with no sequence similarity to occludin. *J Cell Biol* 141: 1539-1550, 1998.

37. **Furuse M, Furuse K, Sasaki H, and Tsukita S.** Conversion of zonulae occludentes from tight to leaky strand type by introducing claudin-2 into Madin-Darby canine kidney I cells. *J Cell Biol* 153: 263-272, 2001.

38. **Furuse M, Hirase T, Itoh M, Nagafuchi A, Yonemura S, and Tsukita S.** Occludin: a novel integral membrane protein localizing at tight junctions. *J Cell Biol* 123: 1777-1788, 1993.

39. **Furuse M, Sasaki H, and Tsukita S.** Manner of interaction of heterogeneous claudin species within and between tight junction strands. *J Cell Biol* 147: 891-903, 1999.

40. **Garayoa M, Villaro AC, Klein U, Zimmermann B, Montuenga LM, and Sesma P.** Immunocytochemical localization of a vacuolar-type ATPase in Malpighian tubules of the ant *Formica polyctena*. *Cell Tissue Res* 282: 343-350, 1995.

41. **Giannakou ME and Dow JA.** Characterization of the Drosophila melanogaster alkali-metal/proton exchanger (NHE) gene family. *J Exp Biol* 204: 3703-3716, 2001.

42. **Gill SS, Chu PB, Smethurst P, Pietrantonio PV, and Ross LS.** Isolation of the V-ATPase A and c subunit cDNAs from mosquito midgut and Malpighian tubules. *Arch Insect Biochem Physiol* 37: 80-90, 1998.

43. **Goodenough DA.** Bulk isolation of mouse hepatocyte gap junctions. Characterization of the principal protein, connexin. *J Cell Biol* 61: 557-563, 1974.

44. **Goodenough DA, Goliger JA, and Paul DL.** Connexins, connexons, and intercellular communication. *Annu Rev Biochem* 65: 475-502, 1996.

45. **Gow A, Southwood CM, Li JS, Pariali M, Riordan GP, Brodie SE, Danias J, Bronstein JM, Kachar B, and Lazzarini RA.** CNS myelin and sertoli cell tight junction strands are absent in Osp/claudin-11 null mice. *Cell* 99: 649-659, 1999.

46. **Grieco MAB and Lopes AG.** 5-hydroxytryptamine regulates the (Na+ + K+)ATPase activity in Malpighian tubules of *Rhodnius prolixus*: evidence for involvement of G-protein and cAMP-dependent protein kinase. *Arch Insect Biochem Physiol* 36: 203-214, 1997.

47. **Gutierrez AM, Hernandez CS, and Whittembury G.** A model for fluid secretion in Rhodnius upper Malpighian tubules (UMT). *J Membr Biol* 202: 105-114, 2004.

48. **Handler JS, Preston AS, and Steele RE.** Factors affecting the differentiation of epithelial transport and responsiveness to hormones. *Fed Proc* 43: 2221-2224, 1984.

49. **Hardin JA, Kimm MH, Wirasinghe M, and Gall DG.** Macromolecular transport across the rabbit proximal and distal colon. *Gut* 44: 218-225, 1999.

50. **Hart SJ, Knezetic JA, and Petzel DH.** Cloning and tissue distribution of two Na+/H+ exchangers from the Malpighian tubules of Aedes aegypti. *Arch Insect Biochem Physiol* 51: 121-135, 2002.

51. **Harvey WR, Maddrell SHP, Telfer WH, and Wieczorek H.** H+ V-ATPases energize animal plasma membranes for secretion and absorption of ions and fluids. *Am Zool* 38: 426 -441, 1998.

52. **Hayes TK, Pannabecker TL, Hinckley DJ, Holman GM, Nachman RJ, Petzel DH, and Beyenbach KW.** Leucokinins, a new family of ion transport stimulators and inhibitors in insect Malpighian tubules. *Life Sci* 44: 1259-1266, 1989.

53. **Hazel MH, Ianowski JP, Christensen RJ, Maddrell SH, and O'Donnell MJ.** Amino acids modulate ion transport and fluid secretion by insect Malpighian tubules. *J Exp Biol* 206: 79-91, 2003.

54. **Hegarty JL, Zhang B, Carroll MC, Cragoe EJJ, and Beyenbach KW.** The effects of amiloride on isolated Malpighian tubules of the yellow fever mosquito (*Aedes aegypti*). *J Insect Physiol* 38: 329-337, 1992.

55. **Hegarty JL, Zhang B, Pannabecker TL, Petzel DH, Baustian MD, and Beyenbach KW.** Dibutyryl cAMP activates bumetanide-sensitive electrolyte transport in Malpighian tubules. *Am J Physiol* 261: C521-529, 1991.

56. **Hidalgo IJ, Raub TJ, and Borchardt RT.** Characterization of the human colon carcinoma cell line (Caco-2) as a model system for intestinal epithelial permeability. *Gastroenterology* 96: 736-749, 1989.

57. **Holman GM, Cook BJ, and Nachman RJ.** Primary structure and synthesis of a blocked myotropic neuropeptide isolated from the cockroach, Leucophaea maderae. *Comp Biochem Physiol C* 85: 219-224, 1986.

58. **Hu M and Borchardt RT.** Mechanism of L-alpha-methyldopa transport through a monolayer of polarized human intestinal epithelial cells (Caco-2). *Pharm Res* 7: 1313-1319, 1990.

59. **Ianowski JP, Christensen RJ, and O'Donnell MJ.** Intracellular ion activities in Malpighian tubule cells of Rhodnius prolixus: evaluation of Na+-K+-2Cl- cotransport across the basolateral membrane. *J Exp Biol* 205: 1645-1655, 2002.

60. **Ianowski JP and O'Donnell MJ.** Basolateral ion transport mechanisms during fluid secretion by Drosophila Malpighian tubules: Na+ recycling, Na+:K+:2Cl- cotransport and Cl- conductance. *J Exp Biol* 207: 2599-2609, 2004.

61. **Ianowski JP and O'Donnell MJ.** Electrochemical gradients for Na+, K+, Cl- and H+ across the apical membrane in Malpighian (renal) tubule cells of Rhodnius prolixus. *J Exp Biol* 209: 1964-1975, 2006.

62. **Ianowski JP and O'Donnell MJ.** Transepithelial potential in Malpighian tubules of Rhodnius prolixus: lumen-negative voltages and the triphasic response to serotonin. *J Insect Physiol* 47: 411-421, 2001.

63. **Jeansonne B, Lu Q, Goodenough DA, and Chen YH.** Claudin-8 interacts with multi-PDZ domain protein 1 (MUPP1) and reduces paracellular conductance in epithelial cells. *Cell Mol Biol (Noisy-le-grand)* 49: 13-21, 2003.

64. **Kang' Ethe W, Aimanova KG, Pullikuth AK, and Gill SS.** NHE8 mediates amiloride sensitive Na+/H+ exchange across mosquito Malpighian tubules and catalyzes Na+ And K+ transport in reconstituted proteoliposomes. *Am J Physiol Renal Physiol*, 2007.

65. **Katahira J, Inoue N, Horiguchi Y, Matsuda M, and Sugimoto N.** Molecular cloning and functional characterization of the receptor for Clostridium perfringens enterotoxin. *J Cell Biol* 136: 1239-1247, 1997.

66. **Koefoed-Johnsen V and Ussing HH.** The nature of the frog skin potential. *Acta Physiol Scand* 42: 298-308, 1958.

67. **Kukulies J and Komnick H.** Plasma membranes, cell junctions and cuticle of the rectal chloride epithelia of the larval dragonfly Aeshna cyanea. *J Cell Sci* 59: 159-182, 1983.

68. **Lebovitz RM, Takeyasu K, and Fambrough DM.** Molecular characterization and expression of the (Na+ + K+)-ATPase alpha-subunit in Drosophila melanogaster. *Embo J* 8: 193-202, 1989.

69. **Leitch B.** Ultrastructure of electrical synapses: review. *Electron Microsc Rev* 5: 311-339, 1992.

70. **Leng XH, Manolson MF, and Forgac M.** Function of the COOH-terminal domain of Vph1p in activity and assembly of the yeast V-ATPase. *J Biol Chem* 273: 6717-6723, 1998.

71. **Lennernas H.** Human intestinal permeability. *J Pharm Sci* 87: 403-410, 1998.

72. **Lennernas H.** Human jejunal effective permeability and its correlation with preclinical drug absorption models. *J Pharm Pharmacol* 49: 627-638, 1997.

73. **Lezaun MJ, Garayoa M, Villaro AC, Montuenga LM, and Sesma P.** Immunocytochemical localization of a vacuolar ATPase in the Malpighian tubules of two nsect species (*Formica polyctena* and *Locusta migratoria*). *Cell Biol Int* 18: 407, 1994.

74. **Linton SM and O'Donnell MJ.** Contributions of K+:Cl- cotransport and Na+/K+-ATPase to basolateral ion transport in malpighian tubules of Drosophila melanogaster. *J Exp Biol* 202: 1561-1570, 1999.

75. **Loh YH, Christoffels A, Brenner S, Hunziker W, and Venkatesh B.** Extensive expansion of the claudin gene family in the teleost fish, Fugu rubripes. *Genome Res* 14: 1248-1257, 2004.

76. **Maddrell SH.** Secretion by the Malpighian tubules of rhodnius. the movements of ions and water. *J Exp Biol* 51: 71-97, 1969.

77. **Maddrell SH.** Transport across insect excretory epithelia. In: *Membrane transport in biology*, edited by Giebisch G, Tosteson DC and Ussing HH. Heidelberg: Springer-Verlag, 1978, p. 239-271.

78. **Maddrell SH and O'Donnell MJ.** Insect Malpighian tubules: V-ATPase action in ion and fluid transport. *J Exp Biol* 172: 417-429, 1992.

79. **Maddrell SH and Overton JA.** Stimulation of sodium transport and fluid secretion by ouabain in an insect malpighian tubule. *J Exp Biol* 137: 265-276, 1988.

80. **Masia R, Aneshansley D, Nagel W, Nachman RJ, and Beyenbach KW.** Voltage clamping single cells in intact malpighian tubules of mosquitoes. *Am J Physiol Renal Physiol* 279: F747-754, 2000.

81. **McCarthy KM, Francis SA, McCormack JM, Lai J, Rogers RA, Skare IB, Lynch RD, and Schneeberger EE.** Inducible expression of claudin-1-myc but not occludin-VSV-G results in aberrant tight junction strand formation in MDCK cells. *J Cell Sci* 113 Pt 19: 3387-3398, 2000.

82. **Misfeldt DS, Hamamoto ST, and Pitelka DR.** Transepithelial transport in cell culture. *Proc Natl Acad Sci U S A* 73: 1212-1216, 1976.

83. **Moser AJ, Giurgiu DI, Morgenstern KE, Abedin ZR, Roslyn JJ, and Abedin MZ.** Calmodulin regulation of gallbladder ion transport becomes dysfunctional during gallstone formation in prairie dogs. *Dig Dis Sci* 45: 1422-1430, 2000.

84. **Nelson N.** Evolution of organellar proton-ATPases. *Biochim Biophys Acta* 1100: 109-124, 1992.

85. **Nicolson SW.** The ionic basis of fluid secretion in insect Malpighian tubules: advances in the last ten years. *J Insect Physiol* 39: 451-453, 1993.

86. **Nicolson SW and Isaacson LC.** Transepithelial and intracellular potentials in isolated Malpighian tubules of tenebrionid beetle. *Am J Physiol* 252: F645-653, 1987.

87. **O'Donnell MJ, Dow JA, Huesmann GR, Tublitz NJ, and Maddrell SH.** Separate control of anion and cation transport in malpighian tubules of Drosophila Melanogaster. *J Exp Biol* 199: 1163-1175, 1996.

88. **O'Donnell MJ, Fletcher M, and Haley CA.** KCl reabsorption by the lower malpighian tubule of rhodnius prolixus: inhibition by Cl(-) channel blockers and acetazolamide. *J Insect Physiol* 43: 657-665, 1997.

89. **O'Donnell MJ and Maddrell SH.** Fluid reabsorption and ion transport by the lower Malpighian tubules of adult female Drosophila. *J Exp Biol* 198: 1647-1653, 1995.

90. **O'Donnell MJ and Maddrell SH.** Paracellular and transcellular routes for water and solute movements across insect epithelia. *J Exp Biol* 106: 231-253, 1983.

91. **O'Donnell MJ and Maddrell SH.** Secretion by the Malpighian tubules of Rhodnius prolixus stal: electrical events. *J Exp Biol* 110: 275-290, 1984.

92. **O'Donnell MJ, Rheault MR, Davies SA, Rosay P, Harvey BJ, Maddrell SH, Kaiser K, and Dow JA.** Hormonally controlled chloride movement across Drosophila tubules is via ion channels in stellate cells. *Am J Physiol* 274: R1039-1049, 1998.

93. **Pannabecker TL.** Physiology of the Malpighian tubule. *Annu Rev Entomol* 40: 493-510, 1995.

94. **Paul SM, Ternet M, Salvaterra PM, and Beitel GJ.** The Na+/K+ ATPase is required for septate junction function and epithelial tube-size control in the Drosophila tracheal system. *Development* 130: 4963-4974, 2003.

95. **Perachia C.** Gap junctions: molecular basis of cell communication in health and disease. In: *Current topics in membranes*, edited by Fambrough DM and Benos DJ. San Diego, CA: Academic Press, 2000.

96. **Petzel DH.** Na(+)/H(+) exchange in mosquito Malpighian tubules. *Am J Physiol Regul Integr Comp Physiol* 279: R1996-2003, 2000.

97. **Petzel DH, Berg MM, and Beyenbach KW.** Hormone-controlled cAMP-mediated fluid secretion in yellow-fever mosquito. *Am J Physiol* 253: R701-711, 1987.

98. **Petzel DH, Pirotte PT, and Van Kerkhove E.** Intracellular and luminal pH measurements of Malpighian tubules of the mosquito Aedes aegypti: the effects of cAMP. *J Insect Physiol* 45: 973-982, 1999.

99. **Phelan P.** Gap junction communication in invertebrates: the innexin gene family. In: *Gap junctions*, edited by Peracchia G. San Diego, USA: Academic Press, 2000, p. 389-422.

100. **Phelan P.** Innexins: members of an evolutionarily conserved family of gap-junction proteins. *Biochim Biophys Acta* 1711: 225-245, 2005.

101. **Phelan P, Bacon JP, Davies JA, Stebbings LA, Todman MG, Avery L, Baines RA, Barnes TM, Ford C, Hekimi S, Lee R, Shaw JE, Starich TA, Curtin KD, Sun YA, et al.** Innexins: a family of invertebrate gap-junction proteins. *Trends Genet* 14: 348-349, 1998.

102. **Phelan P and Starich TA.** Innexins get into the gap. *Bioessays* 23: 388-396, 2001.

103. **Phelan P, Stebbings LA, Baines RA, Bacon JP, Davies JA, and Ford C.** Drosophila Shaking-B protein forms gap junctions in paired Xenopus oocytes. *Nature* 391: 181-184, 1998.

104. **Pietrantonio PV and Gill SS.** Immunolocalization of the 17 kDa vacuolar H(+)-ATPase subunit c in Heliothis virescens midgut and malpighian tubules with an anti-peptide antibody. *J Exp Biol* 198: 2609-2618, 1995.

105. **Powell DW.** Barrier function of epithelia. *Am J Physiol* 241: G275-288, 1981.

106. **Pullikuth AK, Aimanova K, Kang'ethe W, Sanders HR, and Gill SS.** Molecular characterization of sodium/proton exchanger 3 (NHE3) from the yellow fever vector, Aedes aegypti. *J Exp Biol* 209: 3529-3544, 2006.

107. **Quaroni A and Hochman J.** Development of intestinal cell culture models for drug transport and metabolism studies. *Adv Drug Deliv Rev* 22: 3-52, 1996.

108. **Rheault MR and O'Donnell MJ.** Analysis of epithelial K(+) transport in Malpighian tubules of Drosophila melanogaster: evidence for spatial and temporal heterogeneity. *J Exp Biol* 204: 2289-2299, 2001.

109. **Satmary W and Bradley T.** The distribution of cell types in the Malpighian tubules of Aedes taeniorhynchus (Diptera Culicidae). *Int J Insect Morphol Embryol* 13: 209 -214, 1984.

110. **Sawyer DB and Beyenbach KW.** Dibutyryl-cAMP increases basolateral sodium conductance of mosquito Malpighian tubules. *Am J Physiol* 248: R339-345, 1985.

111. **Schneeberger EE and Lynch RD.** Structure, function, and regulation of cellular tight junctions. *Am J Physiol* 262: L647-661, 1992.

112. **Sciortino CM, Shrode LD, Fletcher BR, Harte PJ, and Romero MF.** Localization of endogenous and recombinant Na(+)-driven anion exchanger protein NDAE1 from Drosophila melanogaster. *Am J Physiol Cell Physiol* 281: C449-463, 2001.

113. **Scott BN, Yu MJ, Lee LW, and Beyenbach KW.** Mechanisms of K+ transport across basolateral membranes of principal cells in Malpighian tubules of the yellow fever mosquito, Aedes aegypti. *J Exp Biol* 207: 1655-1663, 2004.

114. **Simon DB, Lu Y, Choate KA, Velazquez H, Al-Sabban E, Praga M, Casari G, Bettinelli A, Colussi G, Rodriguez-Soriano J, McCredie D, Milford D, Sanjad S, and Lifton RP.** Paracellin-1, a renal tight junction protein required for paracellular Mg2+ resorption. *Science* 285: 103-106, 1999.

115. **Sozen MA, Armstrong JD, Yang M, Kaiser K, and Dow JA.** Functional domains are specified to single-cell resolution in a Drosophila epithelium. *Proc Natl Acad Sci U S A* 94: 5207-5212, 1997.

116. **Steele RE, Preston AS, Johnson JP, and Handler JS.** Porous-bottom dishes for culture of polarized cells. *Am J Physiol* 251: C136-139, 1986.

117. **Tang VW and Goodenough DA.** Paracellular ion channel at the tight junction. *Biophys J* 84: 1660-1673, 2003.

118. **Tepass U.** Claudin complexities at the apical junctional complex. *Nat Cell Biol* 5: 595-597, 2003.

119. **Turksen K and Troy TC.** Claudin-6: a novel tight junction molecule is developmentally regulated in mouse embryonic epithelium. *Dev Dyn* 222: 292-300, 2001.

120. **Tyrakowski T, Smuszkiewicz P, Drobnik L, Marzec M, Mlodzik-Danielewicz N, Lelinska A, and Kaczorowski P.** Effects of halothane and isoflurane on stimulated airway transepithelial ion transport. *Pharmacol Rep* 57: 550-555, 2005.

121. **Van Itallie C, Rahner C, and Anderson JM.** Regulated expression of claudin-4 decreases paracellular conductance through a selective decrease in sodium permeability. *J Clin Invest* 107: 1319-1327, 2001.

122. **Wang J, Kean L, Yang J, Allan AK, Davies SA, Herzyk P, and Dow JA.** Function-informed transcriptome analysis of Drosophila renal tubule. *Genome Biol* 5: R69, 2004.

123. **Wang S, Jayaram SA, Hemphala J, Senti KA, Tsarouhas V, Jin H, and Samakovlis C.** Septate-junction-dependent luminal deposition of chitin deacetylases restricts tube elongation in the Drosophila trachea. *Curr Biol* 16: 180-185, 2006.

124. **Weng XH, Huss M, Wieczorek H, and Beyenbach KW.** The V-type H(+)-ATPase in Malpighian tubules of Aedes aegypti: localization and activity. *J Exp Biol* 206: 2211-2219, 2003.

125. **Werle M and Hoffer M.** Glutathione and thiolated chitosan inhibit multidrug resistance P-glycoprotein activity in excised small intestine. *J Control Release* 111: 41-46, 2006.

126. **Wieczorek H, Brown D, Grinstein S, Ehrenfeld J, and Harvey WR.** Animal plasma membrane energization by proton-motive V-ATPases. *Bioessays* 21: 637-648, 1999.

127. **Williams JC and Beyenbach KW.** Differential effects of secretagogues on the electrophysiology of the Malpighian tubules of the yellow fever mosquito. *J Comp Physiol B* 154: 301-309, 1984.

128. **Wu DS and Beyenbach KW.** The dependence of electrical transport pathways in Malpighian tubules on ATP. *J Exp Biol* 206: 233-243, 2003.

129. **Wu VM and Beitel GJ.** A junctional problem of apical proportions: epithelial tube-size control by septate junctions in the Drosophila tracheal system. *Curr Opin Cell Biol* 16: 493-499, 2004.

130. **Wu VM, Schulte J, Hirschi A, Tepass U, and Beitel GJ.** Sinuous is a Drosophila claudin required for septate junction organization and epithelial tube size control. *J Cell Biol* 164: 313-323, 2004.

131. **Yu AS, Enck AH, Lencer WI, and Schneeberger EE.** Claudin-8 expression in Madin-Darby canine kidney cells augments the paracellular barrier to cation permeation. *J Biol Chem* 278: 17350-17359, 2003.

132. **Yu M and Beyenbach KW.** Leucokinin and the modulation of the shunt pathway in Malpighian tubules. *J Insect Physiol* 47: 263-276, 2001.

133. **Yu MJ and Beyenbach KW.** Effects of leucokinin-VIII on Aedes Malpighian tubule segments lacking stellate cells. *J Exp Biol* 207: 519-526, 2004.

134. **Yu MJ and Beyenbach KW.** Leucokinin activates Ca(2+)-dependent signal pathway in principal cells of Aedes aegypti Malpighian tubules. *Am J Physiol Renal Physiol* 283: F499-508, 2002.

135. **Zhang J, Feng Y, and Forgac M.** Proton conduction and bafilomycin binding by the V0 domain of the coated vesicle V-ATPase. *J Biol Chem* 269: 23518-23523, 1994.

136. **Zhang SL, Leyssens A, Van Kerkhove E, Weltens R, Van Driessche W, and Steels P.** Electrophysiological evidence for the presence of an apical H(+)-

ATPase in Malpighian tubules of Formica polyctena: intracellular and luminal pH measurements. *Pflugers Arch* 426: 288-295, 1994.

137. **Zimmermann B and Walz B.** Serotonin-induced intercellular calcium waves in salivary glands of the blowfly Calliphora erythrocephala. *J Physiol* 500 (Pt 1): 17-28, 1997.

CHAPTER 2

CULTURED MONOLAYERS OF THE DOG JEJUNUM WITH THE STRUCTURAL AND FUNCTIONAL PROPERTIES RESEMBLING THE NORMAL EPITHELIUM

Published in Am J Physiol Gastrointest Liver Physiol. 2005 Apr;288(4):G705-717
Used with permission

1. Abstract

The development of a culture of the normal mammalian jejunum motivated this work. Isolated crypt cells of the dog jejunum were induced to form primary cultures on Snapwell filters. Up to seven subcultures were studied under the electron microscope and in Ussing chambers. Epithelial markers were identified by rtPCR, western blot, and immunofluorescent staining. Confluent monolayers exhibit a dense apical brush border, basolateral membrane infoldings, desmosomes and tight junctions expressing ZO-1, occludin-1, and claudin-3 and -4. In OptiMEM medium fortified with epidermal growth factor, hydrocortisone and insulin, monolayer transepithelial voltage was -6.8 mV (apical side), transepithelial resistance was 1050 Ωcm^2, and short-circuit current (I_{sc}) was 8.1 $\mu A/cm^2$. Transcellular and paracellular resistances were estimated as 14.8 $k\Omega cm^2$ and 1.1 $k\Omega cm^2$ respectively. Serosal ouabain reduced voltage and current towards zero, as did apical amiloride. The presence of mRNA of αENaC was confirmed. Na/D-glucose cotransport was identified with an antibody to SGLT1. The unidirectional mucosa to serosa Na^+ flux (19 $nmols \cdot min^{-1} \cdot cm^{-2}$) was twice as large as the reverse flux, and net transepithelial Na^+ flux was nearly double the amiloride-sensitive short-circuit current. In plain Ringer solution, the amiloride-sensitive I_{sc} went towards zero. Under these conditions plus mucosal amiloride, serosal db-cAMP elicited a Cl^--dependent I_{sc} consistent with the stimulation of transepithelial Cl^- secretion. In conclusion, primary cultures and subcultures of the normal mammalian jejunum form polarized epithelial monolayers with 1) the properties of a leaky epithelium, 2) claudins specific to the jejunal tight junction, 3) transepithelial Na^+ absorption mediated in part by SGLT1 and ENaC, and 4) electrogenic Cl^- secretion activated by cAMP.

2. Introduction

Our understanding of transport across the intestine rests largely on the study of intestinal segments perfused in vivo, excised segments in vitro, organ cultures, epithelial cell cultures, and most recently, knock-out animal models. The details of intestinal transport mechanisms and their regulation have been elucidated most clearly in cultured intestinal cells such as Caco-2 (1, 2, 21), T-84 (27), HT-29 (24), Colo 205 (19), SW620 (52) and other epithelial cell lines derived from cancerous tissue. Only a few non-transformed cells intestinal epithelial cells are available such as the intestinal epithelial cells IEC-6 and IEC-18 derived from the normal small intestine of the rat (32, 33, 42), and the IPEC-J2 cell line established from newborn piglet jejunum (44).

In the present study we introduce a new primary culture of the normal jejunum with a focus on the method of producing that culture from crypt cells isolated from the dog jejunum. In addition, we provide a preliminary structural and functional characterization of the epithelial monolayer. Primary cultures and up to seven subcultures consistently formed confluent epithelial monolayers on Snapwell filters. The monolayers exhibit the morphological and functional polarization expected of the normal jejunum, including a prominent apical brush border. The tight junction presents claudin-3 and -4 as in the normal jejunum. The expression of ENaC and an amiloride-sensitive short-circuit current can be attributed to the presence of culture-stimulating agents (epidermal growth factor, hydrocortisone, insulin), because this current disappears in plain Ringer solution lacking culture-stimulating agents. Fortuitously, the expression of an amiloride-sensitive short-circuit current allows an estimate of the electrical resistance of transcellular and paracellular pathways. The estimates reveal a leaky epithelium with a paracellular pathway 13 times as conductive as the transcellular pathway. Measures of the unidirectional isotopic Na^+ fluxes confirmed the leaky nature of the cultured monolayers and pointed to Na^+ transport

systems in addition to that mediated by ENaC. One such transporter is the Na/D-glucose cotransporter SGLT1 identified by western blot. When electrogenic Na^+ absorption via ENaC is minimized by the use of plain Ringer solution containing mucosal amiloride, the addition of db-cAMP to the serosal side activated a Cl^- dependent short-circuit current consistent with the stimulation of transepithelial Cl^- secretion. The culture can be studied for hours in Ussing chambers, thus affording detailed investigations of jejunal transport across a single layer of epithelial jejunal cells under well-defined experimental conditions.

3. Materials and Methods

Epithelial cell isolation and culture. In general, the method to establish primary cultures from the small intestine of adult beagle dogs followed the procedures described for fetal human intestine (39). Segments of the small intestine were obtained from adult beagle dogs (1-2 years old) that were sacrificed for cardiac electrophysiological studies as described by Fox et al. (14) and approved by the Center for Research Animal Resources at Cornell University. Segments of the jejunum (30-50 cm long) were removed and placed on ice. The lumen was washed 4 times with 50 ml ice-cold sterile phosphate-buffered saline (PBS: 136.9 mM NaCl, 2.7 mM KCl, 1.5 mM KH_2PO_4, and 6.5 mM Na_2HPO_4), then filled with a 1.25% Trypsin-0.5 mM EDTA solution, clamped at the two ends, and incubated at room temperature for 10 min. The segments were then cut open longitudinally, laid flat on a sterile glass plate on ice, and the apical surface was scraped gently with a razor blade to remove mucus and most of the villi. The scrapings were discarded. Harder scraping, leaving behind only serosal layers, yielded intact crypts embedded in fragments of surrounding tissue that were collected in 50 ml centrifuge tubes containing serum-free OptiMEM (Invitrogen-GIBCO, Carlsbad, CA) supplemented with 100 U/ml penicillin, 100 μg/ml

streptomycin, and 0.25 μg/ml amphotericin B (Invitrogen-GIBCO-BRL, Antibiotic-Antimycotic solution). After centrifugation at 1000 rpm (220 G), the supernatant was discarded. The pellet was washed 3 times with serum-free OptiMEM and then incubated with serum-free OptiMEM containing 0.4 mg/ml Collagenase type IV (filter sterilized, Sigma, St. Louis, MO) at 37 ^{o}C for 45-60 min, with gentle and brief shaking every 10-15 min. The dissociated epithelial cells were spun down at 1000 rpm (220 G) and washed 5 times with 40 ml of 10% fetal bovine serum (FBS, Hyclone Labs, Logan, UT) in Dulbecco's Modified Eagle medium (DME) supplemented with Antibiotic-Antimycotic solution. After each centrifugation at 1000 rpm, the pellet was resuspended by pipetting up and down vigorously using a 10 ml wide-bore Falcon pipette (Milian USA, Gahana, OH). The final pellet was suspended in 100-250 ml "fortified OptiMEM" (*vide infra*). After allowing large fragments to sediment within 1-2 min, the upper 2/3 of the suspension was plated in 100 mm diameter dishes coated with extracellular matrix ECL (Upstate Biotechnology, Lake Placid, NY) and incubated at 37 ^{o}C and 6% CO_2.

For the culture of monolayers and for their initial physiological characterization we used "fortified OptiMEM" which we define as serum-free OptiMEM supplemented with 10 mM HEPES pH 6.5, 2.5 mM glutamine, 50 U/ml penicillin, 50 μg/ml streptomycin, 2 mM GlutaMAX-I (Invitrogen-GIBCO-BRL), 20 ng/ml epidermal growth factor (human recombinant, Upstate Biotechnology), 150 nM hydrocortisone 21-hemisuccinate sodium salt (Sigma), 10 μg/ml insulin (human recombinant, Sigma), and 4% FBS. After 3 hrs, fortified OptiMEM was aspirated and the attached cells (consisting almost exclusively of intact or large portions of crypts) were rinsed 4 times and refed with fortified OptiMEM and incubated at 37 ^{o}C. After 24 hrs the incubator temperature was changed to 32-34 ^{o}C for the rest of the culture period.

After the primary cultures had grown in 100 mm diameter dishes, between 300,000 and 400,000 cells in 0.5 ml fortified OptiMEM were subcultured onto Snapwell permeable filters (insert growth area 1.13 cm^2, 0.4 μm pore size, Costar, Cambridge, MA) and incubated at 32 ^oC and 6% CO_2 to form DIEC monolayers.

We evaluated the growth of DIEC monolayers by visual inspection under the microscope (Nikon Diaphot) and by daily measurements of the resistance across the filter area with a hand-held Millicell-ERS volt- and ohmmeter (Millipore, Billerica, MA). Since this resistance measurement (between two points with heterogeneous current distribution) is meant to monitor culture growth to confluence we call this resistance 'growth area resistance' (Fig. 2.4e). For measurements of the transepithelial resistance under more homogeneous conditions of transepithelial current distribution, we used current-voltage plots measured across confluent monolayers in the Ussing chamber.

Immunocytochemistry. Cells of primary cultures or passages 1 to 3 were washed 3 times with PBS, fixed with 3% formaldehyde and then directly processed for immunofluorescence staining or permeabilized by one of two methods: 1) incubation with acetone:methanol 1:1 at -20 ^oC for 10 min; or 2) lysis with 0.2 % Triton X-100 in PBS for 2 min at room temperature. Further processing steps are described by Tian and Quaroni (49). The secondary antibodies were FITC- or rhodamine-conjugated goat anti-mouse or donkey anti-rabbit IgG (Boehringer Manheim, Indianapolis, IN) diluted 1:25 in PBS plus 2% bovine serum albumin (BSA). Cells were counterstained with 0.01 % Evans blue and 2 μg/ml DAPI for 2 min. After antibody incubation and washing, the cells were mounted in glycerol:PBS (9:1) and 2.5% 1,4-diazabicyclo-[2.2.2] octane and covered with coverslips. Stained cells were examined with a Zeiss Axiovert 10 microscope equipped with epifluorescence optics and Optronics 3 chip

CCD camera. Digital images were processed with Adobe Photoshop software. We used the following primary antibodies: 1) CY-90 (Sigma) against keratin #18, mouse monoclonal, diluted 1:400; 2) anti desmosomal protein, mouse monoclonal (Sigma), diluted 1:400; 3) anti human occludin, mouse monoclonal, OC-3F10 (Zymed Cat # 33-1500), diluted 1:1000; 4) anti claudin-1, rabbit polyclonal (Zymed, JAY.8, Cat # 51-9000), diluted 1:1000; 5) anti claudin-2, rabbit polyclonal, (Zymed, MH44, Cat # 51-6100), diluted 1:1000; 6) anti claudin-3, rabbit polyclonal, (Zymed, Z23.JM, Cat # 34-1700), diluted 1:1000; 7) anti claudin-4, mouse monoclonal (Zymed, 3E2C1, Cat # 32-9400), diluted 1:2000; 8) anti claudin-5, rabbit polyclonal (Zymed, rabbit Z43.JK, Cat # 35-2500), diluted 1:1000; and 9) anti claudin-5, mouse monoclonal (Zymed, 4C3C2, Cat # 34-1600), diluted 1:2000.

Cells were processed for transmission and scanning electron microscopy as previously described (41).

Western blot. Total cell lysates solubilized in SDS-PAGE sample buffer were subjected to SDS-PAGE and western blot as described previously (49). The DNA concentration was determined using the Hoechst 33258 DNA assay and a mini-fluorometer (Hoefer, Pharmacia Biotech, Piscataway, NJ). The amount of cell lysate applied to each well was normalized to DNA (39). Lysates obtained from 0.2 million cells/sample were subjected to SDS-PAGE on a 7.5-10% acrylamide gel. The proteins were transferred onto a nitrocellulose membrane (High-bond nitrocellulose, Amersham Life Science, Arlington Heights, IL) using a transblot system (BioRad, Hercules, CA) at 100 volts and 5 ^{o}C for 90 min. The membranes were then blocked in PBST (80 mM Na_2HPO_4, 20 mM $NaH_2PO_4 \bullet 2H_2O$, 100 mM NaCl, and 0.1% Tween-20) containing 3% BSA at 4 ^{o}C overnight. Incubation with antibodies, washing, protein detection, antibody stripping and reprobing were performed according to the

ECL-Plus western blotting protocol from Amersham Life Science. Blots were scanned with a Molecular Dynamics Storm 840 scanner (Amersham Pharmacia Biotech, Sunnyvale, CA) in the fluorescence mode. In other experiments we employed fluorescent secondary antibodies and the Li-COR Odyssey Infrared Imaging System (Lincoln, NE). After transfer of the proteins to Hybond-P/ PVDF membrane (Amersham Pharmacia Biotech) and blocking for 4 hr in Odyssey Blocker, incubation with primary antibodies was done in Odyssey Blocker containing 0.1% Tween-20 overnight at 4 ^{o}C. After 4 washes with Tris buffered saline (TBS: 20 mM Tris base, 137 mM NaCl, pH 6) containing 0.1 % Tween-20, the blots were incubated with Alexa Fluor680 goat anti-mouse IgG (1:2500 dilution in Odyssey Blocker, 0.1% Tween-20) for 1 hr at room temperature and shielded from light. After washing, the blots were scanned in the Odyssey Infrared scanner. The primary antibodies used are the same as listed above.

In a separate experiment, the presence of the sodium glucose cotransporter (SGLT1) in DIEC cell lysates was examined by western blot with an antibody specific to rabbit SGLT1. In these studies, SDS-PAGE and the transfer of protein from gel to PVDF membrane was done as described previously (55). After the membrane was incubated for 2 hrs in blocking solution consisting of TBST (20 mM Tris-HCl, 137 mM NaCl, 0.1% Tween, pH 7.6) fortified with 3% BSA, the membrane was then treated for 2 hrs with antibody diluted in TBST plus 1% BSA (1: 1,000). To verify immunoreactivity of SGLT1, the antibody 8821 was first preincubated with 0.5 μg/ml of the immunizing peptide for 2 hrs, which yielded a negative western blot. Both antibody 8821 and immunizing peptide were the gift of Dr. E.M. Wright's (UCLA). The antibody 8821 has been used successfully in the past in investigations of SGLT1 in the dog jejunum in vivo (22).

Electrophysiological studies in Ussing chambers. Electrophysiological measurements were performed on DIEC monolayers mounted in Ussing chambers (CHM5, World Precision Instruments, Sarasota, FL). Monolayers of passage 1 through 7 were studied. Finding consistent electrophysiological properties among them, we did most experiments on passages 1 to 3.

In most transport experiments fortified OptiMEM (10 ml) was present on both sides of the epithelium. Using the methods of atomic absorption spectrophotometry, flame photometry, and coulometry we measured the following partial composition of the OptiMEM culture medium: [Na^+], 157.0 ± 3.7 mM (n = 3); [K^+], 4.6 ± 0.3 mM (n = 3); [Cl^-], 123.7 ± 4.7 mM (n = 3); and protein, 0.56 ± 0.01 mg/ml. According to the manufacturer of OptiMEM culture medium, the glucose concentration is 13.9 mM (personal communication); other ingredients of OptiMEM culture medium are proprietary information.

In experiments examining the ion dependence of the measured short-circuit current, confluent monolayers were taken from their cultures in fortified OptiMEM and mounted in plain Ringer solution lacking culture-stimulating agents. Plain Ringer solution contained in mM: NaCl 120, KCl 5, $NaHCO_3$ 25, $CaCl_2$ 1.2, $MgCl_2$ 1.2, glucose 5, pH 7.3. Low Cl^- Ringer was prepared by replacing 116.8 mM NaCl with Na-isethionate. Glucose-free Ringer solution contained no glucose.

Mucosal and serosal solutions were circulated at a rate of 0.2 ml/sec by air-lifting with 95% O_2 and 5% CO_2. The pH was maintained between 7.35 and 7.38. The temperature was maintained at 32 ^oC with a water bath (Neslab Instruments, Portsmouth, NH). For voltage and current recording we used the multi-channel voltage/current clamp of World Precision Instruments (EVC-4000) and Ag/AgCl voltage/current electrodes embedded in 4% agar and 150 mM NaCl. Voltage and current were measured with respect to ground in the serosal compartment. To

measure the transepithelial resistance, we clamped monolayers at 5mV voltage steps from –20 mV to +20 mV for 5 seconds each and recorded the transepithelial current. The transepithelial resistance (R_t) was calculated as the inverse of the slope of the I-V plot.

After mounting the DIEC monolayers in the Ussing chamber the transepithelial voltage (V_t) was monitored for about 20-30 min until V_t had became stable. Thereafter the bath temperature was gradually increased to 38 ^oC for the next 5 min. The short-circuit current (I_{sc}) was measured at a transepithelial voltage clamp of 0 mV. After I_{sc} had stabilized after about 10 min, experiments were begun. Amiloride (Merck & Co., Whitehouse Station, NJ) was applied to the mucosal or serosal side. The effect of mucosal amiloride concentration on electrical variables was examined in detail since serosal amiloride had no effect. Ouabain and dibutyryl adenosine 3',5'-cyclic monophosphate (db-cAMP) were purchased from Sigma (St. Loius, MO) and presented from the serosal side only. Amiloride and ouabain were dissolved in DMSO, and stored as stock solutions at 1000 times their final concentration in the experiment. The experimental DMSO concentration of 0.1 % had no effect on measured electrical variables.

Transepithelial Na^+ flux measurements. We used $^{22}Na^+$ (Amersham Biosciences, Piscataway, NJ) to measure unidirectional Na^+ fluxes across DIEC monolayers. Radioactivity in known and unknown samples was measured with a Beckman gamma counter (Gamma 300). In the typical isotopic flux experiment the DIEC monolayer was mounted in the Ussing chamber and bathed with fortified OptiMEM on both sides. After V_t had reached steady state at 38 ^oC, the monolayer was voltage clamped at 0 mV and maintained in the short circuit condition for the rest of the experiment. To begin, 10 μCi of $^{22}Na^+$ was added to the mucosal or serosal side. At intervals of 10

min, 1 ml of sample solution was taken from the other side for the measurement of $^{22}Na^{+}$ that had crossed the DIEC monolayer. The counted sample was then returned to the side from where it had been taken. After the 40 min flux period, amiloride (10 μM) was added to the mucosal solution and the flux measurements were repeated, again under short-circuit conditions.

When 1 ml was removed from 10 ml of apical or basolateral solution, the water column dropped by 0.4 cm of water, i.e. 1.5%. The transepithelial hydrostatic pressure difference thus introduced did not cause measurable transepithelial water flows, as water levels remained constant. Moreover, there were no transepithelial streaming potentials, and no effects on short-circuit current and transepithelial resistance. The unidirectional isotopic Na^{+} flux from mucosa to serosa was measured in one set of DIEC monolayers and the reverse flux in another set. Accordingly, the net transepithelial Na^{+} flux is the difference between values of two experimental groups.

rtPCR of dog jejunal αENaC mRNA. Total RNA was extracted from DIEC monolayers at the 3rd passage by CsCl banding as described by Kinston (28). The integrity of RNA was verified by agarose gel electrophoresis and ethidium bromide staining and its quantity was determined spectrophotometrically.

For rtPCR, 1 μl of RNA (1.55 μg/μl) sample was used. The mRNA was reverse-transcribed to cDNA and further amplified by PCR reactions (SuperScriptTM III One-Step RT-PCR System, Invitrogen, Carlsbad, CA). The 25 μl reaction mixture for rtPCR included 12.5 μl of 2X reaction buffer, 1 μl total RNA sample, 1 μl forward primer (10 μM), 1 μl reverse primer (10 μM), 1 μl RT/Taq enzymes mixture, and 8.5 μl H_2O. The first cDNA strands were reverse-transcribed at 52 ^{o}C for 30 min. After denaturing at 94 ^{o}C for 2 min, the cDNA strands were amplified by PCR reactions for

40 cycles. Each cycle entailed incubation at 94 ^{o}C for 15 s, then 52 ^{o}C for 30 s, and 72 ^{o}C for 45 s. Finally, the DNA strands were extended at 72 ^{o}C for 5 min. During the reactions, the following primers were used: αENaC (forward): 5'-AACCTGCCTTTATGGACGAT-3' and αENaC (reverse): 5'-AGGTTGGACAGGAGGGTGAC-3'.

To identify the PCR product, 10 µl of the PCR product was mixed with 2 µl 6X DNA loading buffer (0.25% bromophenol blue, 0.25% xylene cyanol FF, 15% Ficoll in H_2O), applied to 1.5% agarose gel dissolved in 1X TAE buffer (40 mM Tris-acetate, 1 mM EDTA) and separated under 100 V with a horizontal elctrophoresis apparatus (MINI SUB^{TM} DNA CELL, BioRad). The PCR product was purified and submitted for sequencing with the αENaC forward primer to the Bioresource Center of Cornell University.

Statistics. All data are presented as mean ± standard error of the mean. The paired Student t-test was used for the significant difference ($P<0.05$) between control and experimental groups, while the z-test was used for the significant difference between a specific data and a group mean value ($P<0.05$).

4. Results

Cell proliferation and differentiation in primary and secondary cultures. In the present study we produced 17 primary cultures of DIEC. Some primary cultures were taken to up to 7 passages before they lost proliferative activity. As long as the cells could be subcultured, they retained the ability to form confluent monolayers with similar morphological and electrophysiological properties.

While the culture steps producing DIEC is straight forward and reliable, a few steps proved particularly important. First, it was crucial to start cultures with intact or

nearly intact crypts, because isolated epithelial cells or fully differentiated villus cells did not attach to the substrate, nor did they survive for more than 2-3 days. As illustrated in Fig. 2.1a, essentially intact crypt cells have attached to the substrate after only 4 hrs of incubation, and cells at the border of the cluster have started to spread out and migrate. The use of ECL-coated dishes improved significantly (2-3 fold) the number of crypt cells attaching to substrate, but ECL-coated dishes were not essential as qualitatively similar results were obtained with uncoated dishes. Non-epithelial cells, large tissue fragments, and clumps of villus cells did not adhere strongly and were washed out. Proliferative (mitotic) cells could be detected by staining mitotic apparatuses with anti-tubulin antibodies after only one night of incubation. However, mitotic apparatuses were relatively rare and flat and therefore difficult to detect by direct examination of unstained cultures.

Fig. 2.1b shows that the crypt cells had spread out entirely to occupy a much larger surface after one day. The staining of these cultures with anti-keratin antibodies confirmed the epithelial nature of all, or nearly all cells (> 99.9% in 12 samples) present in these primary cultures (Fig. 2.1c). Contamination by fibroblasts and other cell types was negligible. Staining with a monoclonal antibody (TS23) specific for a glycosylated form of Notch-1 expressed in human and rat intestinal stem cells (Quaroni and Beaulieu, submitted) indicated the presence of a subpopulation of stem cells in the primary cultures (Fig. 2.1d).

A second crucial step proved to be temperature control. When cultures were maintained at 37 °C, they remained viable for at least 3-4 weeks, but cell proliferation ceased entirely after one week. In contrast, when cultures were grown at 32-34 °C starting on day 2, regions containing rapidly proliferative cells became evident after 3 to 4 days (see asterisk, Fig. 2.1e). Proliferative cells incorporated bromodeoxyuridine, demonstrating rapid cell division and expansion in the cell population (Fig. 2.1f).

Figure 2.1. Primary cultures of dog intestinal (jejunal) epithelial cells (DIEC) grown in fortified OptiMEM: a) Crypt cells attach to the ECL-coated dish 4 hrs after seeding and wash-out of non-attached cells; b) same culture as in (a) 1 day later. Epithelial cells have now attached and spread out without a significant increase in the number of cells; c) 1 day-old culture stained with an immunofluorescent antibody to keratin, demonstrating the epithelial nature of the culture; d) 1 day-old culture stained with a monoclonal antibody specific to the glycosylated form of Notch-1, identifying crypt stem cells; e) 7 day-old culture maintained at 35 °C, illustrating the presence of clusters of small proliferative cells (asterisk) among older and larger non-proliferative cells; f) same culture as in (e) incubated with BrdU for 24 hrs to visualize proliferative cells (green-blue). BrdU incorporated into cellular DNA was visualized by immunofluorescence staining. Bar = 25 microns in all frames.

Provided by Dr. A. Quaroni

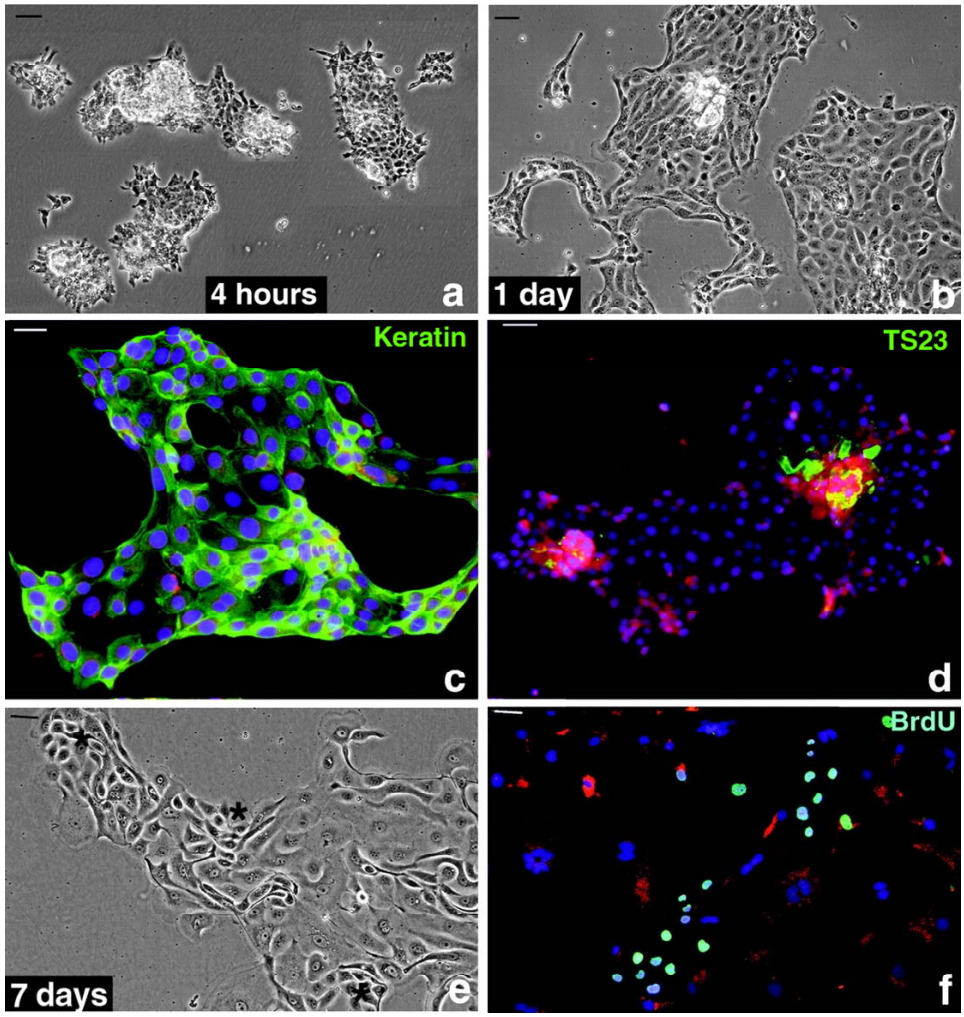
4 hours
a
1 day
b
Keratin
c
TS23
d
7 days
e
BrdU
f

Older, non-proliferative cells became enlarged and apoptotic after about 2 weeks. By that time, the smaller proliferative cells represented the main cell type that could also be serially passaged. We have estimated a population doubling time to be 18-27 hrs in 9 cultures. Proliferative cells could be readily subcultured at least 6 times yielding epithelial cells that were characterized and used in all subsequent studies. We have called these cells 'Dog Intestinal Epithelial Cells' (DIEC).

When confluent, DIEC maintained a typical epithelial morphology and formed tightly confluent DIEC monolayers with frequent, obvious domes when grown on solid (plastic) support, indicating transepithelial ion and water transport in the direction of absorption. The presence of tight junctions could be readily demonstrated by microscopic studies and by western blotting with antibodies to junctional proteins. As illustrated in Fig. 2.2a, of the 5 claudins examined only claudin-3 and -4 were detected in primary (P), 1st, and 2nd passage cultures. In some experiments, small amounts of claudin-1 were also seen. Another tight junction protein, occludin-1, could also be identified by western blot (Fig. 2.2a). Claudin-2 and claudin-5 were not detected in any primary culture or passage. In these experiments, β-tubulin was used as a loading control (Fig. 2.2a).

Immunostaining of primary or secondary cultures localized the expressed junctional proteins to the paracellular pathway. Occludin-1 appeared in a discrete pericellular band as expected from its association with tight junctions (Fig. 2.2b). Likewise, ZO-1 was distributed in a pattern consistent with its presence in tight junctions (Fig. 2.2c). The distribution of claudin-3 and claudin-4 was more diffuse than that of occludin and ZO-1. Claudin-4 and claudin-3 (not shown) appeared to expand

Figure 2.2. Expression of paracellular proteins in dog intestinal epithelial cells (DIEC) grown in fortified OptiMEM. a) Claudins-3 and -4, and occludin-1 were detected by western blot in cell lysates derived from primary cultures (P) and 1st and 2nd passages of DIEC; b) occludin-1 (green); the arrow points to a cell undergoing mitosis; c) zonula occludens-1 (green); d) claudin-4 (green); e) desmosomes (green). The tight junction proteins occludin-1, ZO-1, and claudin-4 were visualized in DIEC of the second passage. Bar = 25 microns in all frames.

Provided by Dr. A. Quaroni

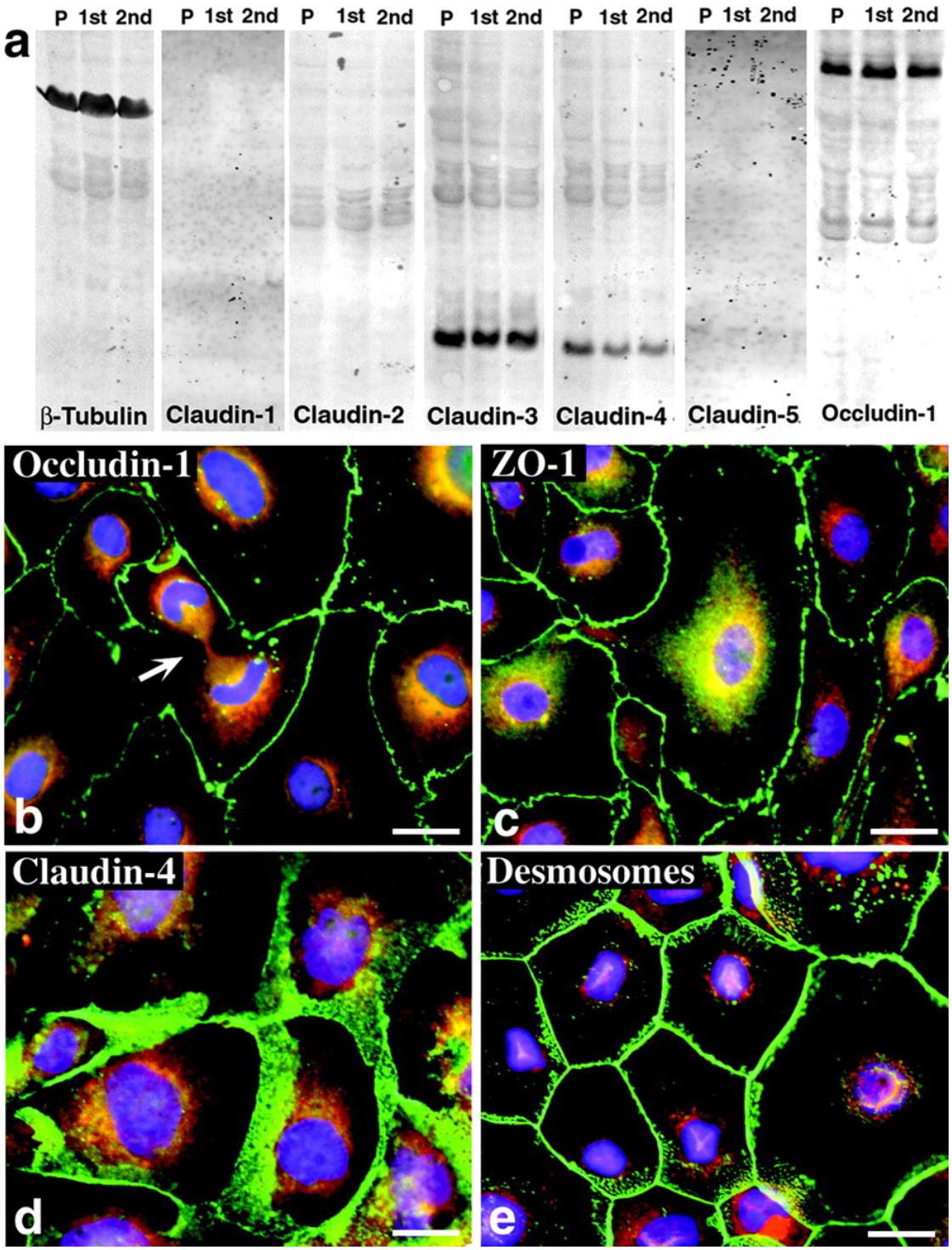
a
P 1st 2nd
β-Tubulin
Claudin-1
Claudin-2
Claudin-3
Claudin-4
Claudin-5
Occludin-1
Occludin-1
b
ZO-1
c
Claudin-4
d
Desmosomes
e

well beyond tight junctions (Fig. 2.2d). The distribution of desmosomes outlines again the paracellular space of confluent epithelial cells (Fig. 2.2e).

Electron microscopy. When DIEC were cultured in plastic dishes in the presence of fortified OptiMEM, both primary cultures and subcultures formed monolayers with the basolateral membrane adhering to the substrate and microvilli on the apical membrane facing the culture medium (Fig. 2.3a). Next to this polarization, transmission electron micrographs revealed extensive infoldings of the basolateral membrane (Fig. 2.3 b,d,e), tight junctions near the apical border (Fig. 2.3d), and desmosomes near the serosal border (Fig. 2.3e). Some cells of the DIEC monolayers contain granules in the apical cytoplasm, possibly identifying primitive goblet cells (Fig. 2.3 a-c). Our attempt to identify goblet cells with antibodies to mucin did not succeed as the rat and human antibodies apparently did not recognize mucin in the dog. Cells without granules are probably epithelial cells with the properties of transepithelial transport.

Scanning electron micrographs of primary and secondary cultures grown on plastic support for 10 days revealed epithelial cells with sparse apical microvilli (Fig. 2.4 a,b). Adjacent epithelial cells overlap, hiding their tight junctions below their lateral edges. In contrast, cultures grown on Millicell HA filters or Snapwells yielded taller cells with a prominent brush border (Fig. 2.4 c,d). DIEC monolayers of this type were used in the transport studies described below.

Daily measurements of the electrical resistance across the insert growth area revealed an exponential rise in resistance as DIEC monolayers become confluent (Fig. 2.4e). After 3 to 4 days the electrical resistance increased sharply, reaching peak resistances 6 to 7 days after seeding the culture. Thereafter, resistance decreased together with increasing variability. In view of the transient nature of the

Figure 2.3. Ultrastructure of DIEC monolayers (second passage) grown on Millicell HA filters in fortified OptiMEM. a,b) Monolayer of polarized epithelial cells. Granule-containing cells (arrows) may be pre-goblet cells; c) granules in the apical cytoplasm at higher magnification; d) tight junctions (arrow) and basolateral membrane infoldings (asterisk) of two neighboring epithelial cells; e) desmosomes (arrow) in the lower lateral interstitial space near the serosal border and basolateral membrane infoldings (asterisk). Images a-c were selected to illustrate the presence of two cell types, granulated and non-granulated cells. Other areas of the DIEC monolayers were devoid of granulated cells.

Provided by Dr. A. Quaroni

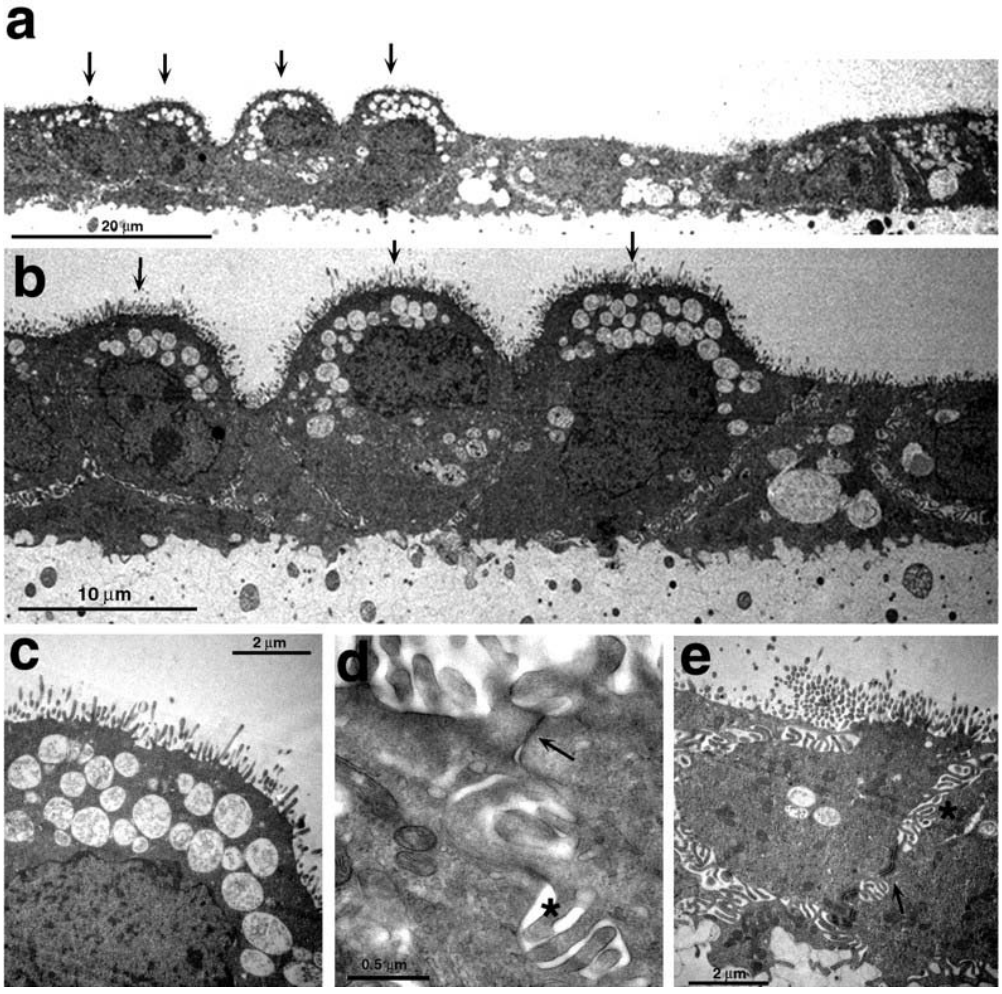
a
20 µm
b
10 µm
c
2 µm
d
0.5 µm
e
2 µm

Figure 2.4. Scanning electron micrograph of DIEC monolayers grown in fortified OptiMEM at 34 °C on plastic dishes (a,b) and on Millicell HA filters (c, d). Monolayers grown on plastic are flat with a sparse apical layer of microvilli, while monolayers on Millicell HA filters are tall and covered with a dense brush border. e) Electrical resistance as a measure of DIEC growth to confluence in fortified OptiMEM. Resistance was measured daily across cultures grown on Millicell HA filters and Snapwells. DIEC monolayers were confluent 6 to 7 days after seeding crypt cells.

Provided by Dr. A. Quaroni

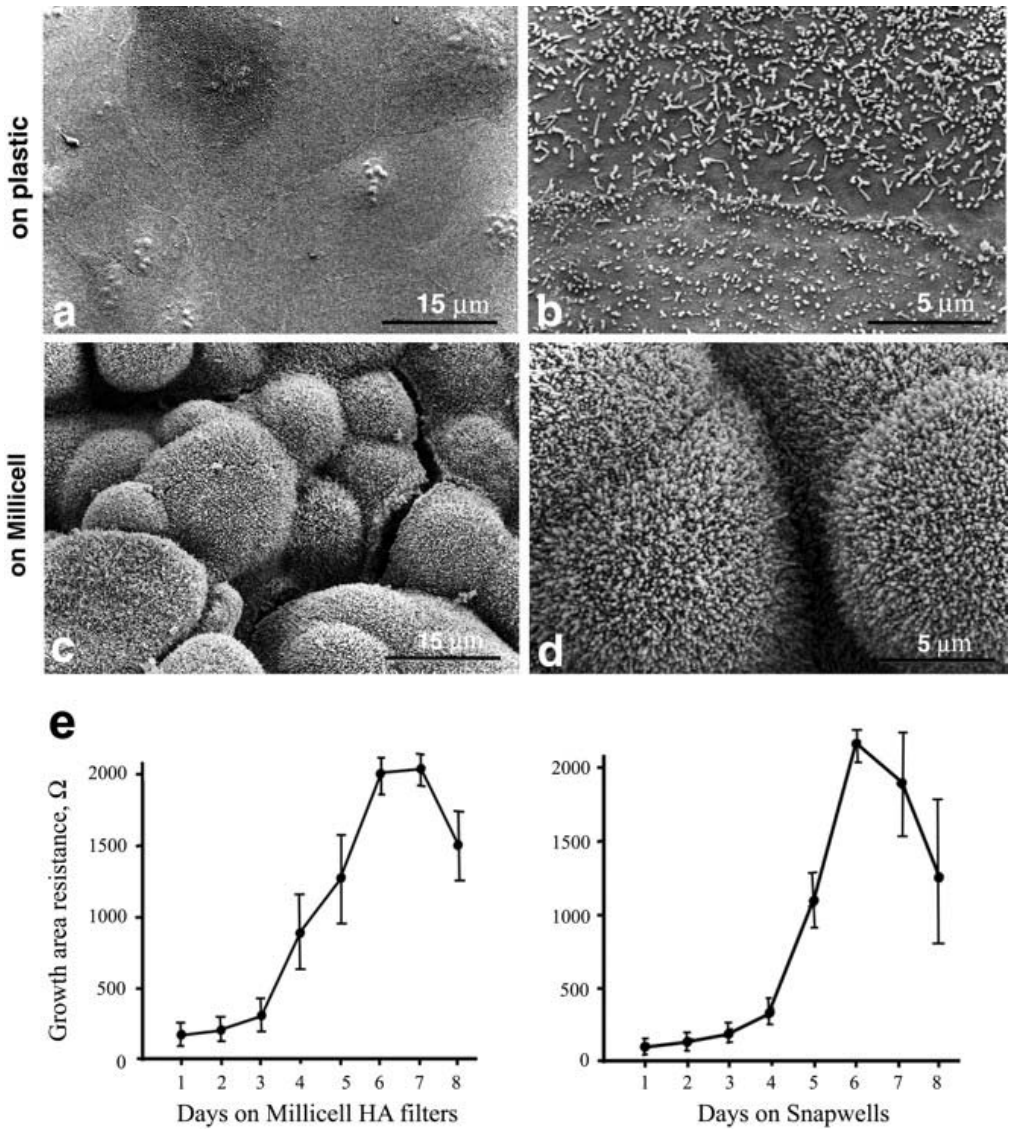
on plastic
on Millicell
a
15 µm
b
5 µm
c
15 µm
d
5 µm
e
Growth area resistance, Ω
2000
1500
1000
500
0
1 2 3 4 5 6 7 8
Days on Millicell HA filters
2000
1500
1000
500
0
1 2 3 4 5 6 7 8
Days on Snapwells

transepithelial resistance, we confined our study or transepithelial transport in Ussing chambers to monolayers between 4 and 6 days old.

Electrophysiology of DIEC monolayers in fortified OptiMEM culture medium. Primary cultures of DIEC were not studied. Instead, our electrophysiological observations focused largely on confluent DIEC monolayers of the first, second, and third passage after noting no major differences with subsequent passages. Monolayers showing signs of apoptosis or degeneration were not used in electrophysiological studies. Under control conditions in fortified OptiMEM containing culture-stimulating agents (epidermal growth factor, hydrocortisone and insuin), the DIEC monolayers had an open circuit voltage (V_t) of -6.8 ± 0.6 mV (n = 36) with a range from -2.0 to -14.4 mV, apical side negative. Apical side positive voltages were never observed. The transepithelial resistance (R_t) was 1050 ± 105 Ωcm^2 on average with a range from 429 to 2173 Ωcm^2 (n = 22). When DIEC monolayers were voltage clamped at 0 mV, the short-circuit current (I_{sc}) was 8.1 ± 0.4 $\mu A/cm^2$ (n = 36) with positive current flowing from the apical to the basolateral side. The short-circuit current ranged from 5.3 to 13.3 $\mu A/cm^2$.

Amiloride-sensitive short-circuit current and expression of ENaC in DIEC monolayers grown and studied in fortified OptiMEM culture medium The effects of amiloride were studied in the presence of fortified OptiMEM (Fig. 2.5). The control transepithelial voltage V_t was -3.6 ± 0.4 mV (n=10), the transepithelial resistance R_t was 694 ± 72 Ωcm^2 (n=7), and the short-circuit current I_{sc} was 8.4 ± 0.6 $\mu A/cm^2$ (n=10; Fig. 2.5a). After amiloride (10 μM) was added to the apical side, V_t dropped immediately and significantly to -0.7 ± 0.2 mV ($P< 0.001$), and I_{sc} significantly decreased to 1.3 ± 0.4 $\mu A/cm^2$ ($P<0.001$, Fig. 2.5a). The inhibitory effects of amiloride

Figure 2.5. Effect of amiloride on transepithelial electrical variables of DIEC monolayers in fortified OptiMEM: a) Amiloride (10 μM) applied to the mucosal solution significantly inhibited transepithelial voltage (V_t) and the short-circuit current (I_{sc}) without an effect on the transepithelial resistance (R_t); b) amiloride applied to the serosal solution had no effect. * $P < 0.001$.

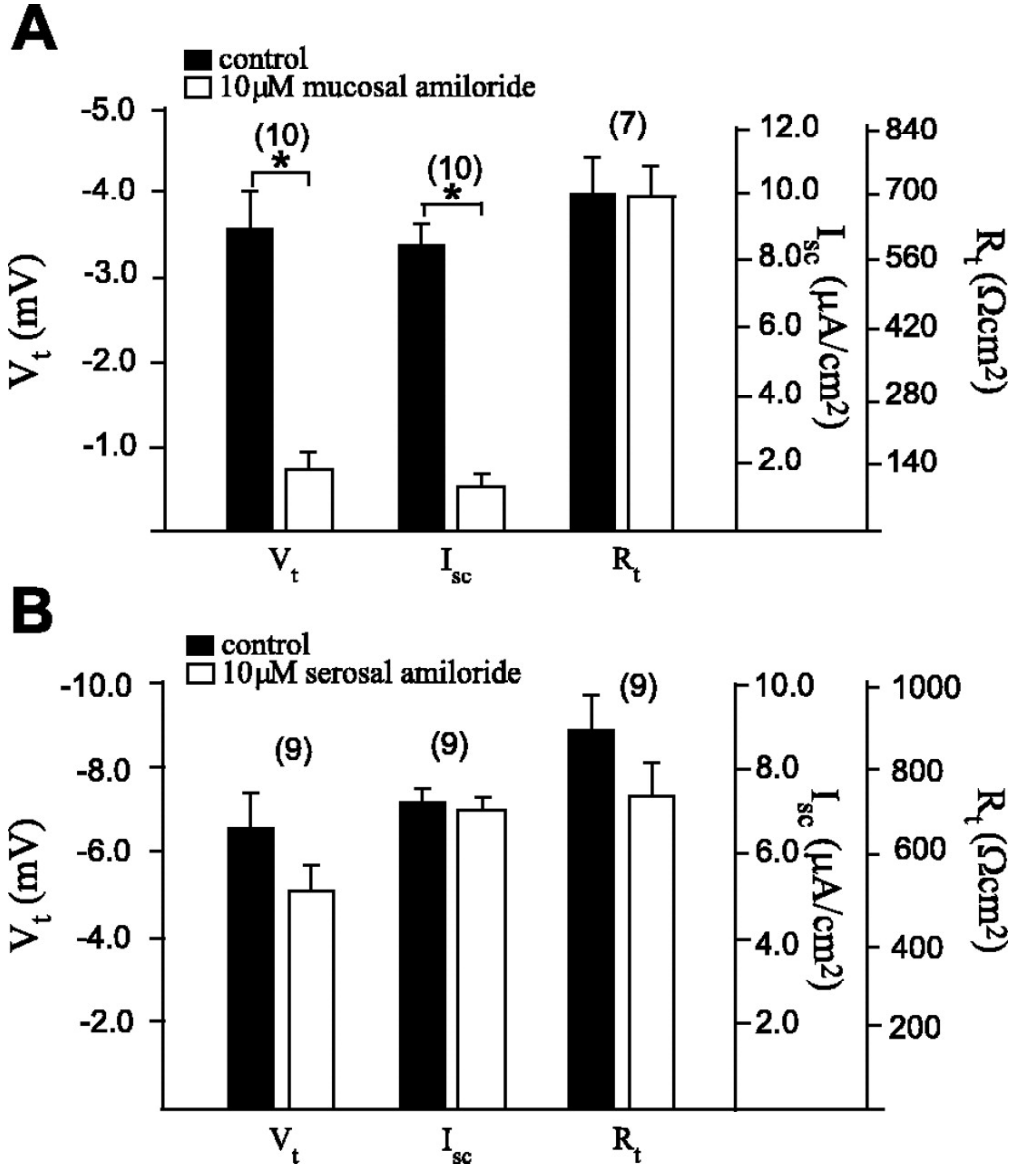
A
control
10μM mucosal amiloride
-5.0
-4.0
-3.0
-2.0
-1.0
(10)
(10)
(7)
*
*
12.0
10.0
8.0
6.0
4.0
2.0
840
700
560
420
280
140
V_t (mV)
I_{sc} (μA/cm^2)
R_t (Ωcm^2)
V_t
I_{sc}
R_t
B
control
10μM serosal amiloride
-10.0
-8.0
-6.0
-4.0
-2.0
(9)
(9)
(9)
10.0
8.0
6.0
4.0
2.0
1000
800
600
400
200
V_t (mV)
I_{sc} (μA/cm^2)
R_t (Ωcm^2)
V_t
I_{sc}
R_t

were immediate, requiring 1 to 2 sec to reach full effect. Even though amiloride significantly inhibited the transepithelial voltage and short-circuit current, it had no significant effect on transepithelial resistance which was 694 ± 72 Ωcm^2 under control conditions and 687 ± 62 Ωcm^2 (n=7) in the presence of amiloride (Fig. 2.5a).

A consistent observation was the subsequent decrease of R_t in the presence of amiloride. After amiloride had inhibited V_t and I_{sc} within 1-2 sec of application, these two variables remained unchanged in the presence of amiloride. In contrast, about 10-20 min later, R_t began to decrease gradually yet significantly, dropping to 81.3 ± 4.3 % ($P<0.001$) of control. The nature of this resistance drop was beyond the scope of the preliminary electrophysiological characterization of DIEC monolayers.

Amiloride (10 μM) added to the basolateral solution had no significant effect on V_t, R_t and I_{sc} (Fig. 2.5b). In these nine DIEC monolayers the control V_t was -6.6 ± 0.8 mV, the R_t was 887 ± 82 Ωcm^2, and the I_{sc} was 7.2 ± 0.3 $\mu A/cm^2$. After adding amiloride to the serosal side, V_t decreased to -5.1 ± 0.6 mV, R_t decreased to 731 ± 80 Ωcm^2, and I_{sc} decreased to 7.0 ± 0.3 $\mu A/cm^2$. None of these changes was significant.

We also examined the effect of amiloride on V_t, I_{sc} and R_t at 32 ^oC, the temperature at which monolayers were cultured. At this temperature, 10 μM amiloride added to the apical side of the monolayer inhibited V_t and I_{sc}, again with no effects on R_t (data not shown).

Fig. 2.6a shows linear current/voltage relationship (I-V plot) measured across DIEC monolayers in the absence and presence of amiloride. The slope of the I-V plots is the transepithelial conductance ($1/R_t$) and the Y-intercept is the short circuit current (I_{sc}). Apical amiloride (10 μM) significantly reduced the short circuit current from 7.5 ± 0.3 $\mu A/cm^2$ to 0.9 ± 0.2 $\mu A/cm^2$ ($P<0.001$) without affecting transepithelial conductance (1.49 and 1.42 mS/cm^2 before and after amiloride, respectively). Significant effects on V_t and I_{sc} but not on R_t suggest that the paracellular conductance

Figure 2.6. Effect of apical amiloride on transepithelial electrical variables of DIEC monolayers in fortified OptiMEM: a) Linear current/voltage plots in the absence and presence of amiloride (10 μM). Amiloride reduces the transepithelial current without affecting the transepithelial conductance. A significant short-circuit current remains at the short-circuit voltage of 0 mV at an amiloride concentration of 10 μM. Data are mean ± SE of 7 monolayers; b) concentration-response curve of the effect of amiloride on the short-circuit current I_{sc}. The amiloride concentration at half maximal inhibition (IC_{50}) is 0.76 μM. No significant short-circuit current remains at the amiloride concentration of 100 μM. V_c, voltage clamp; I_c, clamp current. c) Expression of αENaC mRNA in DIEC monolayers grown in fortified OptiMEM. The 547 base pair cDNA sequence of α-ENaC localized at the expected size of the amplified sequence.

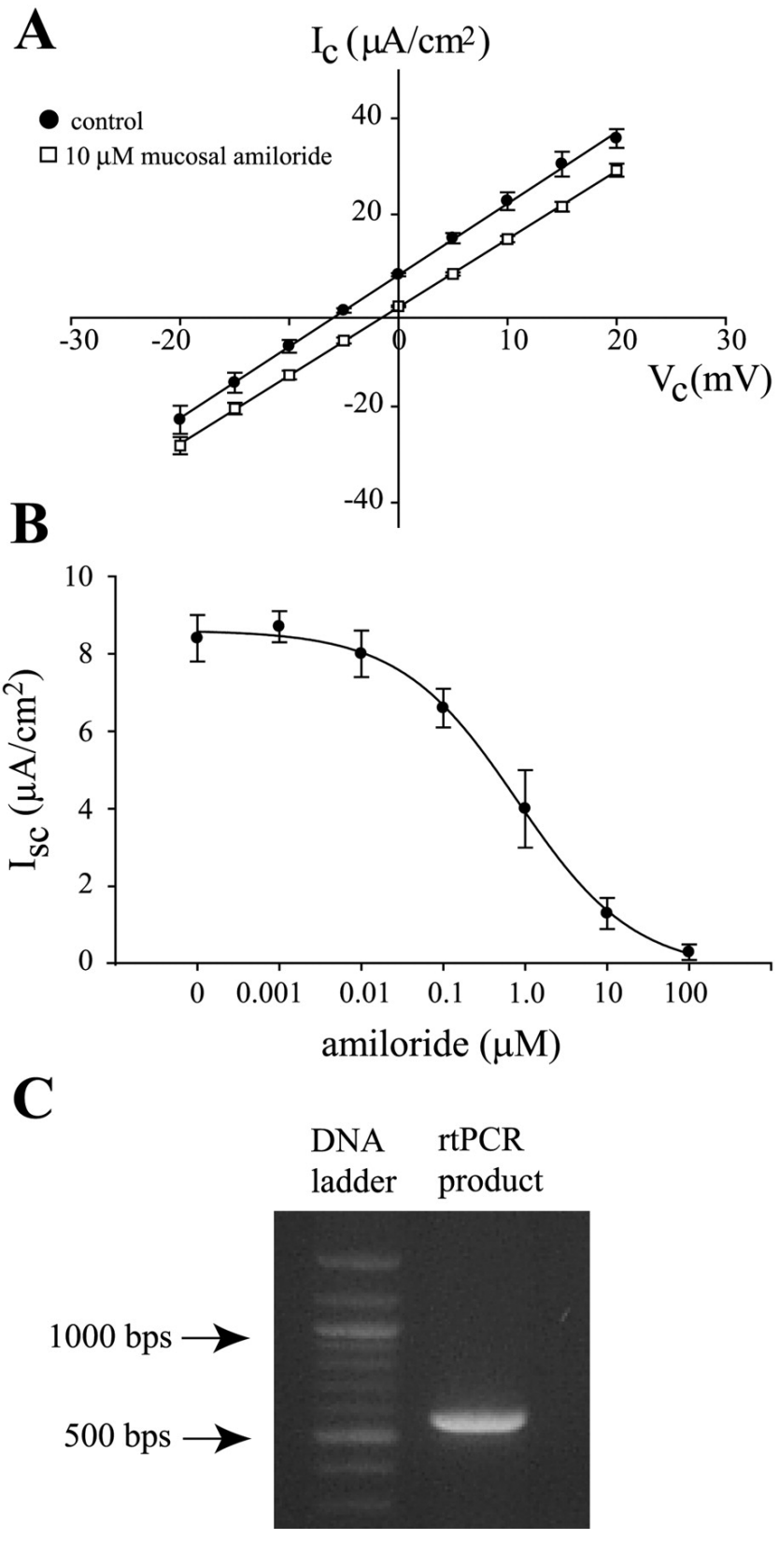
A
I_c (μA/cm²)
control
10 μM mucosal amiloride
40
20
-20
-40
-30
-20
0
10
20
30
V_c(mV)
B
I_{sc} (μA/cm²)
10
8
6
4
2
0
0
0.001
0.01
0.1
1.0
10
100
amiloride (μM)
C
DNA ladder
rtPCR product
1000 bps
500 bps

is much greater than the transcellular conductance, such that changes in transepithelial conductance are undetectable when a transcellular transport pathway is blocked.

A concentration-response curve of the effects of apical amiloride on I_{sc} shows that inhibitory effects begin at an amiloride concentration of 0.1 μM (Fig. 2.6b). A 4-parameter sigmoid curve was fitted to mean values of I_{sc} which drops from approximately 9 $\mu A/cm^2$ in the absence of amiloride to 0.3 ± 0.2 $\mu A/cm^2$ in the presence of an amiloride concentration of 100 μM. The amiloride concentration at half maximal inhibition (IC_{50}) was 0.76 μM. The correlation coefficient of the regression line was 0.9985.

Fig. 2.6c shows the separation of the rtPCR product of αENaC mRNA in agarose gel, revealing a DNA band of 500 bps. After sequencing, the band turned out to be a DNA strand with 547 bps, 100% identical to the reported canine αENaC cDNA (GenBank accession number AF209748).

Effects of amiloride on transepithelial Na^+ fluxes in monolayers grown in fortified OptiMEM culture medium. To examine whether the amiloride-sensitive short-circuit current is carried by Na^+, we measured unidirectional, transepithelial isotopic $^{22}Na^+$ fluxes in the absence and presence of apical amiloride (Table 2.1).

Monolayers were bathed on both sides with fortified OptiMEM containing culture-stimulating agents. Under control conditions the unidirectional Na^+ flux from the mucosal to the serosal side ($J_{m\rightarrow s}$) was 18.6 $nmol \cdot min^{-1} \cdot cm^{-2}$, and the reverse flux, from serosa to mucosa ($J_{s\rightarrow m}$) was 9.7 $nmol \cdot min^{-1} \cdot cm^{-2}$. The net transepithelial Na^+ flux was 8.9 $nmol \cdot min^{-1} \cdot cm^{-2}$ from mucosa to serosa, which is equivalent to a current

Table 2.1. The effects of 10 μM amiloride on unidirectional Na^+ fluxes and short-circuit current.

	J_{m-s} (nmol/min-cm^2)	J_{s-m} (nmol/min-cm^2)	$J_{net\ (m-s)}$		I_{sc} (μA/cm^2)
			as flux (nmol/min-cm^2)	as current (μA/cm^2)	
Control	18.6 ± 2.2 (6)	9.7 ± 2.6 (6)	8.9	14.3 [a]	8.7 ± 1.1 (12)
Mucosal amiloride (10 μM)	18.9 ± 2.6 (6)	11.6 ± 1.7 (6)	7.3	11.7 [a]	1.1 ± 0.2 [b] (12)

Mean ± S.E.; (number of DIEC monolayers). J_{m-s} and J_{s-m} are respectively isotopic Na^+ fluxes from mucosal to serosal and from serosal to mucosal solutions. I_{sc}, short-circuit current. [a]significantly higher ($P<0.001$) from the I_{sc} measured in parallel; z-test. [b]significantly different ($P<0.001$) from control; student t-test.

of 14.3 μA/cm^2. Since the short-circuit current measured in parallel was only 8.7 ± 1.1 μA/cm^2, the transepithelial Na^+ flux significantly exceeds the short-circuit current by a factor of 1.6 ($z = 5.09$, $p<0.001$).

In the presence of amiloride (10 μM), the $J_{m\rightarrow s}$ Na^+ flux remained near control values, 18.9 ± 2.6 nmol·min^{-1}·cm^{-2} (n = 6). Likewise, $J_{s\rightarrow m}$ Na^+ flux, 11.6 ± 1.7 nmol·min^{-1}·cm^{-2}, remained near control values (n = 6). Accordingly, the net transepithelial Na^+ flux was 7.3 nmol·min^{-1}·cm^{-2}, or 11.7 μA/cm^2, not significantly different from control (Table 2.1). In contrast, amiloride caused I_{sc} to drop significantly to 1.1 ± 0.2 μA/cm^2. Thus, amiloride substantially reduced the measured short-circuit current to 13 % of control values without affecting the net transepithelial Na^+ absorptive flux (Table 2.1).

Effects of ouabain on the electrophysiology of monolayers grown in fortified OptiMEM culture medium. In monolayers studied in the presence of fortified OptiMEM containing culture-stimulating agents, the addition of ouabain (1 mM) to the basolateral side inhibited I_{sc} and V_t and decreased R_t (Fig. 2.7). Unlike the immediate effects of amiloride, the effects of ouabain developed slowly. Under control conditions V_t was -9.7 ± 1.9 mV, R_t was 1708 ± 151 Ωcm^2, and I_{sc} was 7.2 ± 0.8 μA/cm^2 in 6 DIEC monolayers. One to two seconds after adding ouabain to the serosal solution, V_t significantly decreased to –8.2 ± 1.4 mV ($P<0.001$) and I_{sc} significantly decreased to 5.9 ± 0.8 μA/cm^2 ($P<0.001$). Twenty minutes later V_t had decreased further to -0.5 ± 0.3 mV ($P<0.001$, compared to control), I_{sc} had fallen to values not significantly different from zero, and R_t had decreased significantly to 1106 ± 111 Ωcm^2 ($P<0.01$).

Figure 2.7. Effect of serosal ouabain on transepithelial electrical variables of DIEC monolayers in fortified OptiMEM. Upon the addition of ouabain, the transepithelial voltage V_t and short-circuit current I_{sc} decreased initially by -3.2 mV and 1.3 $\mu A/cm^2$, respectively. Thereafter, V_t and R_t underwent a slow, gradual decrease until 20 min later when V_t and I_{sc} had decreased to 0, and R_t had decreased significantly as well. NM, not measured; Values are mean ± S.E.; *, $P<0.01$; (number of determinations).

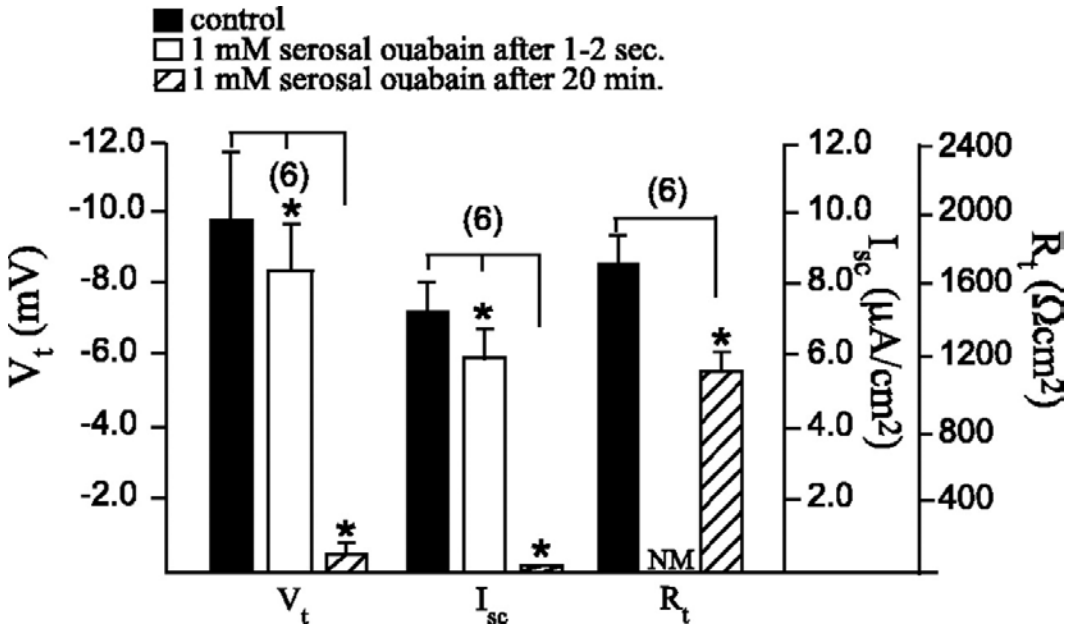
control
1 mM serosal ouabain after 1-2 sec.
1 mM serosal ouabain after 20 min.
-12.0
-10.0
-8.0
-6.0
-4.0
-2.0
V_t (mV)
12.0
10.0
8.0
6.0
4.0
2.0
I_{sc} (μA/cm^2)
2400
2000
1600
1200
800
400
R_t (Ωcm^2)
(6)
(6)
(6)
*
*
*
*
*
NM
V_t
I_{sc}
R_t

Electrophysiological studies of monolayers in plain Ringer solution. When DIEC monolayers cultured in fortified OptiMEM were bathed in Ussing chambers on both sides with plain Ringer solution lacking culture-stimulating agents, the transepithelial voltage decayed in parallel with a decrease in the short-circuit current (Fig. 2.8a). Together with four additional experiments, the transepithelial voltage dropped from –12.5 ± 4.6 mV to –1.5 ± 0.9 mV (n=5) in 10 to 30 min. The I_{sc} dropped from 6.6 ± 1.6 μA/cm^2 to 2.0 ± 0.6 μA/cm^2 (n=5).

Effects of cAMP on monolayer electrophysiology in plain Ringer solutions. Responding to a query of a reviewer we examined DIEC monolayers for transepithelial Cl^- secretion, a functional hallmark of the mammalian jejunum. In these experiments, monolayers were first transferred to plain Ringer solution lacking culture-stimulating agents, and then amiloride (10 μM) was added to the mucosal solution (Fig. 2.8b). Both maneuvers served to abolish the transepithelial Na^+ current mediated in part by ENaC. Under these conditions, I_{sc} was 0.3 ± 0.2 μA/cm^2, V_t was -1.5 ± 0.1 mV, and R_t was 3073 ± 114 Ωcm^2 in 6 monolayers (Fig. 2.8b). Upon the addition of 1 mM db-cAMP to the basolateral solution, V_t and I_{sc} increased gradually and significantly reaching peak values 5 minutes later. Within in the next 5 minutes, I_{sc} went to steady state values of 3.8 ± 0.2 μA/cm^2, V_t went to -6.8 ± 0.4 mV, and R_t decreased to 1718 ± 148 Ωcm^2. The effects of db-cAMP on V_t, R_t, and I_{sc} are highly significant ($P<0.001$).

The same experiment repeated in the presence of low Cl^- Ringer solution (13 mM Cl^-) revealed a marked decrease in the response to db-cAMP (Fig. 2.8c). In the presence of low Cl^- Ringer on both sides of the monolayer and apical amiloride (10 μM), the addition of db-cAMP (1 mM) to the serosal side significantly increased I_{sc} from zero to 2.5 ± 0.1 μA/cm^2 ($P<0.001$); it increased V_t from -1.2 ± 0.1 mV to –3.6 ± 0.3 mV

Figure 2.8. DIEC monolayers studied in Ringer solution lacking culture-stimulating agents. a) Representative decay of the transepithelial voltage and short-circuit current upon the transfer of the DIEC monolayer from fortified OptiMEM containing epidermal growth factor, hydrocortisone and insulin to plain Ringer solution. Upon the transfer a time zero, the transepithelial voltage (V_t) and short-circuit current (I_{sc}) decreased with time. b) Effect of serosal db-cAMP (1 mM) on transepithelial electrical variables of DIEC monolayers in plain Ringer solution containing 130 mM Cl^- on both sides and amiloride (10 μM) on the apical side; c) response to db-cAMP in low Cl^-- Ringer solution containing 13 mM Cl^- on both sides and amiloride (10 μM) on the apical side of the monolayer.

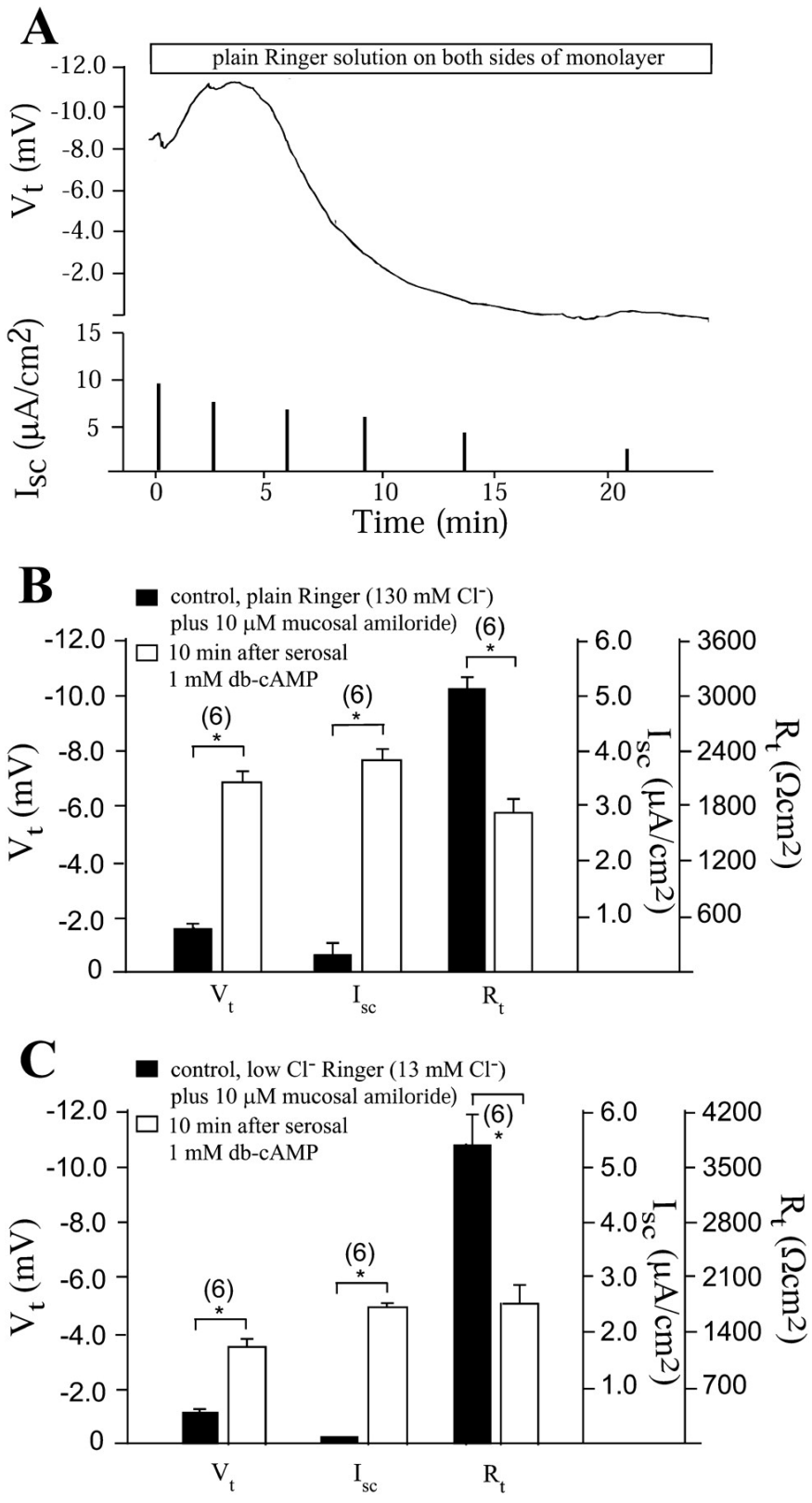
A
plain Ringer solution on both sides of monolayer
Vt (mV)
-12.0
-10.0
-8.0
-6.0
-4.0
-2.0
Isc (μA/cm2)
15
10
5
0
5
10
15
20
Time (min)
B
control, plain Ringer (130 mM Cl-)
plus 10 μM mucosal amiloride)
10 min after serosal
1 mM db-cAMP
(6)
*
Vt (mV)
Isc (μA/cm2)
Rt (Ωcm2)
6.0
5.0
4.0
3.0
2.0
1.0
3600
3000
2400
1800
1200
600
Vt
Isc
Rt
C
control, low Cl- Ringer (13 mM Cl-)
plus 10 μM mucosal amiloride)
10 min after serosal
1 mM db-cAMP
4200
3500
2800
2100
1400
700

($P<0.001$), and it significantly decreased R_t from 3883 ± 388 Ωcm^2 to 1827 ± 255 Ωcm^2 ($P<0.001$) in six monolayers. Although the effects of db-cAMP were statistically significant, they were less than those observed in the presence of plain Ringer solution with a Cl^- concentration of 129.8 mM (Fig. 2.8b,c). These results show that the db-cAMP stimulation of and I_{sc} and V_t was dependent on the presence of Cl^-.

The same conclusion was reached in studies of DIEC monolayers in glucose-free Ringer solution and in the presence of apical amiloride (10 μM). Under these conditions, the addition of 1 mM db-cAMP to the serosal Ringer solution significantly increased V_t from –1.3 ± 0.1 mV to –7.1 ± 0.1 mV ($P<0.001$), it significantly increased I_{sc} from 0.1 ± 0.1 $\mu A/cm^2$ to 4.6 ± 0.4 $\mu A/cm^2$ ($P<0.$ 0.001), and it significantly reduced R_t from 2718 ± 229 Ωcm^2 to 1532 ± 134 Ωcm^2 ($P<0.001$), again in 6 monolayers. Since these effects are quantitatively similar to those observed in the presence of glucose, the significant effects of db-cAMP are not due to the stimulation of electrogenic Na/D-glucose cotransport.

Expression of SGLT1 in DIEC monolayers. Western blot analysis confirmed the presence of SGLT1 in DIEC cultures (Fig. 2.9a). In a protein extract of DIEC, the antibody 8821 specific to mammalian SGLT1 recognized a protein band at 75 kDa where SGLT1 is expected to locate (Fig. 2.9a, left). Antibody specificity was confirmed by tying up the antibody with immunizing peptide which prevented it from binding to SGLT1 in the DIEC extract (Fig. 2.9a, right).

The electrophysiological evidence for the presence of Na^+/D-glucose cotransport was less clear (Fig. 2.9b). In this series of experiments, five DIEC monolayers studied in glucose-free Ringer solution had a V_t of –3.6 ± 0.3 mV, an I_{sc} of 3.2 ± 0.5 $\mu A/cm^2$, and an R_t of 1061 ± 133 Ωcm^2. The addition of 10 mM glucose to both

Figure 2.9. Presence of the Na/D-glucose cotransporter in DIEC monolayers. a) Antibody 8821 raised against SGLT1 recognized the Na/D-glucose cotransporter in an extract of DIEC (left western blot). The right western blot shows non-specific background when antibody 8821 binding to immunizing peptide is not free to bind to SGLT1. b) Effect of 10 mM glucose on transepithelial voltage (V_t), short-circuit current (I_{sc}), and transepithelial resistance (R_t) in DIEC monolayers bathed in plain Ringer solution lacking glucose. The addition of glucose to both sides of the monolayer tended to increase I_{sc} and to decrease R_t but not significantly. R_t was determined as the inverse slope of current-voltage plots.

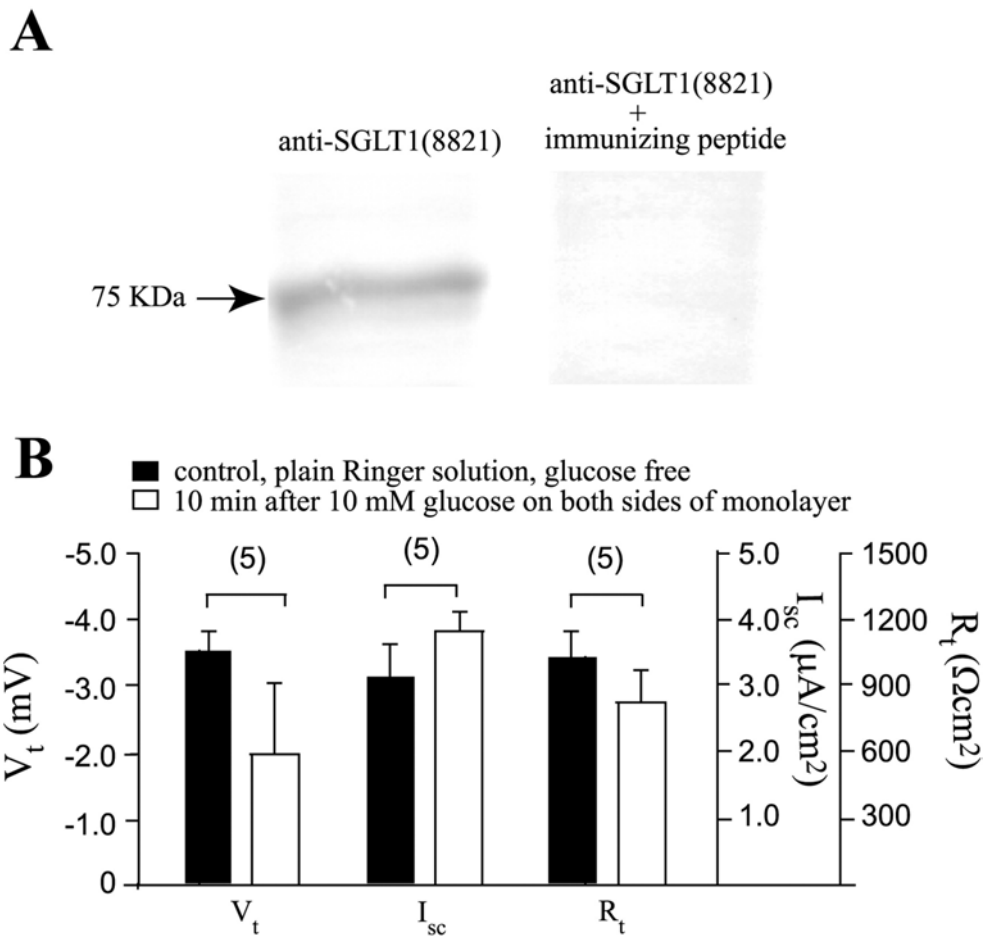
A
anti-SGLT1(8821)
anti-SGLT1(8821)
+
immunizing peptide
75 KDa
B
control, plain Ringer solution, glucose free
10 min after 10 mM glucose on both sides of monolayer
(5)
(5)
(5)
-5.0
-4.0
-3.0
-2.0
-1.0
0
V_t (mV)
5.0
4.0
3.0
2.0
1.0
I_{sc} (μA/cm^2)
1500
1200
900
600
300
R_t (Ωcm^2)
V_t
I_{sc}
R_t

serosal and mucosal solutions decreased V_t to –2.0 ± 1.1 mV, increased I_{sc} to 3.9 ± 0.3 μA/cm^2 and decreased R_t to 830 ± 156 Ωcm^2 (Fig. 2.9b). Though the changes in I_{sc} and R_t were consistent with the stimulation of electrogenic Na^+/D-glucose cotransport, they were not statistically significant.

5. Discussion

Cultures of the mammalian intestine. Fully differentiated epithelial cells derived from the normal mammalian intestine are difficult to culture in vitro (40), and at most have been obtained in non-proliferative states that do not allow significant expansion beyond the primary culture. Most normal cell lines available today have been derived from stem cells or undifferentiated committed crypt cells, but have proved of limited use in studies of nutrient transport across the intestine. The first intestinal epithelial cell line (IEC) was produced by one of us (Quaroni) who started the culture with crypt cells of the newborn rat (42). IEC tends to grow in packed colonies with short and sparse apical microvilli and only limited expression of tight junctions and desmosomes. IEC does not grow well on filter supports, nor does it form tight monolayers suitable for transport studies. Except for aminopeptidase and dipeptidylpeptidase, the usual brush border digestive enzymes are absent, suggesting the largely undifferentiated nature of the IEC culture (40). Furthermore, the cell line lacks most of the active transport systems and the enzymes of the normal epithelium (53).

In the present study we introduce an intestinal cell culture derived from the normal, healthy intestinal mucosa of the dog jejunum. The DIEC culture was directly produced from jejunal crypts, apparently from committed crypt cells. The culture could be carried through at least 6 passages without apparent morphological changes

or loss of ability to form polarized monolayers on filters. When monolayers are grown on filters, epithelial cells display long and dense microvilli at the apical membrane, extensive basolateral membrane infoldings, and well-defined tight junctions and desmosomes (Figs. 2.3,4). The expression of keratin #18 (Fig. 2.1c) and the presence of several tight junction proteins confirm the epithelial nature of the culture (Fig. 2.2). The expression of the epithelial Na^+ channel ENaC (Figs. 2.5,6) was unexpected and most likely due to the presence of epidermal growth factor, corticosterone and insulin in the culture medium (*vide infra*).

Proteins of the tight junction and the paracellular pathway. To date, 24 members of the claudin protein family have been identified in mice and men (50). The claudins have 4 transmembrane domains with N- and C- terminals located in the cytoplasm. Associated with other junctional proteins (occludin, ZO proteins, and junctional adhesion proteins), the claudins define the barrier and permselectivity functions of the paracellular pathway (29, 34). For example, the presence of claudin-16 in tight junctions of the thick ascending limb of the Loop of Henle defines the paracellular Ca^{2+} and Mg^{2+} permselectivity in this part of the nephron (46). More than two claudins may coexist in a tight junction, forming heteropolymers that appear to increase the structural and functional diversity of the paracellular pathway (17).

So far, claudin-3 and claudin-4 have been found in the jejunum (43). Significantly, the same claudins are expressed in the DIEC culture of the dog jejunum, indicating a cultured tight junction that resembles the junction of the normal jejunum. A receptor function has been attributed to these two claudins (5, 26). Binding to the enterotoxin of *Clostridium perfringens*, claudin-3 and claudin-4 are thought to participate in triggering the diarrhea of the *Clostridium* infection. Apparently, claudins can have functions in addition to permissive paracellular transport.

Occludin is another tight junction protein with 4 transmembrane domains. The discrete distribution of occludin in a narrow band surrounding the cells of DIEC monolayers is consistent with its location in tight junctions (Fig. 2.2b). Likewise, the distribution of ZO-1 is limited to the region of the tight junction (Fig. 2.2c).

On first examination, the distribution of claudin-4 suggests its presence in the cytoplasm of cell (Fig. 2.2d). However, upon closer inspection, it appears that the microtome cut takes a tangent to tight junctions. Leaving one epithelial cell, the cut encounters a sharp edge of claudins, suggesting its entry into the tight junction. Passing obliquely through the tight junction, the cut gives rise to the diffuse distribution of claudin-4. In other regions of Fig. 2.2b, claudin is as discretely confined to the cell border, like occludin and ZO-1, consistent with the expression of claudins at plasma membranes (35). Nevertheless, claudins have been observed inside cells. When exogenous claudin-2 and -4 were experimentally expressed in MDCK II cells, they were detected in some intracellular, vacuole-like structures in addition to their expression at the cell border, while native claudins were restricted to the cell border (9). Studies by Kobayashi et al. (30) suggest that foreign claudins can induce the formation of vacuole-like structures in the cytoplasm.

Desmosomes are 'welding spots' that hold cells together and resist tears in epithelial tissues. Desmosomes are abundantly expressed in DIEC monolayers where they outline the lateral interstitial space between epithelial cells and beyond the tight junction (Fig. 2.2e).

DIEC, a leaky epithelium in spite of appreciable transepithelial resistances. In 1972, Frömter and Diamond introduced the concepts of "leaky" and "tight" epithelia (16). In general, leaky epithelia have 1) low values of transepithelial voltage (from 0 to 11 mV) and resistance (from 6 to 200 Ωcm^2), 2) a brush border apical membrane,

and 3) the functional properties of isosmotic fluid transport at high rates. In contrast, tight epithelia have high values of transepithelial voltage (30 to 100 mV) and resistance (300 to 2000 Ωcm^2). Tight epithelia lack a brush border at apical surfaces. The main function of tight epithelia is to generate and maintain high transepithelial concentration differences of solute and water for storage.

In the present study, DIEC monolayers had on average a transepithelial resistance of 1050 Ωcm^2 consistent with a tight epithelium when compared with 50 Ωcm^2, the resistance of the small intestine in vivo (15, 36). On the other hand, a low transepithelial voltage and the presence of a dense brush border indicate a leaky epithelium. Instead of measures of the transepithelial voltage and resistance, Boulpaep et al. have proposed a more appropriate criterion of epithelial leakiness or tightness, namely the ratio of transcellular and paracellular transport in general, and the ratio of transcellular and paracellular resistance in particular (6). To estimate this resistance ratio in DIEC monolayers we have assumed that the electromotive force of the active transport pathway passing through epithelial cells is 120 mV. Since the short-circuit current I_{sc} is 8.1 $\mu A/cm^2$, it follows that the tanscellular resistance is 14815 Ωcm^2. In view of a transepithelial resistance (transcellular and paracellular resistance in parallel) of 1050 Ωcm^2, the paracellular resistance is 1131 Ωcm^2. Thus, the ratio of transcellular and paracellular resistance indicates a paracellular conductance 13 times greater than the transcellular conductance consistent with a leaky epithelium. Such a high paracellular conductance may obscure the effects of amiloride on the transepithelial resistance (Figs. 2.5,6).

Functional characterization of DIEC. Absorption of salt, water and dietary nutrients is the hallmark function of the mammalian small intestine. The human intestine absorbs approximately 600 millimoles of Na^+ and 6.5 liters of water per day.

The absorption of water is coupled to the absorption of solute. In turn, the absorption of solute relies largely on Na-dependent transport mechanisms such as Na/glucose cotransport, Na/amino acid cotransport, Na/H exchange transport, and NaCl absorption via parallel Na/H and Cl/HCO_3 transport. The transport of Na^+ across the small intestine varies 1) along the length of the intestine (radial heterogeneity), 2) along the length from crypt to tip of a villus (axial heterogeneity), and 3) between individual epithelial cells in regions of the villus tip and crypt that express transport systems to varying degree (cellular heterogeneity). DIEC monolayers derived from the normal jejunum appear to illustrate some of these heterogeneities. For one reason, the net absorptive isotopic Na^+ flux was nearly twice the short-circuit current measured in parallel (Table 2.1), suggesting the presence of electroneutral Na^+ transport mechanisms such as NaCl absorption via parallel Na/H and Cl/HCO_3 transport. For another reason, the inequality of current and flux suggests that flux and current do not derive from the same monolayer area, i.e. the monolayer is heterogeneous as the normal jejunum.

Our preliminary functional characterization of DIEC monolayers illustrated the influence of environmental factors on the expression of transport systems. When DIEC monolayers are grown and studied in OptiMEM solution containing the culture-stimulating agents epidermal growth factor, hydrocortisone, and insulin, the monolayers display an amiloride-sensitive short-circuit current mediated by ENaC (Fig. 2.6). This current disappears in plain Ringer solution (Fig. 2.8a). The subsequent addition of cAMP to the serosal side activates a Cl^- dependent current consistent with transepithelial secretion of Cl^- (Fig. 2.8b,c). Thus DIEC monolayers can be manipulated to express electrogenic Na^+ absorption under one set of conditions and electrogenic Cl^- secretion under another.

When grown and studied in fortified OptiMEM solution, the inhibition of the short-circuit current with amiloride presented from the mucosal side (and not the serosal side, Fig. 2.5) and the inhibitory effects of serosal ouabain on voltage and short-circuit current (Fig. 2.7), outline the rudiments of the Ussing model of epithelial Na^+ transport (51). The amiloride concentration-response curve revealed an IC_{50} of 0.76 μM (Fig. 2.6b), similar to that measured in other epithelia expressing ENaC (4). The immediate effect of ouabain on V_t and I_{sc} probably results from the blockade of the electrogenic Na^+/K^+ ATPase operating with a stoichiometric exchange of 3 Na^+ ions for 2 K^+ ions. The ouabain-sensitive pump current was measured as 1.3 ± 0.2 $\mu A/cm^2$, which is significantly different from zero ($P<0.001$). The gradual decline of V_t and I_{sc} in the presence of ouabain probably reflects the dissipation of Na^+, K^+ and voltage gradients across cell membranes.

Isotopic Na^+ flux measurements in DIEC monolayers grown and studied in fortified OptiMEM show that ENaC-mediated transepithelial Na^+ transport accounts for only 18% of the net absorptive transepithelial Na^+ transport (Table 2.1). Since these measurements were made in the absence of transepithelial voltage and concentration differences, DIEC monolayers must possess additional transepithelial active transport mechanisms for Na^+. Indeed, an antibody specific to SGLT1 recognizes a protein in DIEC lysates that localizes at the expected position (Fig. 2.9a). That the same antibody recognizes SGLT1 in the dog jejunum in vivo indicates that our culture expresses Na/D-glucose cotransport as the normal jejunum (22). Next to Na/D-glucose cotransport, DIEC monolayers may express other Na^+-dependent solute transport systems that were not investigated in the present study.

Significantly, amiloride-sensitive transepithelial voltage and short-circuit current disappeared in monolayers when fortified OptiMEM, containing growth factor, hydrocortisone and insulin, was replaced with plain Ringer solution (Fig. 2.8a). In the

presence of plain Ringer solution on both sides of the monolayer, the transepithelial voltage and short-circuit current decayed with a time course expected from the endocytic deactivation of ENaC (7, 8). The decay of voltage and current suggest that the presence of growth factor, glucocorticoid and insulin in the culture medium had activated the expression of ENaC (38, 45). Still, the presence of ENaC in a cell culture of the small intestine may not be so unusual as it first appears. In rats, the surgical removal of the colon (ileoanal anastomosis) induces ENaC expression in the ileum (31). Furthermore, the induction of ENaC activity has been attributed to serum- and glucocorticoid-induced kinase (sgk1) that is present in both jejunum and ileum (10).

Next to transepithelial Na^+ absorption, the transepithelial secretion of fluid driven by secretory Cl^- transport is a functional hallmark of the jejunum. In particular, Cl^- driven fluid secretion is thought to take place in the crypt region of villi and mediated by epithelial cells that harbor Cl^- channels in the apical membrane and the Na/K/2Cl cotransporter in the basolateral membrane (13, 54). Up to now, at least 3 different Cl^- channels have been found in the small intestine: the stretch activated Cl^- channel, the Ca^{2+} activated Cl^- channel, and CFTR that is activated by phospharylation via PKA and cAMP (3). DIEC monolayers apparently exhibit Cl^- secretion via CFTR in view of the effects of db-cAMP (Fig. 2.8b,c). The nucleotide induced a significant increase in short-circuit current (from mucosa to serosa) when ENaC channels were blocked with amiloride. The cAMP stimulated I_{sc} was dependent on the presence of Cl^- in the bath medium consistent with the stimulation of transepithelial Cl^- secretion. Furthermore the sustained stimulation of I_{sc} distinguishes CFTR channels from Ca^{2+} activated and stretch activated Cl^- channels which respond only transiently to activation (3, 13).

Of note is the significant decrease of the transepithelial resistance upon stimulation with cAMP (Fig. 2.8b,c). The activation of CFTR in the apical membrane of DIEC monolayers was not expected to decrease much the transepithelial resistance in view of the low paracellular resistance relative to the transcellular resistance that prevented a significant increase in transepithelial resistance in the presence of amiloride (Figs.2.5a,6a). Thus, cAMP may have affected the paracellular pathway in addition to CFTR in the apical membrane of DIEC. Indeed, the nucleotide is thought to increase tight junction permeability (25). The molecular mechanism is not completely understood, but the PKA phosphorylation of Thr^{207} of claudin-5, one of the tight junction proteins, is known to trigger the rapid decrease in transendothelial resistance in rat lung endothelium (47).

Sodium dependent glucose cotransport via SGLT1 is another hallmark of the jejunum. Glucose enters the cell from the intestinal lumen against its chemical gradient at the expense of the Na^+ electrochemical gradient across the apical membrane. Glucose leaves the cells across the basolateral membrane down its chemical gradient through another sugar transporter of the family of GLUT glucose transporters (48).

Western blot analysis revealed the presence of SGLT1 in DIEC monolayers. The electrophysiological evidence for SGLT1 was less clear. The addition of 10 mM glucose to glucose-free medium tended to increase the short-circuit current but the change was not statistically significant (Fig. 2.9b). SGLT1 is also present in other cultures of the mammalian intestine such as Caco-2, HT29 cl.19A, and HT29-D4. However, it is active only in fully differentiated HT29-D4 cell monolayers (12, 18, 20), suggesting that SGLT1 activity correlates with cell differentiation (11). Indeed, SGLT genes are transcribed and translated only in mature enterocytes at villus tips (23). Thus it is likely that the number of tip cells present in DIEC monolayers may be

sufficient to yield a positive western blot but insufficient to yield significant transepithelial electrical changes when stimulated with glucose.

Na/D-glucose cotransport can be activated by cAMP, as in HRT-18 cells (37). However, in DIEC monolayers the cAMP stimulation of the short-circuit current was due primarily to the stimulation of a Cl^- dependent current (Figs. 2.8,9).

As a good model for the study of intestinal transport, a monolayer must resemble the in vivo condition, physically, morphologically and biochemically. In the present study, we have examined the morphological and electrophysiological characteristics of a new intestinal culture derived from the normal dog jejunum. DIEC monolayers resemble to normal epithelium to a remarkable degree. They display the morphological polarization of the jejunum with a prominent brush border, basolateral membrane infoldings, and the functional polarization of transporters in expected basolateral and apical membrane domains of the jejunum. Likewise, DIEC tight junctions possess the claudin proteins of the normal jejunum. Yet we leave many transport questions open to further studies, and the expression of digestive enzymes has yet to be examined. As a culture of the normal small intestine, DIEC monolayers may find wide application serving basic and applied motivations, from studies of the mechanism and regulation of transepithelial solute and water transport, to drug absorption, intestinal clearance of xenobiotics, and high throughput evaluations of pharmaceutical agents.

6. References

1. **Adibi SA.** Regulation of expression of the intestinal oligopeptide transporter (Pept-1) in health and disease. *Am J Physiol Gastrointest Liver Physiol* 285: G779-788, 2003.

2. **Artursson P, Palm K, and Luthman K.** Caco-2 monolayers in experimental and theoretical predictions of drug transport. *Adv Drug Deliv Rev* 46: 27-43, 2001.

3. **Basavappa S, Vulapalli SR, Zhang H, Yule D, Coon S, and Sundaram U.** Chloride channels in the small intestinal cell line IEC-18. *J Cell Physiol*, 2004 [Epub ahead of print].

4. **Benos DJ.** Amiloride: a molecular probe of sodium transport in tissues and cells. *Am J Physiol Cell Physiol* 242: C131-145, 1982.

5. **Berkes J, Viswanathan VK, Savkovic SD, and Hecht G.** Intestinal epithelial responses to enteric pathogens: effects on the tight junction barrier, ion transport, and inflammation. *Gut* 52: 439-451, 2003.

6. **Boulpaep EL.** In: *The paracellular pathway*, edited by Purcell EF. New York, NY: Josiah Macy, Jr. Foundation, 1982, p. 131-132.

7. **Butterworth MB, Helman SI, and Els WJ.** cAMP-sensitive endocytic trafficking in A6 epithelia. *Am J Physiol Cell Physiol* 280: C752-762, 2001.

8. **Carattino MD, Hill WG, and Kleyman TR.** Arachidonic acid regulates surface expression of epithelial sodium channels. *J Biol Chem* 278: 36202-36213, 2003.

9. **Colegio OR, Van Itallie C, Rahner C, and Anderson JM.** Claudin extracellular domains determine paracellular charge selectivity and resistance but not tight junction fibril architecture. *Am J Physiol Cell Physiol* 284: C1346-1354, 2003.

10. **Coric T, Hernandez N, de la Rosa DA, Shao D, Wang T, and Canessa CM.** Expression of ENaC and serum- and glucocorticoid-induced kinase 1 in the rat intestinal epithelium. *Am J Physiol Gastrointest Liver Physiol* 286: G663-670, 2004.

11. **Delezay O, Baghdiguian S, and Fantini J.** The development of Na^+-dependent glucose transport during differentiation of an intestinal epithelial cell clone is regulated by protein kinase C. *J Biol Chem* 270: 12536-12541, 1995.

12. **Delezay O, Verrier B, Mabrouk K, van Rietschoten J, Fantini J, Mauchamp J, and Gerard C.** Characterization of an electrogenic sodium/glucose cotransporter in a human colon epithelial cell line. *J Cell Physiol* 163: 120-128, 1995.

13. **Field M.** Intestinal ion transport and the pathophysiology of diarrhea. *J Clin Invest* 111: 931-943, 2003.

14. **Fox JJ, Riccio ML, Hua F, Bodenschatz E, and Gilmour RF, Jr.** Spatiotemporal transition to conduction block in canine ventricle. *Circ Res* 90: 289-296, 2002.

15. **Fromm M, Schulzke JD, and Hegel U.** Epithelial and subepithelial contributions to transmural electrical resistance of intact rat jejunum, in vitro. *Pflugers Arch* 405: 400-402, 1985.

16. **Fromter E and Diamond J.** Route of passive ion permeation in epithelia. *Nat New Biol* 235: 9-13, 1972.

17. **Furuse M, Sasaki H, and Tsukita S.** Manner of interaction of heterogeneous claudin species within and between tight junction strands. *J Cell Biol* 147: 891-903, 1999.

18. **Grasset E, Bernabeu J, and Pinto M.** Epithelial properties of human colonic carcinoma cell line Caco-2: effect of secretagogues. *Am J Physiol Cell Physiol* 248: C410-418, 1985.

19. **Hariton-Gazal E, Rosenbluh J, Graessmann A, Gilon C, and Loyter A.** Direct translocation of histone molecules across cell membranes. *J Cell Sci* 116: 4577-4586, 2003.

20. **Hemlin M and Huang X.** Na^+/glucose cotransport in the colonic adenocarcinoma cell line HT29 cl.19A: effect of cAMP. *Acta Physiol Scand* 160: 185-194, 1997.

21. **Hidalgo IJ, Raub TJ, and Borchardt RT.** Characterization of the human colon carcinoma cell line (Caco-2) as a model system for intestinal epithelial permeability. *Gastroenterology* 96: 736-749, 1989.

22. **Hines OJ, Whang EE, Bilchik AJ, Zinner MJ, Welton ML, Lane J, McFadden DW, and Ashley SW.** Role of Na^+-glucose cotransport in jejunal meal-induced absorption. *Dig Dis Sci* 45: 1-6, 2000.

23. **Hwang ES, Hirayama BA, and Wright EM.** Distribution of the SGLT1 Na^+/glucose cotransporter and mRNA along the crypt-villus axis of rabbit small intestine. *Biochem Biophys Res Commun* 181: 1208-1217, 1991.

24. **Itoh A, Tsujikawa T, Fujiyama Y, and Bamba T.** Enhancement of aquaporin-3 by vasoactive intestinal polypeptide in a human colonic epithelial cell line. *J Gastroenterol Hepatol* 18: 203-210, 2003.

25. **Karczewski J and Groot J.** Molecular physiology and pathophysiology of tight junctions III. Tight junction regulation by intracellular messengers: differences in response within and between epithelia. *Am J Physiol Gastrointest Liver Physiol* 279: G660-665, 2000.

26. **Katahira J, Inoue N, Horiguchi Y, Matsuda M, and Sugimoto N.** Molecular cloning and functional characterization of the receptor for *Clostridium perfringens* enterotoxin. *J Cell Biol* 136: 1239-1247, 1997.

27. **Keely SJ and Barrett KE.** p38 mitogen-activated protein kinase inhibits calcium-dependent chloride secretion in T84 colonic epithelial cells. *Am J Physiol Cell Physiol* 284: C339-348, 2003.

28. **Kinston RE.** Preparation and analysis of RNA. In: *Current Protocols in Molecular Biology*. New York, NY: John Wiley & Sons, 2002, p. 4.2.3-4.2.5.

29. **Kiuchi-Saishin Y, Gotoh S, Furuse M, Takasuga A, Tano Y, and Tsukita S.** Differential expression patterns of claudins, tight junction membrane proteins, in mouse nephron segments. *J Am Soc Nephrol* 13: 875-886, 2002.

30. **Kobayashi J, Inai T, and Shibata Y.** Formation of tight junction strands by expression of claudin-1 mutants in their ZO-1 binding site in MDCK cells. *Histochem Cell Biol* 117: 29-39, 2002.

31. **Koyama K, Sasaki I, Naito H, Funayama Y, Fukushima K, Unno M, Matsuno S, Hayashi H, and Suzuki Y.** Induction of epithelial Na^+ channel in rat ileum after proctocolectomy. *Am J Physiol Gastrointest Liver Physiol* 276: G975-984, 1999.

32. **Li T, Ito K, and Horie T.** Transport of fluorescein methotrexate by multidrug resistance-associated protein 3 in IEC-6 cells. *Am J Physiol Gastrointest Liver Physiol* 285: G602-610, 2003.

33. **Ma TY, Hollander D, Bhalla D, Nguyen H, and Krugliak P.** IEC-18, a nontransformed small intestinal cell line for studying epithelial permeability. *J Lab Clin Med* 120: 329-341, 1992.

34. **Mankertz J, Hillenbrand B, Tavalali S, Huber O, Fromm M, and Schulzke JD.** Functional crosstalk between Wnt signaling and Cdx-related transcriptional activation in the regulation of the claudin-2 promoter activity. *Biochem Biophys Res Commun* 314: 1001-1007, 2004.

35. **Morita K, Furuse M, Fujimoto K, and Tsukita S.** Claudin multigene family encoding four-transmembrane domain protein components of tight junction strands. *Proc Natl Acad Sci U S A* 96: 511-516, 1999.

36. **Munck BG and Schultz SG.** Properties of the passive conductance pathway across in vitro rat jejunum. *J Membr Biol* 16: 163-174, 1974.

37. **Nath SK, Rautureau M, Heyman M, Reggio H, L'Helgoualc'h A, and Desjeux JF.** Emergence of Na^+-glucose cotransport in an epithelial secretory cell line sensitive to cholera toxin. *Am J Physiol Gastrointest Liver Physiol* 256: G335-341, 1989.

38. **Pearce D.** SGK1 regulation of epithelial sodium transport. *Cell Physiol Biochem* 13: 13-20, 2003.

39. **Quaroni A and Beaulieu JF.** Cell dynamics and differentiation of conditionally immortalized human intestinal epithelial cells. *Gastroenterology* 113: 1198-1213, 1997.

40. **Quaroni A and Hochman J.** Development of intestinal cell culture models for drug transport and metabolism studies. *Adv Drug Deliv Rev* 22: 3-52, 1996.

41. **Quaroni A and Isselbacher KJ.** Cytotoxic effects and metabolism of benzo[a]pyrene and 7,12-dimethylbenz[a]anthracene in duodenal and ileal epithelial cell cultures. *J Natl Cancer Inst* 67: 1353-1362, 1981.

42. **Quaroni A, Wands J, Trelstad RL, and Isselbacher KJ.** Epithelioid cell cultures from rat small intestine. Characterization by morphologic and immunologic criteria. *J Cell Biol* 80: 248-265, 1979.

43. **Rahner C, Mitic LL, and Anderson JM.** Heterogeneity in expression and subcellular localization of claudins 2, 3, 4, and 5 in the rat liver, pancreas, and gut. *Gastroenterology* 120: 411-422, 2001.

44. **Rhoads JM, Chen W, Chu P, Berschneider HM, Argenzio RA, and Paradiso AM.** L-glutamine and L-asparagine stimulate Na^+-H^+ exchange in porcine jejunal enterocytes. *Am J Physiol Gastrointest Liver Physiol* 266: G828-838, 1994.

45. **Schulz-Baldes A, Berger S, Grahammer F, Warth R, Goldschmidt I, Peters J, Schutz G, Greger R, and Bleich M.** Induction of the epithelial Na^+ channel via glucocorticoids in mineralocorticoid receptor knockout mice. *Pflugers Arch* 443: 297-305, 2001.

46. **Simon DB, Lu Y, Choate KA, Velazquez H, Al-Sabban E, Praga M, Casari G, Bettinelli A, Colussi G, Rodriguez-Soriano J, McCredie D, Milford D, Sanjad S, and Lifton RP.** Paracellin-1, a renal tight junction protein required for paracellular Mg^{2+} resorption. *Science* 285: 103-106, 1999.

47. **Soma T, Chiba H, Kato-Mori Y, Wada T, Yamashita T, Kojima T, and Sawada N.** $Thr^{(207)}$ of claudin-5 is involved in size-selective loosening of the endothelial barrier by cyclic AMP. *Exp Cell Res* 300: 202-212, 2004.

48. **Thorens B.** Facilitated glucose transporters in epithelial cells. *Annu Rev Physiol* 55: 591-608, 1993.

49. **Tian JQ and Quaroni A.** Involvement of p21(WAF1/Cip1) and p27(Kip1) in intestinal epithelial cell differentiation. *Am J Physiol Cell Physiol* 276: C1245-1258, 1999.

50. **Tsukita S and Furuse M.** Claudin-based barrier in simple and stratified cellular sheets. *Curr Opin Cell Biol* 14: 531-536, 2002.

51. **Ussing HH and Zerahn K.** Active transport of sodium as the source of electric current in the short-circuited isolated frog skin. *Acta Physiol Scand* 23: 110-127, 1951.

52. **Varga A, Nugel H, Baehr R, Marx U, Hever A, Nacsa J, Ocsovszky I, and Molnar J.** Reversal of multidrug resistance by amitriptyline in vitro. *Anticancer Res* 16: 209-211, 1996.

53. **Versantvoort CHM, Ondrewater RCA, Duizer E, Van de Sandt JJM, Gilde AJ, and Groten JP.** Monolayers of IEC-18 cells as an in vitro model for screening the passive transcellular and paracellular transport across the intestinal barrier: comparison of active and passive transport with the human colon carcinoma Caco-2 cell line. *Environ Toxicol Pharmacol* 11: 335-344, 2002.

54. **Welsh MJ, Smith PL, Fromm M, and Frizzell RA.** Crypts are the site of intestinal fluid and electrolyte secretion. *Science* 218: 1219-1221, 1982.

55. **Weng XH, Huss M, Wieczorek H, and Beyenbach KW.** The V-type H^+-ATPase in Malpighian tubules of *Aedes aegypti*: localization and activity. *J Exp Biol* 206: 2211-2219, 2003.

CHAPTER 3

THE V-TYPE H^+-ATPASE IN MALPIGHIAN TUBULES OF *AEDES AEGYPTI*: LOCALIZATION AND ACTIVITY

Published in J Exp Biol. 2003 Jul;206(13):2211-2219
Used with permission

1. Abstract

The V-type H^+ ATPase is thought to provide the driving force for transepithelial electrolyte and fluid secretion in Malpighian tubules. To confirm the presence of this proton pump in Malpighian tubules of the yellow fever mosquito *Aedes aegypti*, we used several antibodies raised against the V-type H^+ ATPase of *Manduca sexta*. Western blot analysis confirmed the presence of the V-type H^+ ATPase in Malpighian tubules of *Aedes aegypti*. In situ immunostaining identified the V-type H^+ ATPase at the apical membrane of the mitochondrion-rich brush border of principal cells. The V-type H^+ ATPase was not found in stellate cells. Measurements of ATPase activity revealed bafilomycin-sensitive and NO_3^--sensitive ATPase activity to account from 50% to 60% of total ATPase activity in crude extracts of Malpighian tubules. No significant ouabain- or vanadate-sensitive Na^+/K^+ ATPase activity was detected. These results support the conclusion reached previously in electrophysiological studies that the mechanisms for transepithelial electrolyte secretion in the *Aedes* Malpighian tubules rely on the V-type H^+ ATPase as the principal energizer of epithelial transport. Measures of transepithelial Na^+ and K^+ secretion and estimates of the H^+ flux mediated by the V-type H^+ ATPase suggest a 1:1 stoichiometry for Na^+/H^+ and K^+/H^+ exchange transport across the apical membrane.

2. Introduction

The V-type H^+ ATPase was first discovered in endomembranes such as the vacuoles of cells (26). In recent years, this proton pump is increasingly found also in plasma membranes of cells (13). Here the V-type H^+ ATPase functions as an electrogenic pump, transporting protons from the cytoplasm to the extracellular fluid and generating cell-negative membrane voltages. The membrane voltage can then serve to drive ion transport through ion-specific channels, and the electrochemical

proton potential can serve to drive secondary active transport processes such as cation/H^+ exchange or anion/H^+ cotransport (12). In view of the diversity of transport processes supported by the V-type H^+ ATPase, Wieczorek and Harvey have introduced the H^+ paradigm of epithelial transport that takes its place next to the classical Na^+/K^+ paradigm of Koefoed-Johnsen and Ussing (42).

Bafilomycin A_1, a specific inhibitor of the V-type H^+ ATPase, completely inhibits transepithelial NaCl and KCl secretion, and with it, fluid secretion in Malpighian tubules of *Aedes aegypti* (5). Simultaneously, both apical and basolateral membrane voltages and the transepithelial voltage decrease to zero. These studies strongly suggest the H^+ paradigm of epithelial transport for Malpighian tubules.

In the present study we used an antibody specific to the B subunit of V-type H^+ ATPase to localize the proton pump to the apical brush border membrane of principal cells, but not stellate cells, of Malpighian tubules of the yellow fever mosquito. We also measured enzyme activities of the V-type H^+ ATPase and the Na^+/K^+ ATPase. We found much activity of the former and little of the latter

3. **Materials and Methods**

Mosquitoes, and preparation of crude extracts of Malpighian tubules. The mosquito colony was maintained as described by (31). On the day of the experiment a female mosquito (3-7 days post-eclosion) was cold anesthetized and decapitated. Malpighian tubules of female mosquitoes were removed under Ringer solution from their attachment to the gut and transferred to Ringer solution on ice. Ringer solution contained: 150 mM NaCl, 3.4 mM KCl, 1.7 mM $CaCl_2$, 1.8 mM $NaHCO_3$, 1.0 mM $MgSO_4$, 5 mM glucose, 25 mM HEPES, pH 7.1. For SDS-PAGE and western blot, 250 Malpighian tubules were isolated from 50 female mosquitoes and collected in 1.5 ml of ice-cold mosquito Ringer solution. The Ringer solution was then aspirated and

replaced with 100 µl of ice-cold lysis buffer, consisting of 20 mM Tris, 2 mM EGTA, 2 mM EDTA, 25 µg aprotinin, 0.5 mM phenylmethylsulfonyl fluoride (PMSF), 25 µg leupeptin, and 1% Triton X-100. The tubules were homogenized on ice with a Teflon pestle.

Protein content of Malpighian tubules. Total protein in Malpighian tubules of *Aedes aegypti* was determined with a "BioRad *DC* Protein Assay kit" (BioRad, Hercules, CA). The method is similar to the well-documented Lowry assay, which is based on the reaction of proteins with an alkaline copper tartrate solution and Folin reagent (22). In a typical protein determination we prepared CTE as described above using 100 Malpighian tubules from female mosquitoes only. The CTE volume was 100 µl. To 20 µl of this CTE and to 20 µl of bovine serum albumin (BSA) standards, 100 µl of reagent A (alkaline copper tartrate solution, BioRad, Hercules, CA) was added and then 800 µl of reagent B (Folin reagent, BioRad, Hercules, CA). After 15 minutes, the absorbance was read at 750 nm using a Beckman spectrophotometer (DU-65) against the BSA standards series ranging from 0.25 mg/ml to 1.5 mg/ml.

SDS-PAGE and western blot. SDS-PAGE was performed as described previously (43). In brief, 10 µl sample buffer (5-fold strength) was added to a 40 µl of CTE such that final concentrations of sample buffer were 125 mM Tris-HCl, 5% sucrose, 2% SDS, 0.005% bromphenolblue and 2% β-mercaptoethanol in a final volume of 50 µl at pH 6.8. After boiling for 3 minutes on a hotplate and then cooling on ice, aliquots of 7 µl (~11 µg protein) were loaded on each lane of the gel (BioRad Mini Protean 3 chamber, T 17%/C 0.4%). The electrophoresis was started with a current of 20 mA.

After the sample had entered the stacking-gel, the current was increased to 45 mA. The proteins were transferred to nitrocellulose membranes by semidry-blotting (60 minutes, 1 mA/cm^2) using a three buffer-system according to (16), modified by the addition of 20% methanol. SDS-PAGE lanes in the nitrocellulose membrane were cut from the western blot lanes and stained with Ponceau S.

The western blot membrane (nitrocellulose) was incubated for 60 minutes in blocking solution consisting of TBSNT (20 mM Tris-HCl, pH 7.5, 500 mM NaCl, 0.02% NaN_3, 0.05% Tween) fortified with 3% fish gelatine. The membrane was then treated for 60 minutes with three different primary antibodies diluted in TBSNT plus 1% fish gelatine (1: 1,000). The antibodies were: 1) Ab 353-2 against the V_1 complex of the V-type H^+ ATPase (15), 2) Ab 488-1 against the C subunit (25), and 3) Ab C23 against the B subunit of the V-type H^+ ATPase (15). In each case the antigen was isolated from *Manduca sexta* in the laboratory of Wieczorek. Antibodies (antisera) were prepared in guinea pigs by Charles River (Germany).

The western blot membrane was washed with TBSNT in a shaking bath 3 times, 5 minutes each. The secondary antibody (anti-guinea-pig alkaline phosphatase conjugated, Sigma A-5062) was added after dilution in TBSNT plus 1% fish gelatine (1: 30,000). Sixty minutes later the membrane was washed again with TBSNT 3 times for 5 minutes each. After rinsing with double distilled water (ddH_2O), the membrane was treated with 10 ml substrate-solution consisting of 50 mM Tris-HCl, pH 9.5, 100 mM NaCl, 50 mM $MgCl_2$, 0.34 mg/ml nitro blue tetrazolium (NBT, Sigma, St. Louis, MO) and 0.17 mg/ml 5-bromo-4-chloro-3-indolyl phosphate p-toluidine (BCIP, Sigma, St. Louis, MO). When protein bands became visible after 2 to 10 minutes, the membrane was rinsed with ddH_2O and dried at room temperature.

Immunohistochemistry. One hundred Malpighian tubules were removed from female mosquitoes as described above and collected in approximately 1 ml of mosquito Ringer solution (47). The Ringer solution was aspirated and the tubules were transferred for fixation to 5 ml of 10% formaldehyde buffered with 33.3 mM NaH_2PO_4 and 45.8 mM Na_2HPO_4 at pH 7.2~7.4. After 2.5 hours of fixation the tubules were transferred to a stainless steel embedding mold, dehydrated in a series of ethanol concentrations ranging from 30% to 100% at 10% increments, and embedded in paraffin wax. Serial sections were cut to a thickness of 4 μm. The sections were deparaffinized in xylene, rehydrated in a series of ethanol (100%, 95%, 70%) and washed in phosphate buffered saline (PBS: 145mM NaCl, 3.2 mM NaH_2PO_4, 7.2 mM Na_2HPO_4, pH 7.2~7.4). The sections were then treated with 0.5% H_2O_2 for 10 minutes to suppress endogenous peroxidase activity.

Slides treated in conventional ways showed little staining with the antibody C23. In contrast, pre-treating slides for 5 minutes in 0.1 M citric buffer at pH 6.0 and 80~90 ^oC (microwave) markedly improved the localization of antibody. The method is known as heat-induced-antigen-retrieval (HIAR), frequently used to increase the "antigenicity" of the antigens in formalin-fixed and paraffin-embedded sections (37). Although the mechanism of action of HIAR is not clear, it is believed that the procedure loosens or breaks cross-linkages of antigen and fixative, freeing epitopes for binding to antibody (37).

Unspecific binding was blocked with 10% normal rabbit serum (Zymed, San Francisco, CA) for 20 minutes before the slides were treated with primary antibody at 37 ^oC for 2 hours. The primary antibody, Ab C23, was the same polyclonal antibody used in western blot analysis (diluted 1:2000 in PBS). The secondary antibody, BIOTINylated rabbit-anti-guinea pig IgG (Zymed, San Francisco, CA) was 50-fold diluted in PBS and applied at room temperature for 20 minutes. Immunoreactivity

was visualized by incubating the sections in streptavidin/peroxidase solution (prediluted, Zymed histostain® kit, Zymed, San Francisco, CA) for 15 minutes and then in aminoethyl carbazole (AEC) chromogen substrate solution (Zymed, San Francisco, CA) for 2 minutes. Finally, the sections were counterstained with hematoxylin stain Gill's Formation #2 (Fisher, Fair Lawn, NJ) for 10 seconds at room temperature.

ATPase activity measurements. Total ATPase activity was measured spectrophotometrically as the oxidation of NADH, which was coupled to ATP hydrolysis as described by (36). The activity of the Na^+/K^+ ATPase was measured as the ouabain- or vandate-sensitive ATPase activity, and the V-type H^+ ATPase activity was measured as the bafilomycin- or nitrate-sensitive ATPase activity, as described by (21).

To free ATPase we lysed Malpighian tubules in hypo-osmotic lysis buffer (20 mM Tris-HCl, 2 mM EGTA, pH 7.1). In a typical experiment, 225 Malpighian tubules from 45 female mosquitoes were homogenized on ice with a Teflon coated pestle in 130 µl of lysis buffer. After ultrasonication for 1 minute, the tubule extract was divided into 6 aliquots of 20 µl each and stored at -20 ^oC.

On the day of the assay, the reaction buffer (125 mM Tris buffer, 1 mM EGTA, 120 mM NaCl, 12.5 mM KCl, 5mM NaN_3, 5 mM $MgCl_2$, 5 mM ATP, 2.5 mM phosphoenolpyruvate, with or without ATPase inhibitor) was preincubated with 0.125 mM NADH (Sigma, St. Louis, MO) and 10 units each of L-lactic dehydrogenase (LDH, type XI, Sigma, St. Louis, MO) and pyruvate kinase (PK, Sigma, St. Louis, MO) for 30 minutes at room temperature. The ATPase reaction was started by adding 20 µl of tubule extract in a cuvette. The closed cuvette was quickly inverted for

mixing and inserted into the spectrophotometer (General purpose UV/VIS DU520, Beckman).

The oxidation of NADH was measured as a function of time at 340 nm, the wavelength of NADH absorption. The linear portion of this function (the slope OD/hour) was divided by the NADH extinction coefficient (6.22 $OD*mM^{-1}$) and normalized to protein concentration to obtain the ATPase activity in tubule extracts (36).

The V-type H^+ ATPase was calculated as the bafilomycin- or NO_3-suppressible portion of the total ATPase activity, while the Na^+/K^+ ATPase activity was determined as the ouabain- or vanadate-suppressible portion. Bafilomycin was used at a concentration of 0.025 mM, NO_3^- 100 mM, ouabain (Sigma) 1 mM, and vanadate 0.1 mM (21).

Statistical treatment of the data. ATPase activity data are presented as mean ± standard error. The paired Student t-test was used for the significant difference ($P<0.05$) between control and experimental groups.

4. RESULTS

Protein content of Malpighian tubules. The protein concentration in 20 µl of CTE, equivalent to 20 Malpighian tubules was 0.77 ± 0.04 µg/µl in 5 determinations. Hence, the protein content is on average 0.77 µg per tubule.

SDS-PAGE and western blot. SDS-PAGE of the extract of Aedes Malpighian tubules reveals protein bands that co-localize with proteins of the V-type H^+ ATPase

purified from the tobacco hornworm Manduca sexta, suggesting that the tubule extract contains proteins of the V-type H^+ ATPase (Fig. 3.1A). Western blot analysis confirms the presence of the V-type H^+ ATPase in Aedes Malpighian tubules (Fig 3.1B). The mixture of antibodies (Ab 353-2) raised against proteins of the cytoplasmic V_1 complex identified more than 15 proteins in the purified V-type H^+ ATPase of Manduca sexta (lane 1, Fig. 3.1B). Five protein bands with molecular weights of 16, 27, 43, 56 and 67 kDa stained prominently (lane 1, Fig. 3.1B). Three of these proteins with molecular weights 16, 56 and 67 kDa were also recognized by the antibody mixture in the extract of Aedes Malpighian tubules (lane 2). The 67 kDa protein is most likely the A subunit of the V_1 complex (44).

Ab 488-1 is a polyclonal antibody raised against the C subunit of the V_1 complex. The antibody clearly recognized subunit C in both the holoenzyme from *Manduca sexta* (lane 3) and crude extract of *Aedes* Malpighian tubules (lane 4, Fig. 3.1B). Likewise, the polyclonal antibody Ab C23 raised against B subunit of the V_1 complex identified this subunit in the holoenzyme of *Manduca* (lane 5, Fig. 1B) and in the crude extract of *Aedes* Malpighian tubules (lane 6, Fig. 3.1B).

Immunolabeling performed with preimmuno-serum (control) exhibited no labeling (not shown). Thus, Fig. 3.1 confirms the presence of the V-type H^+ ATPase in Malpighian tubules of *Aedes aegypti* on the basis of antibodies raised against proteins of the V-type H^+ ATPase purified from *Manduca sexta*.

Immunohistochemistry.

Fig. 3.2 illustrates two sequential microtome sections from the same paraffin block of Malpighian tubules of *Aedes aegypti*. The two sections received the same experimental treatment, including heat-induced antigen retrieval, exposure to

Figure 3.1. Molecular identification of the V-type H^+ ATPase in Malpighian tubules of the yellow fever mosquito. A) SDS-PAGE, lane 1: standard molecular weight proteins; lane 2: holoenzyme of the V-type H^+ ATPase of *Manduca sexta*; lane3: crude tubule extract of Malpighian tubules of *Aedes aegypti,* B) western blot; antibodies raised against the V-type H^+ ATPase of *Manduca sexta* recognized similar proteins in extracts of Malpighian tubules of *Aedes aegypti*. Lanes 1, 3 and 5 are the holoenzyme; lane 2, 4 and 6 are the crude extracts of *Aedes* Malpighian tubules. Ab 353-2, Ab 488-1 and Ab C23 are respectively antibodies against the V_1 complex, C subunit and B subunit of the proton pump.

Provided by Dr. M. Huss

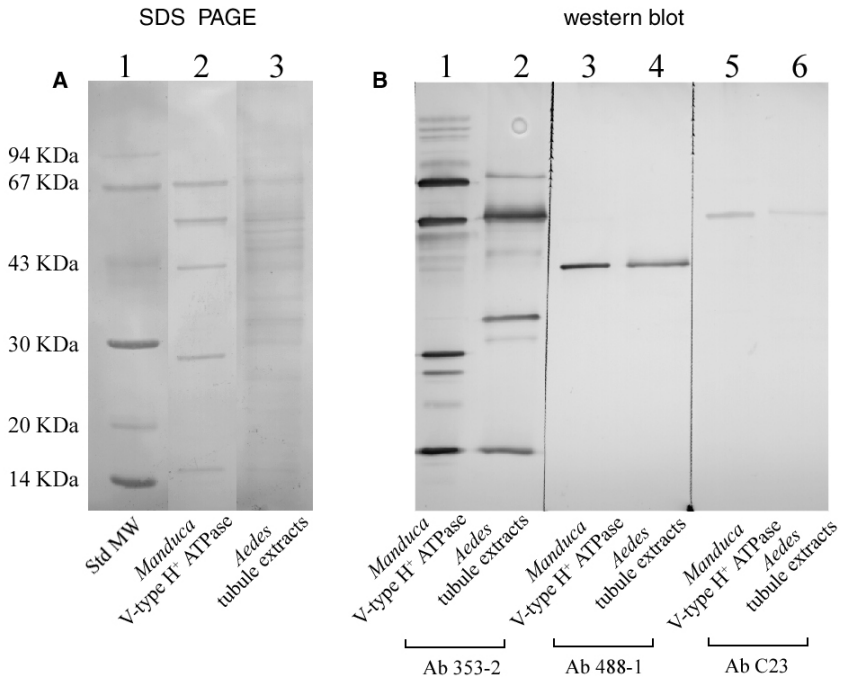
SDS PAGE
western blot
A
B
1
2
3
4
5
6
94 KDa
67 KDa
43 KDa
30 KDa
20 KDa
14 KDa
Std MW
Manduca V-type H+ ATPase
Aedes tubule extracts
Ab 353-2
Ab 488-1
Ab C23

Figure 3.2. Immunolocalization of the V-type H^+ ATPase in Malpighian tubules of *Aedes aegypti*. Paraffin sections of mosquito Malpighian tubules were labeled with a polyclonal antibody specific to the 56 kDa B subunit of the V-type H^+ ATPase (see Fig. 3.1B). A) Paraffin section labeled with preimmuno-serum as a negative control, B) paraffin section labeled with C23 polyclonal antibody; sc: stellate cell, bar: 100 μm. The inset section illustrates stellate cells without staining. Arrowheads point to small stellate cells without a prominent brush border, bar: 200 μm.

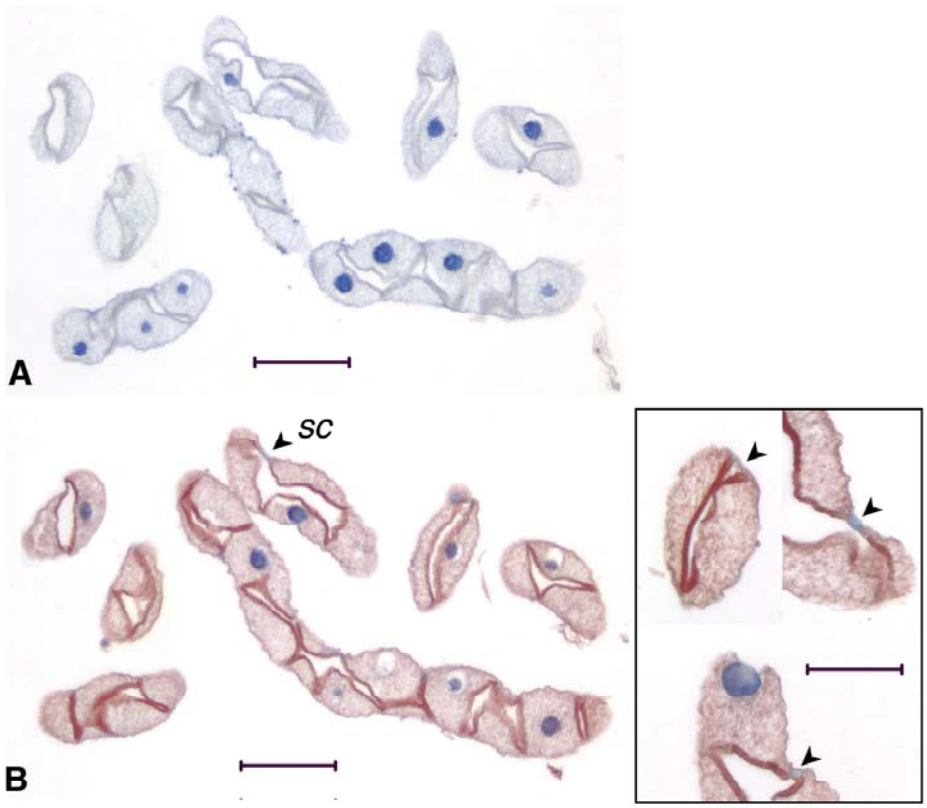
A
B
SC

secondary antibody, and staining with hematoxylin. The only difference is the additional exposure of section B to Ab C23, the primary antibody specific to the B subunit of the V-type H^+ ATPase. Section A was exposed to the preimmuno-serum.

Tubules appear in a mix of longitudinal and oblique sections (Fig. 3.2). The tubule lumen occasionally comes into view as the unstained clear space enclosed by the apical brush border of mostly principal cells. Single principal cell of the tubule reveals a large nucleus (18 μm) when the cut has passed through the center. Principal cells are further characterized by a tall dense brush border. Most cells of the tubule are principal cells (86%); the remainder are stellate cells (35).

The obvious difference between sections A and B is the positive stain of the antibody specific to the V-type H^+ ATPase in section B. The antibody C23 recognized the B subunit of the V-type H^+ ATPase most prominently in the brush border of principal cells, consistent with a high density of this proton pump at the apical membrane. Light staining of the cytoplasm of principal cells suggests the presence of the V-type H^+ ATPase (or parts thereof containing the B subunit) associated with cytoplasmic structures. However, the antibody did not stain stellate cells, neither plasma membrane nor cytoplasm.

ATPase activities.

Fig. 3.3 illustrates the enzyme activities of the V-type H^+ ATPase and the Na^+/K^+ ATPase in extracts of *Aedes* Malpighian tubules. Total ATPase activity was 3.14 ± 0.35 μmol/hour per mg protein in 10 control determinations. The bafilomycin A_1 sensitive ATPase activity was 1.58 ± 0.30 μmol/hour per mg protein in 10 determinations, significantly different from zero ($P = 2.5 \times 10^{-4}$). The KNO_3 sensitive ATPase activity was 1.88 ± 0.20 μmol/hour per mg protein in 7 determinations, also significantly different from zero ($P = 4.8 \times 10^{-5}$). The two V-type H^+ ATPase

Figure 3.3. ATPase activities in crude extract of Malpighian tubules of *Aedes aegypti*. The V-type H^+ ATPase activity was measured as the bafilomycin- and NO_3^- -sensitive ATPase activity. The Na^+/K^+ ATPase activity was measured as the ouabain- and vanadate-sensitive ATPase activity. The following inhibitor concentrations were used: bafilomycin A_1, 0.025 mM; nitrate, 100 mM; ouabain, 1 mM; vanadate, 0.1 mM. *, $P<0.01$; (number of determinations)

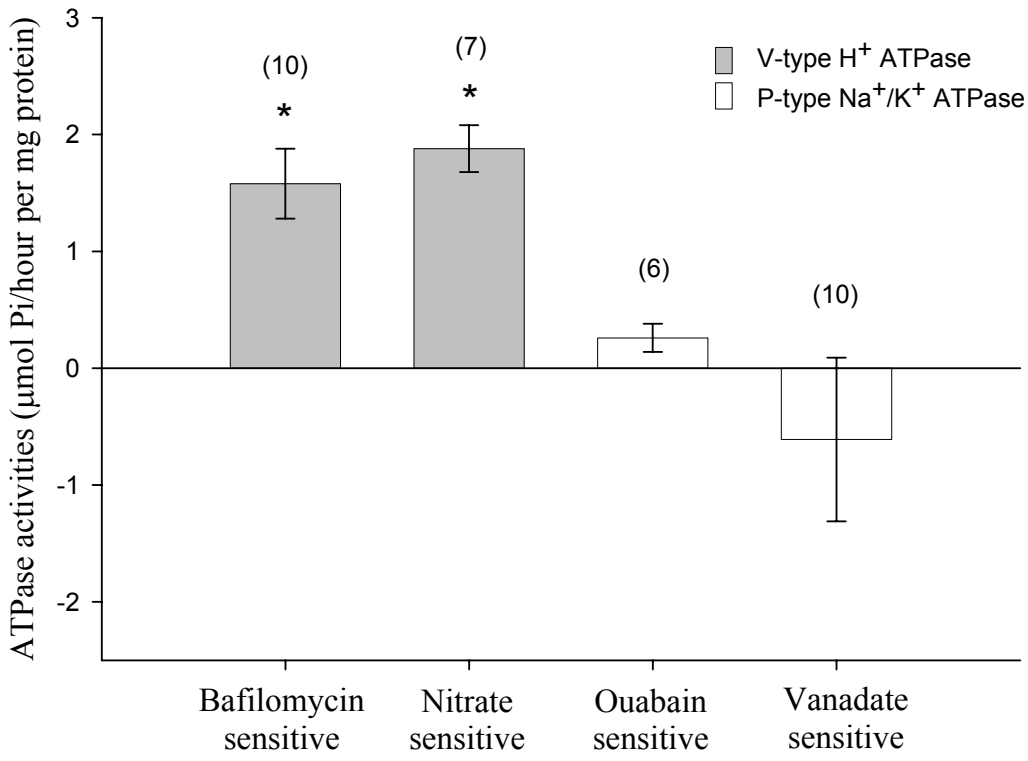
ATPase activities (µmol Pi/hour per mg protein)
3
2
1
0
-1
-2
(10)
*
(7)
*
(6)
(10)
V-type H+ ATPase
P-type Na+/K+ ATPase
Bafilomycin sensitive
Nitrate sensitive
Ouabain sensitive
Vanadate sensitive

activities measured with two different pump inhibitors, bafilomycin A_1 and NO_3^-, were not significantly different, consistent with the complete inhibition of the V-type H^+ ATPase.

Inhibitors of the Na^+/K^+ ATPase had no significant effect on the total ATPase activity. The ouabain-sensitive ATPase activity was 0.26 ± 0.12 μmol/hour per mg protein in 10 determinations, which is not significantly different from zero. Likewise, the nonsensical negative ATPase activity (-0.61 ± 0.70 μmol/hour per mg protein) measured in the presence of vanadate is not significantly different from zero. Again, the use of two different inhibitors, ouabain and vanadate, yielded similar activities of the Na^+/K^+ ATPase consistent with complete inhibition.

5. Discussion

The presence of the V-type H^+ ATPase in Malpighian tubules of Aedes aegypti. The V-type H^+ ATPase is a multi-subunit protein composed of two major functional domains, a cytoplasmic V_1 complex and a membrane integrated V_0 complex. The V_1 complex is the site for ATP binding and hydrolysis. It is composed of eight different subunits A-H including subunit B that was targeted in the present study using the antibody C23. The B subunit is a 56 kDa polypeptide with high sequence identity among several species (27). It is one of the two sites in the V_1 complex that binds ATP, the other is the A subunit (42). The C subunit is a 43 kDa polypeptide to which polyclonal antibody 488-1 binds. The function of the C subunit is not well understood. It is thought to be located outside the V_1 complex and part of the cytoplasmic peripheral linkage that couples V_1 and V_0 complexes. The V_0 complex is composed of five different subunits, designated a to d, that collectively function as the proton translocation pathway (9).

The two polyclonal antibodies, C23 and 488-1, raised against respectively the B and C subunits of the proton pump in the midgut of *Manduca sexta* identified their intended targets in the purified V-type H^+ ATPase and in crude extract of *Aedes* Malpighian tubules (Fig. 3.1B, lanes 3-6), thereby confirming the presence of the two subunits, and hence the presence of the V-type H^+ ATPase in Malpighian tubules of the yellow fever mosquito. Other laboratories have successfully used antibodies to various subunits of the V-type H^+ ATPase to identify this proton pump in Malpighian tubules of the ant, moth and locust (10, 20, 34).

Localization of the V-type H^+ ATPase in the brush border membrane of principal cells. The V-type H^+ ATPase was first identified as an enzyme associated with endosomal membranes of lysosomes, clathrin coated vesicles, and vacuoles of yeast and plants (26, 40). In endosomal membranes, the V_1 complex faces the cytoplasm and the V_0 complex points into the endosomal compartment. Thus protons are moved from the cytoplasm to the endosomal compartment, raising endosomal H^+ concentrations above cytoplasmic concentrations and generating an endosomal membrane potential that is positive inside. Both H^+ and voltage gradients serve a variety of functions. Voltage may drive the entry of Cl^- into the endosome, acidifying the endosomal compartment with HCl, when the endosomal membrane houses Cl^- channels next to the V-type H^+ ATPase (23). The presence of malate channels serves electrogenic uptake of $malate^{2-}$ (32).

In epithelial membranes of animal cells, the V-type H^+ ATPase is often located at the apical side, where again voltage and H^+ gradients can serve activities ranging from signal transduction (7) to nutrient uptake (50) and electrolyte transport (42). The present study shows that the V-type H^+ ATPase is densely expressed in the brush border of principal cells of Malpighian tubules of *Aedes aegypti* (Fig. 3.2). The brush

border is also densely populated by mitochondria (3). Virtually every microvillus is home to a mitochondrion (3). The close spatial relationship between ATP synthesis (mitochondria) and ATP utilization (the V-type H^+ ATPase) suggests a close temporal relationship between metabolism and transepithelial transport (Fig. 3.4A). Indeed, the inhibition of ATP synthesis by dinitrophenol depolarizes the apical membrane voltage from 111 mV to 9 mV within a minute, consistent with the rapid inhibition of transepithelial transport (30). More recent studies confirm that intracellular ATP concentration and electrogenesis by the V-type H^+ ATPase in the apical, microvillar plasma membrane are intimately coupled (46).

In *Aedes* Malpighian tubules, the V-type H^+ ATPase energizes transport not only across the apical membrane, but also across the epithelial shunt and across the basolateral membrane on the other side of the cell (3). As illustrated in Fig. 3.4, the transport of protons from the microvillar cytoplasm to the extracellular space of the brush border constitutes a pump current that must return to the cytoplasmic side of the V-type H^+ ATPase (3). Current passing through the epithelial shunt is carried by Cl^- passing from hemolymph to tubule lumen as the mechanism of transepithelial Cl^- secretion (24). Current passing from the hemolymph into principal cells is carried by K^+ as the major mechanism of secretory K^+ entry into the cell (4).

Although we expected to find the V-type H^+ ATPase at the apical membrane, we cannot be sure about the immunohistochemical evidence for the presence of this proton pump in the cytoplasm of principal cells (Fig. 3.2). The staining of the cytoplasm may reflect antibody binding to parts of the holoenzyme such as V_1 complex. The reversible dissociation of the V_1 complex from the holoenzyme is known as a mechanism for regulating the transport activity of the V-type H^+ ATPase (42). But this dissociation should leave the V_1 complex in close proximity to the site of its dissociation from the holoenzyme, namely in microvilli of the brush border. It

should not yield the diffuse distribution of the B subunit in the cytoplasm. For these reasons we believe that the cytoplasmic signal reflects various aspects of holoenzyme synthesis, sorting and trafficking, although the association of the V-type H^+ ATPase with endosomal membranes of principal cells can not be excluded.

The V-type H^+ ATPase is absent from stellate cells in Malpighian tubules of *Aedes aegypti* (Fig. 3.2). Stellate cells in Malpighian tubules of *Drosophila melanogaster* do not express the V-type H^+ ATPase according to enhancer trapping studies in Dow's lab (39). Moreover, stellate cells are thought to provide the transepithelial Cl^- shunt pathway in *Drosophilia* Malpighian tubules (29). Such a transport role fits also our finding of Cl^--channels in apical membrane patches of *Aedes* Malpighian tubules (28). Mediating passive transepithelial Cl^- transport, stellate cells may not need the V-type H^+ ATPase.

ATPase activities. Between 50% and 60% of the total ATPase activity in extracts of *Aedes* Malpighian tubules can be attributed to a nitrate- and bafilomycin- sensitive component that reflects the activity of the V-type H^+ ATPase. The remaining ATPase activity is likely due to protein kinases, nucleotide cyclases, myosin, DNA helicases, and other ATP-consuming processes. Bafilomycin A_1 is known to inhibit the free V-type H^+ ATPase with an I_{50} of 0.4 nmol/mg protein (6). Our use of a concentration 6000 times (2500 nmol/mg) that much should have completely inhibited the V-type H^+ ATPase in the tubule extracts used in the present study. Consistent with the complete inhibition by bafilomycin is a similar V-type H^+ ATPase activity measured in Malpighian tubules with a maximal dose of nitrate (Fig. 3.3). Nitrate inhibits the free V-type H^+ ATPase with an I_{50} of 50 mM (8).

Bafilomycin is thought to block the proton channel of the V-type H^+ ATPase (48). In contrast, there are two mechanisms for inhibiting the V-type H^+ ATPase by nitrate:

1) via oxidation of the cystine residue on the A subunit with the effect of preventing ATP hydrolysis, and 2) via dissociation of the V_1 from the V_0 complex (8).

Even though the V-type H^+ ATPase activity was measured in a crude extract of Malpighian tubules, the activity most probably reflects the activity of the intact proton pump, i.e. the holoenzyme. The cytosolic V_1 complex is capable of hydrolyzing ATP in a Ca^{2+}-dependent manner, but this hydrolysis is blocked by Mg^{2+} concentrations as low as 0.1 mM (11). The Mg^{2+} concentration in our ATPase assays was 5 mM which should have inhibited any ATP hydrolysis by dissociated V_1 complexes. When the V_1 complex is attached to the V_0 complex and in membrane-bound form, the hydrolysis of ATP is Mg^{2+}- rather than Ca^{2+}-dependent (11). It is believed that the hydrophobic environment of the membrane changes the conformation of the V_1 complex thereby switching the metal requirement to Mg^{2+} (11). Accordingly, the presence of 5 mM Mg^{2+} in our ATP assay should have maximized V-type H^+ ATPase activity of the holoenzyme in apical membrane fragments but inhibited ATP hydrolysis by the dissociated V_1 complexes.

In the present study we measured no detectable ouabain or vanadate sensitive Na^+/K^+ ATPase activity in crude extracts of *Aedes* Malpighian tubules (Fig. 3.3). Likewise, we observed no immediate effects of 1 mM oubain on the transepithelial voltage and resistance of isolated *Aedes* Malpighian tubules (45). In contrast, significant effects of ouabain, such as the partial (~50%) inhibition of transepithelial fluid secretion, were observed after ouabain treatment for more than half an hour (14). In view of the strong expression of the V-type H^+ ATPase detected by immunostaining (Fig. 3.2) and by biochemical (Fig. 3.3) and electrophysiological assays (3, 46), it appears that the V-type H^+ ATPase serves first and foremost epithelial transport mechanisms, and that the Na^+/K^+ ATPase, if it is present, may perhaps serve cell household functions. Accordingly, ouabain will have no immediate effect on

transepithelial transport, but it may compromise transepithelial transport after normal cell household functions have been impaired. Further experiments using a more sensitive assay for the Na^+/K^+ ATPase activity, or immunostaining methods, may help to reveal the presence of the Na^+/K^+ pump in Malpighian tubules of *Aedes aegypti*.

Kinetics and thermodynamics of transport across the apical membrane. Fig. 3.4 illustrates the present model of transepithelial NaCl and KCl secretion by Malpighian tubules of the yellow fever mosquito dependent on the central role of the V-type H^+ ATPase located in the apical membrane of principal cells. Since proton-translocating ATPases can transport as many as 3 protons per ATP hydrolyzed (41), the hydrolysis of 1.7 μmol ATP/hour per mg protein is equivalent to H^+ transport across the apical membrane of the tubule at a rate of 5.1 μmol/hour per mg protein. A single Malpighian tubule of the yellow fever mosquito contains approximately 0.77 μg of protein. Hence, a proton transport rate of 65 pmol/min can be estimated for the whole tubule under control conditions. The estimated proton transport rate comes close to 74 pmol/min, the rate of transepithelial secretion of Na^+ and K^+ (3). The approximation suggests electroneutral Na^+/H^+ and K^+/H^+ exchange transport across the apical membrane with a stoichiometry of 1:1.

Since electroneutral Na^+/H^+ and K^+/H^+ cannot be driven by voltage, the question arises whether the pH difference across the apical membrane has the thermodynamic strength to drive Na^+ and K^+ from cell to lumen in exchange for H^+? A proton transport rate of 65 pmol/min across the apical membrane is expected to decrease the pH in the tubule lumen to values less than 1 in the time of only 1 minute, providing a driving force far greater than needed. However, measurements of the pH in the tubule lumen of Malpighian tubules invariably are close to 7, and measures of cytoplasmic pH are not that far off (2, 33, 49). What then is the minimum pH difference across the

Figure 3.4. Models of transepithelial NaCl and KCl secretion across Malpighian tubules of the yellow fever mosquito. A) Molecular model of transcellular Na^+ and K^+ secretion and paracellular Cl^- secretion, B) electrical equivalent circuit of transepithelial electrolyte secretion. Na^+ and K^+ are actively transported through principal cells and Cl^- is passively transported from hemolymph to tubule lumen through the shunt pathway. E, electromotive force; V, voltage; R, resistance; t, transepithelial; bl and a are basolateral and apical membrane respectively; sh, shunt (From Beyenbach, K.W., 2001, *News Physiol. Sci.* **16**, 145-151)

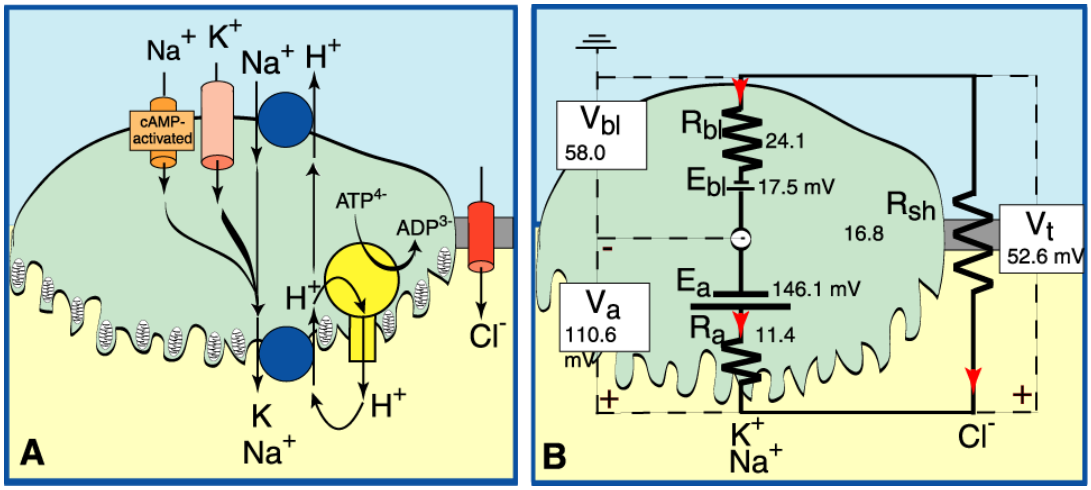
Na+ K+
Na+ H+
cAMP-activated
ATP4-
ADP3-
H+
Cl-
K
Na+
H+
A
Vbl
58.0
Rbl
24.1
Ebl
17.5 mV
Rsh
16.8
Vt
52.6 mV
Ea
146.1 mV
Va
110.6 mV
Ra
11.4
K+
Na+
Cl-
B

apical membrane that is needed to drive Na^+/H^+ and K^+/H^+ exchange transport in *Aedes* Malpighian tubule? The answer to this question requires knowledge of cytoplasmic cation concentrations in principal cells.

In Malpighian tubules of ants, the intracellular K^+ concentration (67 mM) is near electrochemical equilibrium with the K^+ concentration in the hemolymph (18). The equilibrium distribution of K^+ holds probably also true in Malpighian tubules of *Aedes aegypti* in view of a K^+ conductance as large as 64% of the basolateral membrane conductance (4). Accordingly, in the presence of a peritubular K^+ concentration of 3.4 mM and a basolateral membrane voltage of -58 mV, the intracellular K^+ concentration can be estimated as 31.5 mM under control conditions, when the K^+ concentration in secreted (luminal) fluid is 91 mM (3). Thus the movement of K^+ from 31.5 mM in the cell to 91 mM in the lumen requires a nearly 3-fold H^+ concentration difference, or a pH difference of 0.5 across the apical membrane. If the intracellular pH is 7.2, then a lumen pH of 6.7 would be sufficient to drive K^+/H^+ exchange across the apical membrane with a transport stoichiometry of 1:1.

Since fluid secreted into the tubule lumen is not sufficiently acidic to drive cation/H^+ antiport, the pH of an unstirred layer in the brush border might be low enough as in amphibian skin (17). In addition, large negative surface charges of the apical membrane due to fixed negative charges of glycosylated proteins, glycolipids, and adsorbed proteins, may support a surface pH considerably lower than that in the aqueous solution of the tubule lumen (1). Finally, the glycocalyx of the brush border may limit the diffusion of H^+, generating an acid microenvironment akin to that in the intestinal brush border (38). These considerations of the kinetics and thermodynamics of transport suggest, but do not prove, that the transport of K^+/H^+ and Na^+/H^+ across the apical membrane of principal cells of the *Aedes* Malpighian tubule can be electroneutral, as previously suggested for Malpighian tubules of the ant *Formica* (19,

49). Additional experiments are needed to resolve the mechanism, stoichiometry, and regulation of cation/H^+ exchange across the apical membrane.

6. Reference:

1. **Aronson PS and Giebisch G.** Mechanisms of chloride transport in the proximal tubule. *American Journal of Physiology* 273: F179-F192, 1997.

2. **Bertram G and Wessing A.** Intracellular pH regulation by the plasma membrane V-ATPase in Malpighian tubules of *Drosophila* larvae. *Journal of Comparative Physiology B, Biochemical, Systemic, and Environmental Physiology* 164: 238-246, 1994.

3. **Beyenbach KW.** Energizing epithelial transport with the vacuolar H^+ ATPase. *News Physiol Sci* 16: 145-151, 2001.

4. **Beyenbach KW and Masia R.** Membrane conductances of principal cells in Malpighian tubules of *Aedes aegypti*. *Journal of Insect Physiology* 48: 375-386, 2002.

5. **Beyenbach KW, Pannabecker TL, and Nagel W.** Central role of the apical membrane H^+-ATPase in electrogenesis and epithelial transport in Malpighian tubules. *J Exp Biol* 203 Pt 9: 1459-1468, 2000.

6. **Bowman EJ, Siebers A, and Altendorf K.** Bafilomycins: a class of inhibitors of membrane ATPases from microorganisms, animal cells, and plant cells. *Proc Natl Acad Sci USA* 85: 7972-7976, 1988.

7. **Camello C, Pariente JA, Salido GM, and Camello PJ.** Role of proton gradients and vacuolar H^+-ATPases in the refilling of intracellular calcium stores in exocrine cells. *Curr Biol* 10: 161-164, 2000.

8. **Dschida WJ and Bowman BJ.** The vacuolar ATPase: Sulfite stabilization and the mechanism of nitrate inactivation. *J Biol Chem* 270: 1557-1563, 1995.

9. **Forgac M.** Structure, function and regulation of the vacuolar H^+-ATPases. *FEBS Lett* 440: 258-263, 1998.

10. **Garayoa M, Villaro AC, Klein U, Zimmermann B, Montuenga LM, and Sesma P.** Immunocytochemical localization of a vacuolar-type ATPase in Malpighian tubules of the ant *Formica polyctena*. *Cell and Tissue Research* 282: 343-350, 1995.

11. **Graf R, Harvey WR, and Wieczorek H.** Purification and properties of a cytosolic V_1-ATPase. *Journal of Biological Chemistry* 271: 20908-20913, 1996.

12. **Harvey WR, Maddrell SHP, Telfer WH, and Wieczorek H.** H^+ V-ATPases energize animal plasma membranes for secretion and absorption of ions and fluids. *American Zoologist* 38: 426-441, 1998.

13. **Harvey WR and Wieczorek H.** Animal plasma membrane energization by chemiosmotic H^+ V-ATPases. *J Exp Biol* 200: 203-216, 1997.

14. **Hegarty JL, Zhang B, Pannabecker TL, Petzel DH, Baustian MD, and Beyenbach KW.** Dibutyryl cAMP activates bumetanide-sensitive electrolyte transport in Malpighian tubules. *Am J Physiol* 261: C521-C529, 1991.

15. **Huss M.** PhD Dissertation. Struktur, funktion und regulation der plasmamembran V-ATPase von *Manduca Sexta*. University of Osnabrueck http://elib.ub.uni-osnabrueck.de/publications/diss/E-Diss165_thesis.pdf, 2001.

16. **Kyhse Andersen J.** Electroblotting of multiple gels: a simple apparatus without buffer tank for rapid transfer of proteins from polyacrylamide to nitrocellulose. *J Biochem Biophys Methods* 10: 203-210, 1984.

17. **Larsen EH, Christoffersen BC, Jensen LJ, Sorensen JB, and Willumsen NJ.** Role of mitochondria-rich cells in epithelial chloride uptake. *Exp Physiol* 81: 525-534, 1996.

18. **Leyssens A, Dijkstra S, Van Kerkhove E, and Steels P.** Mechanisms of K^+ uptake across the basal membrane of Malpighian tubules of *Formica polyctena*: the effect of ions and inhibitors. *J Exp Biol* 195: 123-145, 1994.

19. **Leyssens A, Steels P, Lohrmann E, Weltens R, and Van Kerkhove E.** Both dinitrophenol and Ba^{2+} reduce KCl and fluid secretion in Malpighian tubules of *Formica*: the role of the apical H^+ and K^+ concentration gradient. *Journal of Insect Physiology* 39: 431-446, 1993.

20. **Lezaun MJ, Garayoa M, Villaro AC, Montuenga L, and Sesma P.** Immunocytochemical localization of a vacuolar ATPase in the Malpighian tubules of two insect species (*Formica polyctena* and *Locusta migratoria*). *Cell Biology International* 18: 407, 1994.

21. **Lin H and Randall DJ.** Proton-ATPase activity in crude homogenates of fish gill tissue: Inhibitor sensitivity and environmental and hormonal regulation. *Journal of Experimental Biology* 180: 163-174, 1993.

22. **Lowry OH, Rosebrough NJ, Farr AL, and Randall RJ.** Protein measurement with the Folin phenol reagent. *Journal of Biological Chemistry* 193: 265-275, 1951.

23. **Marshansky V and Vinay P.** Proton gradient formation in early endosomes from proximal tubules. *Biochimica et Biophysica Acta* 1284: 171-180, 1996.

24. **Masia R, Aneshansley D, Nagel W, Nachman RJ, and Beyenbach KW.** Voltage clamping single cells in intact Malpighian tubules of mosquitoes. *American Journal of Physiology* 279: F747-F754, 2000.

25. **Merzendorfer H, Reineke S, Zhao XF, Jacobmeier B, Harvey WR, and Wieczorek H.** The multigene family of the tobacco hornworm V-ATPase: novel subunits a, C, D, H, and putative isoforms. *Biochim Biophys Acta* 1467: 369-379, 2000.

26. **Nelson N.** Evolution of organellar proton-ATPases. *Biochim Biophys Acta* 1100: 109-124, 1992.

27. **Novak FJ, Graf R, Waring RB, Wolfersberger MG, Wieczorek H, and Harvey WR.** Primary structure of V-ATPase subunit B from *Manduca sexta* midgut. *Biochim Biophys Acta* 1132: 67-71, 1992.

28. **O'Connor KR and Beyenbach KW.** Chloride channels in apical membrane patches of stellate cells of Malpighian tubules of *Aedes aegypti*. *J Exp Biol* 204: 367-378, 2001.

29. **O'Donnell MJ, Rheault MR, Davies SA, Rosay P, Harvey BJ, Maddrell SH, Kaiser K, and Dow JA.** Hormonally controlled chloride movement across *Drosophila* tubules is via ion channels in stellate cells. *Am J Physiol* 274: R1039-R1049, 1998.

30. **Pannabecker TL, Aneshansley DJ, and Beyenbach KW.** Unique electrophysiological effects of dinitrophenol in Malpighian tubules. *American Journal of Physiology* 263: R609-R614, 1992.

31. **Pannabecker TL, Hayes TK, and Beyenbach KW.** Regulation of epithelial shunt conductance by the peptide leucokinin. *Journal of Membrane Biology* 132: 63-76, 1993.

32. **Pantoja O and Smith JA.** Sensitivity of the plant vacuolar malate channel to pH, Ca^{2+} and anion-channel blockers. *Journal of Membrane Biology* 186: 31-42, 2002.

33. **Petzel DH, Pirotte PT, and Van KE.** Intracellular and luminal pH measurements of Malpighian tubules of the mosquito *Aedes aegypti*: The effects of cAMP. *Journal of Insect Physiology* 45: 973-982, 1999.

34. **Pietrantonio PV and Gill SS.** Immunolocalization of the 17 kDa vacuolar H^+-ATPase subunit c in *Heliothis virescens* midgut and Malpighian tubules with an anti-peptide antibody. *J Exp Biol* 198 (Pt 12): 2609-2618, 1995.

35. **Satmary WM and Bradley TJ.** The distribution of cell types in the Malpighian tubules of *Aedes taeniorhynchus* (Diptera Culicidae). *International Journal of Insect Morphology and Embryology* 13: 209-214, 1984.

36. **Scharschmidt BF, Keeffe EB, Blankenship NM, and Ockner RK.** Validation of a recording spectrophotometric method for measurement of membrane-associated Mg^{2+}- and Na^{+}/K^{+}-ATPase activity. *J Lab Clin Med* 93: 790-799, 1979.

37. **Shi SR, Cote RJ, and Taylor CR.** Antigen retrieval techniques: current perspectives. *J Histochem Cytochem* 49: 931-937, 2001.

38. **Shimada T.** Factors affecting the microclimate pH in rat jejunum. *J Physiol* 392: 113-127, 1987.

39. **Sozen MA, Armstrong JD, Yang M, Kaiser K, and Dow JA.** Functional domains are specified to single-cell resolution in a *Drosophila* epithelium. *Proceedings of the National Academy of Sciences of the United States of America* 94: 5207-5212, 1997.

40. **Stevens TH and Forgac M.** Structure, function and regulation of the vacuolar H^{+}-ATPase. *Annu Rev Cell Dev Biol* 13: 779-808, 1997.

41. **Tomashek JJ and Brusilow WSA.** Stoichiometry of energy coupling by proton-translocating ATPases: A history of variability. *Journal of Bioenergetics and Biomembranes* 32: 493-500, 2000.

42. **Wieczorek H, Brown D, Grinstein S, Ehrenfeld J, and Harvey WR.** Animal plasma membrane energization by proton-motive V-ATPases. *Bioessays* 21: 637-648, 1999.

43. **Wieczorek H, Cioffi M, Klein U, Harvey WR, Schweikl H, and Wolfersberger MG.** Isolation of goblet cell apical membrane from tobacco hornworm midgut and purification of its vacuolar-type ATPase. *Methods Enzymol* 192: 608-616, 1990.

44. **Wieczorek H, Gruber G, Harvey WR, Huss M, and Merzendorfer H.** The plasma membrane H+-V-ATPase from tobacco hornworm midgut. *J Bioenerg Biomembr* 31: 67-74, 1999.

45. **Williams JCJ and Beyenbach KW.** Differential effects of secretagogues on the electrophysiology of the Malpighian tubules of the yellow-fever mosquito *Aedes aegypti*. *J Comp Physiol (B)* 154: 301-310, 1984.

46. **Wu DS and Beyenbach KW.** The dependence of electrical transport pathways in Malpighian tubules on ATP. *J Exp Biol* 206: 233-243, 2003.

47. **Yu M and Beyenbach KW.** Leucokinin and the modulation of the shunt pathway in Malpighian tubules. *J Insect Physiol* 47: 263-276, 2001.

48. **Zhang J, Feng Y, and Forgac M.** Proton conduction and bafilomycin binding by the V_0 domain of the coated vesicle V-ATPase. *J Biol Chem* 269: 23518-23523, 1994.

49. **Zhang S, Leyssens A, Kerkhove EV, Weltens R, Driessche WV, and Steels P.** Electrophysiological evidence for the presence of an apical H^+-ATPase in Malpighian tubules of *Formica polyctena*: intracellular and luminal pH measurements. *Pfluegers Archiv (European Journal of Physiology)* 426: 288-295, 1994.

50. **Zhuang Z, Linser PJ, and Harvey WR.** Antibody to H^+ V-ATPase subunit E colocalizes with portasomes in alkaline larval midgut of a freshwater mosquito (*Aedes aegypti*). *J Exp Biol* 202 (Pt 18): 2449-2460, 1999.

CHAPTER 4

ELECTRICAL COUPLING OF PRINCIPAL CELLS VIA GAP JUNCTIONS IN THE MALPIGHIAN TUBULES OF *AEDES AEGYPTI*

1. Abstract

The present study was undertaken to examine Malpighian tubules of the yellow fever mosquito for the presence of gap junctions. Current was injected into one principal cell of the isolated Malpighian tubule and membrane voltage deflections were measured in that cell and 2 consecutive neighboring principal cells. By short-circuiting the transepithelial voltage with the diuretic peptide leucokinin we largely eliminated electrical coupling of the cells through the tubule lumen thereby focusing the data analysis on coupling through gap junctions. The analysis of an equivalent electrical circuit yielded an average gap junction resistance (R_{gj}) of 431 kΩ. The good agreement between the measured input resistance of one principal cell (195 kΩ) coupled to other cells and the input resistances predicted from the equivalent circuit (210 kΩ) validates the use of leucokinin to estimate the gap junction resistance. The addition of the Ca-ionophore A23187 (2 μM) to the peritubular Ringer bath did not affect the gap junction resistance, but metabolic inhibition of the tubule with dinotrophenol (0.5 mM) increased the gap junction resistance from 526 kΩ to 30.8 MΩ, suggesting the regulation of gap junctions by ATP. Lucifer Yellow injected into one principal cell appeared in the tubule lumen but not in neighboring cells. Accordingly, gap junctions allow the passage of current but not Lucifer yellow. The demonstration of gap junctions in Malpighian tubule of *Aedes aegypti* promotes our previous model of the tubule as a single cable to a double cable that improves estimates of electrophysiological variables and the interpretation of electrophysiological data.

2. Introduction

Malpighian tubules of insects initiate the formation of urine by secreting fluid in blind-ended (distal) segments of the tubule. Distal segments of the Malpighian tubule in the yellow fever mosquito, *Aedes aegypti*, consist of two types of epithelial cells: principal cells and stellate cells with a relative distribution of 5:1 (28). However, principal cells make up about 90% of the tubule mass on account of their large size (2). While it is clear that principal cells mediate transepithelial secretion of K^+ and Na^+ from hemolymph to tubule lumen by active transport (3, 5), our previous studies also suggested the electrical coupling of principal cells. For example, current-voltage plots of a single principal cell in an isolated Malpighian tubule yielded rather low cell input resistance that, when compared to measurements of the transepithelial resistance, suggested the electrical coupling of 5 to 6 principal cells (20).

There are two major pathways for coupling epithelial cells in a tubular epithelium. One pathway leads through gap junctions, the other passes through the apical membrane of one cell, through the tubule lumen, and across the apical membrane into neighboring cells. Accordingly, gap junctions couple neighboring cells directly, and the tubule lumen couples them indirectly. Although gap junctions are widely distributed in insects (24, 25), their presence in Malpighian tubules has not been established to this date.

In the present study we present electrophysiological evidence for the presence of gap junctions between principal cells of Malpighian tubules of the yellow fever mosquito. The gap junctions permit the passage of current from one cell to the next but not the dye Lucifer Yellow. Metabolic inhibition of the tubule which is known to reduce intracellular ATP concentrations (36) and to halt transepithelial electrolyte and fluid secretion (6, 7, 21), increases the gap junction resistance about 60-fold, consistent with the regulation of gap junction permeability by ATP.

3. Material and Methods

Mosquitoes and Malpighian tubules. The colony of mosquitoes (*Aedes aegytpi*) was maintained as described previously (22) except for feeding larvae with ground up TetraMin Tropical Flakes. On the day of the experiment a female mosquito (3-7 days post-eclosion) was cold anesthetized and decapitated. A Malpighian tubule was removed under Ringer solution from its attachment to the gut and transferred to Ringer solution in a Lucite perfusion chamber with a filling volume of 1.0 ml. The bottom of the chamber was covered with Parafilm"M" (American National Can, Greenwich, CT) to which Malpighian tubules adhere and stabilize for impalements with microelectrodes. The tubules were viewed from above with a stereoscope microscope at ×50 magnification (Wild, Heerbrugg, Switzerland).

Ringer solution and drugs. Ringer solution contained the following, in mM: 150.0 NaCl, 25.0 HEPES, 3.4 KCl, 1.8 $NaHCO_3$, 1.0 $MgCl_2$, 1.7 $CaCl_2$, and 5.0 glucose. The pH was adjusted to 7.1 with NaOH. The osmolality of the Ringer solution was 320 mosmol/kgH_2O. Synthetic leucokinin-VIII was a gift from Ron Nachman (Texas A&M University).

Electrophysiological studies. All electrophysiological measurements were made in Malpighian tubules resting on Parafilm"M" in the Ringer bath. Malpighian tubules of adult female mosquitoes are on average 3.5 mm long. As shown in Fig. 4.1a, three adjacent principal cells of a Malpighian tubule were selected for impalement with

Figure 4.1. Electrophysiological estimate of the gap junction resistance in isolated Malpighian tubules of the yellow fever mosquito; a) Three adjacent principal cells of a Malpighian tubule are impaled with conventional microelectrodes for measurements of basolateral membrane voltages (V_{bl}). In addition, principal cell 1 is voltage-clamped at desired basolateral membrane voltages with current microelectrode impaling this cell, and the V_{bl} deflections are recorded in cells 1,2 and 3; b) Electrical equivalent circuit of the Malpighian tubule modeled as a double cable. Radial electrical coupling links active transcellular and passive paracellular pathways. Axial electrical coupling links neighboring cells through gap junctions and the luminal fluid. V, voltage; R, resistance; E, electromotive force; gj, gap junction; a, bl, apical and basolateral membrane of principal cell; sh, paracellular shunt pathway, and lu, tubule lumen.

a.

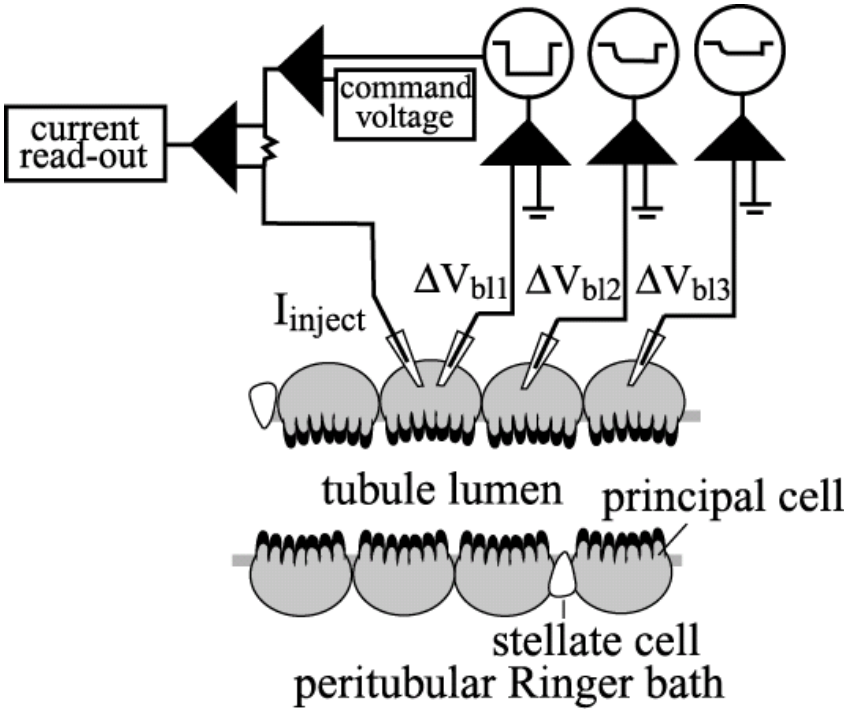
command voltage
current read-out
ΔV_{bl1} ΔV_{bl2} ΔV_{bl3}
I_{inject}
tubule lumen
principal cell
stellate cell
peritubular Ringer bath

b.

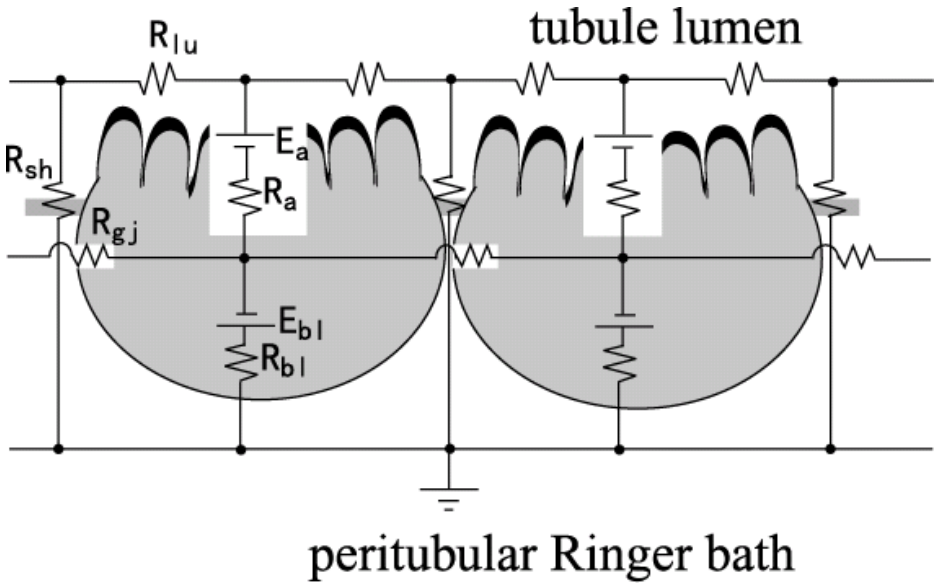
R_{lu}
tubule lumen
R_{sh}
E_a
R_a
R_{gj}
E_{bl}
R_{bl}
peritubular Ringer bath

conventional microelectrodes. Principal cell 1 was selected between 5 and 10 cells away from the blind end of the tubule, and principal cells 2 and 3 were selected towards to the open-end of the tubule. Principal cell 1 was impaled with both current and voltage microelectrodes. The latter measured the basolateral membrane voltage (V_{bl1}), as well as ΔV_{bl1} during voltage clamp. Principal cells 2 and 3 were each impaled with a voltage microelectrode for the measurement of respectively ΔV_{bl2} and ΔV_{bl3} when current was injected into cell 1.

Microelectrodes (Omega dot borosilicate glass capillaries, 30-30-1; Frederick Haer & Co, St Bowdoinham, ME) were pulled on a programmable puller (Model P-97; Sutter Instruments, Novato, CA) to yield resistances between 20 and 30 MΩ when filled with 3 M KCl. The microelectrodes were bridged to the measuring hardware using Ag/AgCl junctions that were prepared by first degreasing the silver wire with alcohol, and then by Cl-plating it in 0.1 M HCl for 20 min at a current of 50 μA. The bath was grounded with an Ag/AgCl wire lodged in a 4% agar bridge of Ringer solution.

The electronic hardware consisted of 1) the GeneClamp model 500B voltage and patch clamp amplifier, 2) head stage HS-2A gain 10MGU for current injection, and 3) head stage HS-2A gain 1LU for voltage recording (Axon Instruments, Sunnyvale, CA). Voltage deflections in principal cells 2 and 3 were recorded with custom-made high-impedance amplifiers (Burr-Brown, 10^{11} Ω). We used Clampfit (pClamp 9) for data analysis (Axon Instruments, Sunnyvale, CA).

All current and voltage data were stored in digital form with the aid of a computer and the A/D converter DigiData1332x (Axon Instruments, Sunnyvale, CA). Current and voltage data from principal cell 1 were also displayed on an oscilloscope (Iwatsu, Japan) and on a strip chart recorder (model BD 41; Kipp and Zonen, Crown Graphic).

Equivalent circuit analysis. The transepithelial secretion of electrolytes in Malpighian tubules of *Aedes aegypti* can be modeled with an electrical equivalent circuit consisting of two major transepithelial transport pathways, one active, the other passive (Fig. 4.1b). The active transport pathway is taken by Na^+ and K^+ through principal cells. It consists of the electromotive forces (E) and the membrane resistance (R) located in apical (a) and basolateral (bl) membranes. The passive pathway is located outside principal cells and is represented by the single shunt resistance (R_{sh}). Electrophysiological evidence has shown that this shunt pathway is the paracellular pathway in *Aedes* Malpighian tubules (21). The paracellular pathway becomes highly permselective to Cl^- in the presence of leucokinin (4, 22). Since both transcellular and paracellular pathways span the epithelium, they are electrically coupled such that cationic current through principal cells equals anionic current through the shunt (Fig. 4.1b). Indeed, the quantity of Cl^- secreted into the tubule lumen approximates the quantities of Na^+ and K^+ secreted into the tubule lumen (3, 5, 35).

In the past we have modeled the Malpighian tubule as a simple electrical cable with only one axial resistance, i.e. the resistance of the tubule lumen also referred as the core resistance (5, 6, 21, 22, 29, 36, 38). In the present study, we model the Malpighian tubule as a cable with two parallel axial resistances, the resistance of the tubule lumen (R_{lu}) and the gap junction resistance (R_{gj}) as shown in Fig. 4.1b. To obtain values of R_{gj}, we simplified the equivalent electrical circuit of Fig. 4.1b by taking advantage of the known effects of the diuretic hormone leucokinin-VIII on the tubule. Leucokinin is known to nearly short circuit the transepithelial voltage (22). It does so by decreasing the paracellular shunt resistance R_{sh} from 57.8 Ωcm^2 to 9.9 Ωcm^2, thereby decreasing the transepithelial voltage from 59 mV to 6 mV (22). Even though the transepithelial voltage does not drop to 0 mV (the true short-circuit condition), the simultaneous and substantial drop in both transepithelial resistance and

voltage indicate that the tubule is essentially short-circuited. The assumption that the tubule is completely short-circuited places the tubule lumen at the same ground potential in the peritubular bath which allows the reduction of the complex electrical circuit of Fig. 4.1b to the much simplified circuit shown in Fig. 4.2b. As will be shown in the Results and Discussion, the assumption that leucokinin completely short-circuits the epithelium introduces negligible error in the data analysis. In brief, the simplification of the electrical circuit of Fig. 4.1b places the resistances R_a, R_{lu} in parallel to R_{bl}. Representing these two parallel resistances as a single non-junctional resistance (R_{nj}) yields a circuit consisting of R_{nj} and the gap junction resistance R_{gj} alone. The two resistances R_{nj} and R_{gj} can be determined as follows.

Fig. 4.2b shows that current injected into principal cell 1 can take three routes. One route is through R_{nj1} to ground, and the second route is from cell 1 to the upstream principal cell through the gap junction R_{gj1}', and the third route is to downstream principal cell through R_{gj1}. Since the gap junction current passing into left and right cells can be assumed to be the same, the current injected into principal cell 1 (I_{inject}) is the sum of three currents (eq. 1)

$$I_{inject} = 2I_{gj1} + I_{nj1} \qquad (1)$$

where I_{gj1} is the gap junction current passing into cell 2 and I_{nj1} is the non-junctional current passing out of cell 1. Fig. 4.2b illustrates further that I_{gj1} is the sum of the gap junction current I_{gj2} and the non-junctional current I_{nj2} passing out of principal cell 2 (eq. 2).

$$I_{gj1} = I_{gj2} + I_{nj2} \qquad (2)$$

I_{gj1} is also the current passing through gap junction 1 according to the difference between the voltage deflections in cell 1 and 2 consequent to the current injected into cell 1 (eq. 3).

Figure. 4.2. Simplifying the double cable model of the Malpighian tubule. The diuretic peptide leucokinin is known to increase the paracellular Cl^- conductance, effectively reducing the shunt resistance R_{sh} to zero (see Fig. 4.1b). a) in the absence of Rsh, both tubule lumen and peritubular medium are at the same ground potential, which renders the apical membrane resistance (R_a) and the tubule lumen (R_{lu}) parallel to the resistance of the basolateral membrane R_{bl}; b) the circuit can be further by combining the parallel resistances as the non-junctional resistance (R_{nj}), leaving a circuit consisting only of the non-junctional resistance and the gap junctional (R_{gj}).

a

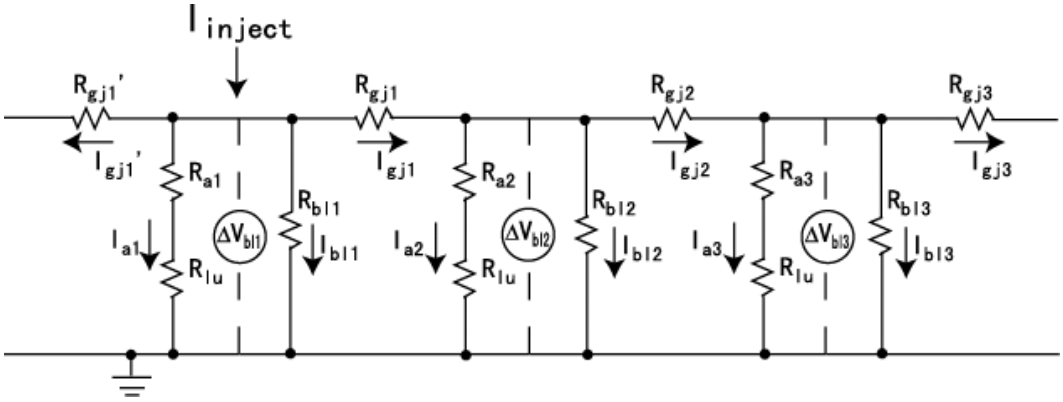
I inject
R gj1'
R gj1
R gj2
R gj3
I gj1'
I gj1
I gj2
I gj3
R a1
R a2
R a3
R b11
R b12
R b13
I a1
I a2
I a3
ΔV bl1
ΔV bl2
ΔV bl3
I b11
I b12
I b13
R lu
R lu
R lu

b

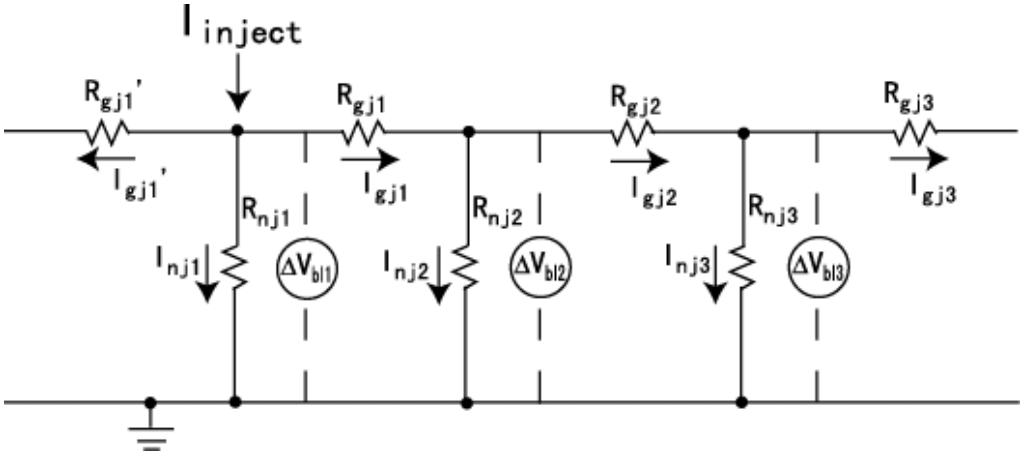
I inject
R gj1'
R gj1
R gj2
R gj3
I gj1'
I gj1
I gj2
I gj3
R nj1
R nj2
R nj3
I nj1
I nj2
I nj3
ΔV bl1
ΔV bl2
ΔV bl3

$$I_{gj1} = \frac{\Delta V_{bl1} - \Delta V_{bl2}}{R_{gj1}} \quad (3)$$

A similar statement can be written for the current I_{gj2} passing from cell 2 to cell 3 (eq. 4).

$$I_{gj2} = \frac{\Delta V_{bl2} - \Delta V_{bl3}}{R_{gj2}} \quad (4)$$

Currents passing through non-junctional resistances obey Ohm's law as follows

$$I_{nj1} = \frac{\Delta V_{bl1}}{R_{nj1}} \quad (5)$$

$$I_{nj2} = \frac{\Delta V_{bl2}}{R_{nj2}} \quad (6)$$

Since it can be assumed that $R_{gj1} = R_{gj2}$ and $R_{nj1} = R_{nj2}$, equations 2 to 6 can be combined to yield

$$I_{inject} = 2\left(\frac{\Delta V_{bl1} - \Delta V_{bl2}}{R_{gj}}\right) + \left(\frac{\Delta V_{bl1} - 2\Delta V_{bl2} + \Delta V_{bl3}}{R_{gj}}\right) \times \frac{\Delta V_{bl1}}{\Delta V_{bl2}} \quad (7)$$

Solving for the gap junction resistance R_{gj} yields

$$R_{gj} = \frac{\frac{\Delta V_{bl1}}{\Delta V_{bl2}} \times (\Delta V_{bl1} - 2\Delta V_{bl2} + \Delta V_{bl3}) + 2(\Delta V_{bl1} - \Delta V_{bl2})}{I_{inject}} \quad (8)$$

and solving for the non-junctional resistance R_{nj} yields

$$R_{nj} = \frac{R_{gj} \times \Delta V_{bl2}}{\Delta V_{bl1} - 2\Delta V_{bl2} + \Delta V_{bl3}} \quad (9)$$

In the typical experiment we first treated the Malpighian tubule to 1 μM leucokinin VIII for 5 min, and then voltage-clamped cell 1 to a hyperpolarizing voltage of 40 mV for 50 ms. We then recorded the steady current injected into cell 1 (I_{inject}) and the steady state basolateral membrane voltage deflections (ΔV_{bl}) in cells1, 2 and 3.

The input resistance. Voltage-clamping cell 1 yields the direct measurement of the input resistance (R_{pc}) as the ratio of $\Delta V_{bl1}/\Delta I_{inject}$ (Fig. 4.1). The input resistance includes cell 1 and all other cells coupled to it as illustrated in Fig. 4.2b. The input resistance can also be predicted from the values of R_{gj} and R_{nj} determined in the circuit analysis above (eqs. 8, 9). Good agreement between measured values of R_{pc} and predicted values would support our measurement of the gap junction resistance by way of the equivalent circuit analysis. To predict values of R_{pc} from values of R_{gj} and R_{nj}, the experimental preparation illustrated in Fig. 4.1a is redrawn in Fig. 4.3 from the perspective of current injected into cell 1 and flowing symmetrically from it into cells upstream and downstream the tubule. The parallel symmetry of all resistances in Fig. 4.3 allows the reduction of all resistances to a single resistance, the predicted R_{pc}. In this data reduction we have limited the number of coupled cells to 7 (See Fig. 4.3) since previous studies have suggested the electrical coupling of 5 to 6 principal cells (20).

Cable analysis. According to the equivalent electrical circuit shown in Fig. 4.2b, current injected into one principal cell passes 1) along a chain of neighboring cells through gap junctions and 2) across cell membranes though non-junctional resistances to ground. As current is injected into cell 1, the voltage deflections (ΔV) decay exponentially from cell to cell along the length of the tubule according to equation 10 where x is the distance from the injected cell (cell 1) and λ is the cell length constant.

Figure. 4.3. Estimate of the input resistance (R_{pc}) from measured values of non-junctional and gap-junctional resistances. The electrical circuit of Fig. 4.2b is redrawn to show the symmetric distribution of current injected into cell 1. R_{pc} can be measured directly as the ratio $\Delta V_{bl1}/ I_{inject}$.

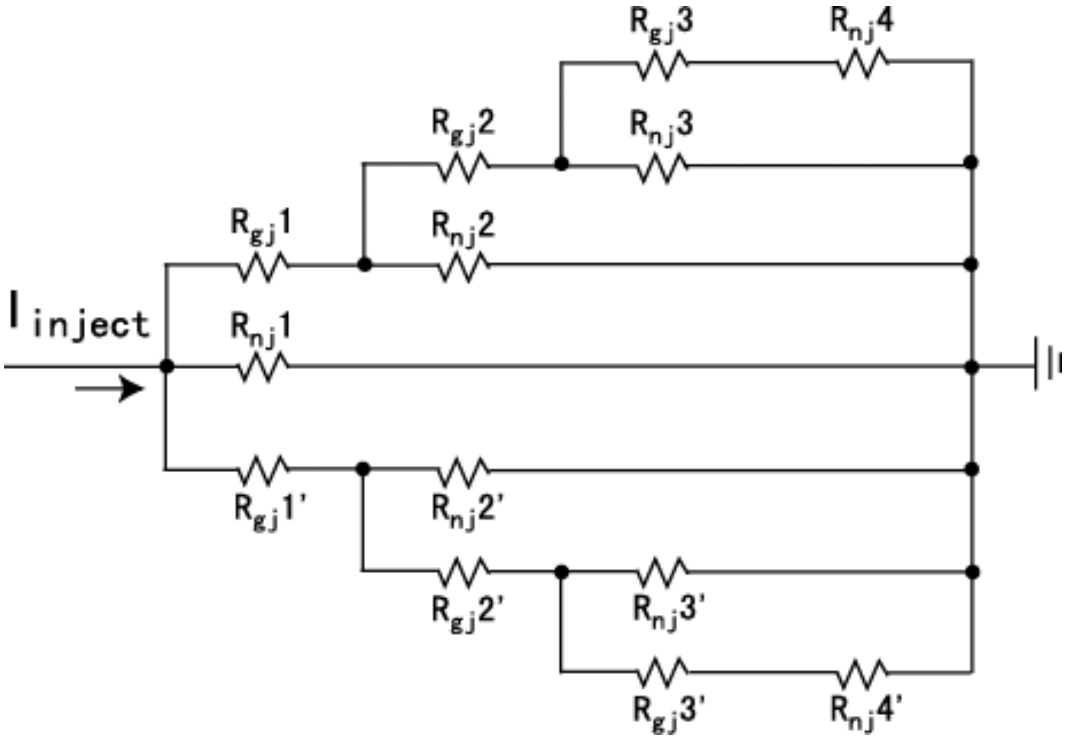
$R_{gj}3$
$R_{nj}4$
$R_{gj}2$
$R_{nj}3$
$R_{gj}1$
$R_{nj}2$
I_{inject}
$R_{nj}1$
$R_{gj}1'$
$R_{nj}2'$
$R_{gj}2'$
$R_{nj}3'$
$R_{gj}3'$
$R_{nj}4'$

$$\Delta V_x = \Delta V_{bl1} \times e^{-\frac{x}{\lambda}} \tag{10}$$

According to cable analysis the length constant λ (ΔV_x at 37% of ΔV_{bl1}) is

$$\lambda = \sqrt{\frac{r_r}{r_a}} \tag{11}$$

where r_r is the length-specific resistance of the cell wall in the radial direction, and r_a is the length-specific resistance of the cell wall in the axial direction. Specifically,

$$r_a = \frac{2\Delta V_{bl1}}{(\Delta I_{inject})\lambda} \tag{12}$$

$$r_r = \frac{2(\Delta V_{bl1})\lambda}{\Delta I_{inject}} \tag{13}$$

where ΔI_{inject} is the current injected into cell 1 (Fig. 4.2b), but one half of the injected current passes upstream and the other downstream the tubule.

Since r_r and r_a are normalized to tubule length, the gap junction resistance R_{gj} and the non-junctional resistance can be estimated. The estimate of R_{gj} neglects the cytoplasmic resistance in view of the large size of principal cells. Since 2 gap junctions are expected to couple cell 1 to cell 3, R_{gj} is

$$R_{gj} = \frac{(r_a)l}{2} \tag{14}$$

and R_{nj} is

$$R_{nj} = \frac{(r_r)2}{l} \tag{15}$$

where *l* is the distance between the voltage electrodes in cell 1 and 3. On average this distance was 247.9 ± 7.5 μm in 14 experiments (Fig. 4.1a).

Lucifer Yellow injections of principal cells. The coupling of principal cells via gap junctions was examined by injecting one principal cell with Lucifer Yellow to observe whether it could appear in neighboring principal cells. After dissection, the Malpighian tubule was transferred to a perfusion bath pre-coated with 0.125 mg/ml poly-L-lysine (Sigma, St. Louis, MO). Malpighian tubules stick to lysine-coated glass as they do Parafilm"M", preventing their movement when a single principal cell is injected with dye. Microinjecting pipettes were made from borosilicate glass (TW100F-4, WPI, Sarasota, FL) using a horizontal puller (P87, Sutter Instrument Co., Novato, CA) and a two-step pulling protocol. Injection pipettes had an average resistance of 4.33 ± 0.37 MΩ (n=9) when filled with 3 M KCl. For injections of Lucifer Yellow, the pipette was back-filled by capillary action with a 2.5 mM Lucifer Yellow CH dilithium salt (Sigma, St. Louis, MO) dissolved in water. After impaling a principal cell, a hydrostatic pressure of approximately 5,172 mmHg was applied to the pipette for 250 ms with the aid of a pneumatic picopump (PV830, WPI, Sarasota, FL). The pressure pulse injected a volume of approximately 0.7 pl as determined in pre-experiment pipette calibrations. Lucifer Yellow injected into a principal cell was immediately visible when viewed with an inverted microscope (Diaphot, Nikon, Kawasaki, Japan) equipped with a B-3A filter (Chroma Technology, Brattleboro, VT) and a mercury lamp light source (Chiu Technical Corp., Kings Park, NY). We typically watched the tubule for more than one hour for signs of Lucifer Yellow diffusing from the injected principal cells to the adjacent principal cells or stellate

cells. To prevent photo bleaching of the dye, we turned on the light source only briefly every 10 min.

Computational simulation of the electrical properties of a Malpighian tubule. After finding the evidence for gap junctions in *Aedes* Malpighian and determining the gap junction resistance, it was clear that an electrical model of the Malpighian tubule should be a double cable. In previous studies we have treated the tubule as a single cable in order to determine electromotive forces (emf) and the resistances of transcellular and paracellular transport pathways (6, 21, 22). It was therefore important to reevaluate all emfs and resistances for the double cable model of the tubule. In brief, we modeled the tubule as a linear series of 10 principal cells (21) where each cell was represented by the electrical circuit shown in Fig. 4.1b. Moreover, the ten principal cells were modeled to represent the physiological condition where the cells electrically separate the tubule lumen from the hemolymph in the insect or the peritubular bath in the isolated perfused Malpighian tubule. The analysis of this tubule model with the software of Electronics Workbench® 5.12 (National Instruments, Austin, Texas) allows current to be injected at any position in the circuit to observe voltage deflections across any two points of the circuit. By simulating our previous *in vitro* microperfusion experiment, where a known current was injected into the tubule lumen at one end of the tubule (21), we fitted emfs and resistances of the tubule to the real voltage data collected previously in the single cable analysis. However, since the data were fitted to a double cable model of the tubule we obtained new values of emfs and resistances.

Statistical evaluation of data. Each tubule/cell was used as its own control so that the data could be analyzed for the difference between paired samples, control vs. experimental (paired Student's *t*-test).

4. Results

Estimate of the gap junction resistance by equivalent circuit analysis. Fig. 4.4 illustrates a typical experiment for estimating the gap junction resistance R_{gj} and the non-junctional resistance R_{nj} in a Malpighian tubule. Cells 1, 2 and 3 were impaled with current and voltage electrodes as shown in Fig. 4.1a. After obtaining a current-voltage (I-V) plot under control conditions (Fig. 4.4a), the tubule was treated with leucokinin-VIII to reduce the shunt resistance R_{sh}, and a second I-V plot was taken. Only cell 1 was voltage-clamped to four preset hyperpolarizing voltages 10 mV apart, 50 ms each. The voltage clamp steps in cell 2 and 3 progressively decreased due to current loss across cell membranes and through gap junctions (Fig. 4.4b). In the presence of leucokinin the voltage deflections decrease in principal cells 2 and 3 in view of 1) the increase in the Cl^- conductance of the paracellular shunt pathway (37), and 2) the increase in the Ca^{2+} conductance of the basolateral membrane of principal cells (38).

Table 4.1 summarizes the results of 14 experiments. Under control conditions the basolateral membrane voltage (V_{bl}) was –82.2 mV in principal cell 1 (and similar in cells 2 and 3, data not shown). Clamping V_{bl1} to a hyperpolarizing voltage 40 mV above the resting membrane voltage required the intracellular injection of 168.8 nA (Table 4.1). Consequent to the current injection, the basolateral membrane voltages in principal cells 2 and 3 (ΔV_{bl}) hyperpolarized by 20.7 mV and 11.9 mV respectively.

Figure 4.4. Current-voltage relationships in principal cells in the absence and presence of leucokinin VIII. a) Current and voltage profiles when cell 1 is voltage-clamped at 4 progressive hyperpolarizing voltages of 10 mV each. Steady state voltages and currents were taken at 45 ms after the each voltage clamp step; b) current-voltage plots in three consecutive cells before and after treatment of LKVIII. V_{bl}, basolateral membrane voltage; 1, 2, 3, cell 1, 2 and 3 respectively.

a.

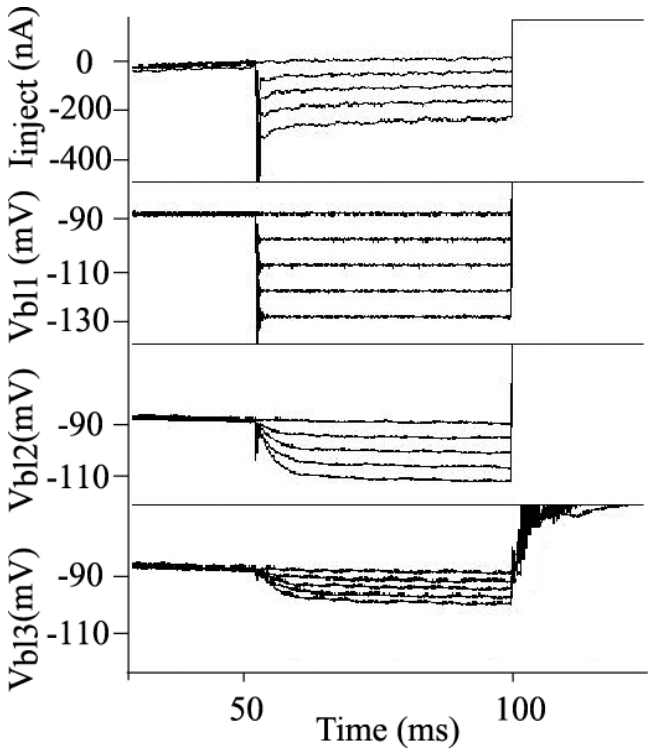
Iinject (nA)
0
-200
-400
Vb11 (mV)
-90
-110
-130
Vb12(mV)
-90
-110
Vb13(mV)
-90
-110
50
100
Time (ms)

b.

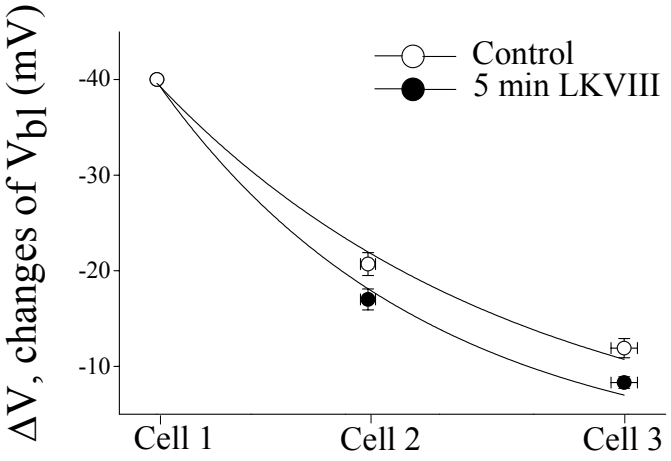
ΔV, changes of Vb1 (mV)
-40
-30
-20
-10
Control
5 min LKVIII
Cell 1
Cell 2
Cell 3

Table 4.1. Measurement of the gap junction resistance R_{gj} in Malpighian tubules of *Aedes aegypti* by circuit analysis.

	Control	**Leucokinin-VIII**
V_{bl1} (mV)	-82.2 ± 2.5	-100.4 ± 2.7*
I_{inject} (nA)	168.8 ± 13.5	211.5 ± 16.1*
ΔV_{bl1} (mV)	40	40
ΔV_{bl2} (mV)	20.7 ± 1.2	17.0 ± 1.0*
ΔV_{bl3} (mV)	11.9 ± 1.0	8.3 ± 0.6*
R_{gj} (kΩ)		431.0 ± 56.5
R_{nj} (kΩ)		546.7 ± 59.3
Measured R_{pc} (kΩ)	246.5 ± 17.8	194.8 ± 14.3*
Predicted R_{pc} (kΩ)		209.6 ± 15.4

Values are means ± SE of 14 experiments; * significantly different ($P<0.05$) from control by the paired Student's t-test. V_{bl}, basolateral membrane voltage; 1,2,3 principal cell 1,2 and 3 respectively; R_{nj}, non-junctional resistance; R_{pc}, input resistance of the current-injected principal cell. Leucokinin-VIII is used to eliminate electrical coupling of principal cells through the tubule lumen.

In the presence of leucokinin-VIII V_{bl} significantly hyperpolarized from to -100.4 mV (Table 4.1). The hyperpolarization of V_{bl} is due to the increased coupling of the basolateral membrane voltage to the apical membrane voltage as the shunt resistance drops to 12% of control values, nearly short-circuiting the transepithelial voltage (22). In the presence of leucokinin-VIII, cells 1, 2, and 3 are electrically coupled by primarily gap junctions (see Methods). According to the experimental design developed in equations 1-9, the voltage deflections in cells 2 and 3 allow estimates of the gap junction resistance, 431.0 kΩ, and the non-junctional resistance, 546.7 kΩ (Table 4.1). Importantly, these values were derived from the current-voltage plots and the circuit analysis as described in eq. 1-9, i.e. independently of the cell input resistance.

Measured and predicted input resistances. Table 4.1 shows the input resistance of principal cell 1 (R_{pc}) measured as the ratio of $\Delta V_{bl1}/\Delta I_{inject}$ (inverse of the slope of the I-V plot) was 246.5 kΩ under control conditions. The input resistance fell significantly to194.8 kΩ in the presence of leucokinin-VIII. The decrease reflects in part 1) the increased transcellular secretion of Na^+ and K^+ in the presence of the diuretic hormone leucokinin (4, 14, 22), and 2) the activation of Ca^{2+} channels in the basolateral membrane (38).

Using the values of R_{gj} and R_{nj}, the input resistance can be calculated by reducing all resistances in Fig. 4.3 to the single resistance R_{pc}. The reduction predicts an R_{pc} of 209.6 kΩ in the presence of leucokinin-VIII (Table 4.1), which comes close to the measured R_{pc}, 194.8 kΩ, in the same tubules.

Cable analysis of R_{gj} and R_{nj}. In the same fourteen tubules we had measured the distance between voltage electrodes 1,2, and 3 impaling principal cells 1,2 and 3

respectively. A two-parameter exponential decay curve was fitted to mean values of voltage deflections along the tubule. The equation of this curve was

$$\Delta V_x = (-38.5\, mV) \times e^{-\frac{x}{0.016}}$$

with a length constant λ of 0.016 cm or 160 μm (and a regression correlation coefficient of 0.99). Using equations 12 and 13 yields 26.7 MΩ/cm as the gap junction resistance and 6.5 kΩcm as the non-junctional resistance, both normalized to tubule length, in the presence of leucokinin-VIII (Table 4.2). Equations 14 and 15 yields the single cell gap junction resistance R_{gj} of 327.3 kΩ and 524.9 kΩ as the non-junctional resistance R_{nj} in 14 tubule experiments (Table 4.2).

Diffusional coupling of principal cells tested with Lucifer Yellow. As shown in Fig. 4.5, one principal cell of the Malpighian tubule was microinjected with Lucifer Yellow at time zero. At the time of injection, the fluorescence of Lucifer Yellow was confined in the injected principal cells. About five seconds after the injection, the fluorescence of Lucifer Yellow started to appear in the tubule lumen and one minute later the dye exited the lumen at the open end of the tubule, indicating the secretion of Lucifer Yellow across the apical membrane of the injected principal cell. *Although* the fluorescent intensity of Lucifer Yellow faded with time in the injected cell (Fig.4.5), no fluorescence was observed in the neighboring principal cells or in the stellate cells, not even after 60 minutes. We made these observations consistently in eight additional tubule experiments.

Physiological regulation of gap junctions. Since it is known that intracellular calcium and metabolic inhibitors can close gap junctions, we tested the effects of the

Table 4.2. Measurement of the gap junction resistance R_{gj} in Malpighian tubules of *Aedes aegypti* by cable analysis.

	Control	**Leucokinin-VIII**
ΔV_{bl1} (mV)	40	40
I_{inject} (nA)	168.8 ± 13.5	211.5 ± 16.1*
Length constant λ (cm)		0.016 ± 0.001
Radial resistance r_m (kΩcm)		6.5 ± 0.5
Axial resistance (MΩ/cm)		26.7 ± 2.6
R_{gj} (kΩ)		327.3 ± 32.7
R_{nj} (kΩ)		524.9 ± 42.6

Values are means ± SE of the same 14 experiments of Table 4.1; * significantly different ($P<0.05$) from control by the paired Student's t-test. V_{bl1}, basolateral membrane voltage of principal cell 1; I_{inject}, current injected into principal cell 1; R_{nj}, non-junctional resistance.

Figure. 4.5. The absence of chemical coupling in a representative Malpighian tubule of *Aedes aegypti*. One principal cell was injected with Lucifer Yellow dye and the gap junction permeability to the dye was monitor with the fluorescence of the dye at time indicated (numbers: in minutes).

Provided by Dr. MJ Yu

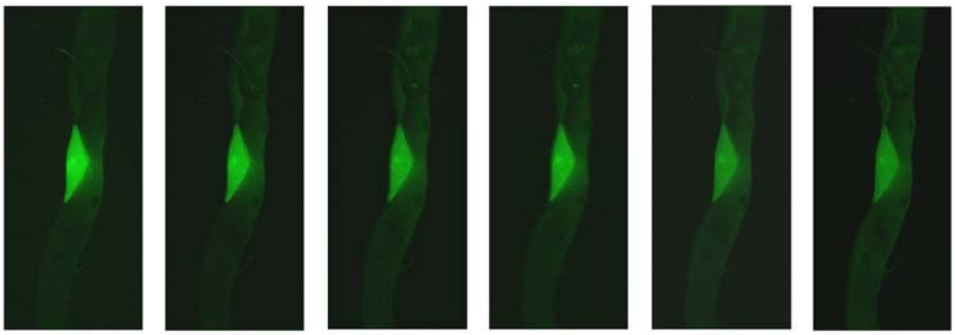
10
20
30
40
50
60

calcium ionophore A23187 and dinitrophenol (DNP) on the gap junction resistance (R_{gj}) and the non-junctional resistance (R_{nj}). In these experiments we first treated the isolated Malpighian tubule with 1 μM LKVIII to measure R_{gj} and R_{nj} by the circuit analysis described above (Figs. 4.1,2, Table 4.1). After 5 min in the presence of LKVIII we added 2 μM A23187 to the peritubular medium and took measurements of R_{gj} and R_{nj} 5 min later. We then added 0.5 mM DNP to the peritubular Ringer bath (in the presence of LKVIII and A23187) and measured R_{gj} and R_{nj} 2 min later. Table 4.3 summarizes the results of 8 tubule experiments.

The addition of LKVIII to the peritubular bath significantly ($p< 0.05$) hyperpolarized the basolateral membrane voltage in principal cell 1 from -83.5 to -103.3 mV (Table 4.3). The circuit analysis of voltage deflections in neighboring cells (eq. 1-9) yielded an average gap junction resistance of 468.0 kΩ and a non-junctional resistance of 578.5 kΩ in the presence of leucokinin-VIII in eight Malpighian tubules.

After 5 min in the presence of A23187, V_{bl1} was -99.3 mV which is not significantly different from -103.3 mV before application of A23187 (Table 4.3). Likewise, the increase in the gap junction resistance from 468.0 kΩ to 526.1 kΩ is not statistically significant. In contrast, the decrease in the non-junctional resistance (R_{nj}) from 578.5 kΩ to 504.0 kΩ reached statistical significance. The decrease in R_{nj} is further reflected in the significant decrease in the measured input resistance (R_{pc}) from 214.9 kΩ to 193.7 kΩ in the presence of A23187 (Table 4.3).

Upon the addition of 0.5 mM dinitrophenol (DNP) to the peritubular medium, the basolateral membrane voltage significantly dropped from -99.3 mV to -13.5 mV (Table 4.3). In parallel, the gap junction resistance R_{gj} increased nearly 60-fold from 526.1 kΩ to 30,762 kΩ. The non-junctional resistance R_{nj} increased 3-fold from 504.0 kΩ to 1483.8 kΩ. The significant effects of DNP on R_{gj} and R_{nj} are reflected in the

Table 4.3. The effects of the Ca^{2+} ionophore A23187 (2 μM)and dinitrophenol (DNP, 0.5 mM) on the gap junction resistance (R_{gj}).

	Control (8)	Leucokinin-VIII (1 μM) (8)	A23187 (2 μM) (8)	Dinitrophenol (0.5 mM) (6)
V_{bl1} (mV)	-83.5 ± 3.3	-103.3 ± 2.1*	-99.3 ± 3.6	-13.5 ± 4.3*
R_{pc} (kΩ)	273.7 ± 22.1	214.9 ± 9.3*	193.7 ± 5.8*	1,474.3 ± 191.3*
R_{gj} (kΩ)		468.0 ± 72.2	526.1 ± 76.6	30,762.1 ± 6594.6*
R_{nj} (kΩ)		578.5 ± 60.9	504.0 ± 63.1*	1,483.8 ± 109.2*

Values are means ± SE (number of tubule experiments); * significantly different ($P<0.05$) from the previous treatment or control by the paired Student's t-test. V_{bl1}, basolateral membrane voltage of principal cell 1; R_{pc}, input resistance of the current-injected principal cell ; R_{nj}, non-junctional resistance. Tubules were first treated with leucokinin-VIII, then with A23187 in the presence of leucokinin-VIII , and finally with dinitrophenol in the

significant increase in the measured input resistance which increased from 193.7 kΩ to 1474.3 kΩ in the presence of DNP (Table 4.3).

5. Discussion

The electrophysiological evidence for gap junctions in Malpighian tubules of Aedes aegypti. We have used two independent experimental approaches to measure the gap junction resistance between principal cells of Malpighian tubules of the yellow fever mosquito. In the first method we modeled the Malpighian tubule as an electrical cable inside an electrical cable (double cable, Fig. 4.1) and used circuit analysis to measure the gap junction resistance. In the second method we used cable analysis of the voltage deflections along principal cells when only one principal cell was voltage clamped. Importantly, both circuit analysis and cable analysis were performed in each tubule. The circuit analysis of 14 tubules yielded a gap junction resistance of 431 kΩ (Table 4.1), and the cable analysis yielded a gap junction resistance of 327 kΩ in the same tubules (Table 4.2). Although the two measurements are significantly different, they both document electrical coupling between principal cells. We consider the circuit analysis to deliver the more accurate measurement of the gap junction resistance for the following reason: The circuit analysis which is independent of the input resistance (eqs. 1-9) yields values of the gap junctional and non-junctional resistances from which the input resistance can be predicted. The predicted input resistance is 210 kΩ (Fig. 4.3). The measured input resistance, 195 kΩ, is not significantly different, which strengthen the case for measuring the gap junction resistance by circuit analysis. We have less confidence in the cable analysis as it requires more assumptions than the circuit analysis.

The gap junction resistance of 431 kΩ reflects the contributions of all gap junctions that connect one principal cell with a single neighboring principal cell.

Expressing this resistance as conductance yields 2.32 μS. The single gap junction conductance between two cells of clone C6/36 derived from the mosquito *Aedes albopictus* is 375 pS (12). Assuming a similar conductance in Malpighian tubules of *Aedes aegypti*, we estimate 6,200 gap junctions between one principal cell and the next in the *Aedes* Malpighian tubule. The estimate appears rather high. However, insect epithelia capable of high secretion rates appear to exhibit an unusual degree of electrical coupling. Applying cable analysis in studies of the electrical coupling of epithelial cells in *Drosophila* salivary glands, Loewenstein et al. measured gap junction resistances of 62 kΩ, equivalent to a gap junction conductance of 16.1 μS (19). Cable analysis in *Aedes* Malpighian tubule yields a gap junction resistance of 3.0 μS (Table 4.2). Thus, epithelial cells in insect salivary glands display more than 5 times the electrical coupling we observe through gap junctions we observe in Malpighian tubules.

It is possible that the electrical coupling between principal cells involves gap junctions as well as cytoplasmic bridges (8). Cytoplasmic bridges are thought to represent aqueous continua large enough to permit the passage of large particles and even organelles (8, 16). In cell pairs of an *Aedes* cell line, Bukaushas et al. (9) contribute to cytoplasmic bridges the passage of Lucifer Yellow (443 Da) and a molecule ten times as heavy FITC-dextran (4,400 Da). Since Lucifer Yellow, the smaller molecule of the two, was unable to diffuse from one principal cells to the next, it is unlikely that cytoplasmic bridges account much for electrical coupling in *Aedes* Malpighian tubules.

Our measurement of the gap junction resistance in the *Aedes* Malpighian tubule takes on added significance because it reflects the gap junction resistance taken under conditions when the isolated tubule secretes fluid in vitro as it does in vivo. In other studies, the gap junction resistance was determined in salivary glands with a lumen

perfused with sucrose (18), in cell pairs of cloned insect cells (11, 12), in cell pairs isolated from salivary glands (33), in cultured insect cell lines (10), and *Xenopus* oocytes expression system (26).

Critical assumptions. Our measurement of the gap junction resistance in *Aedes* Malpighian tubules depends on two critical assumptions: 1) the current distribution assumption, and 2) the leucokinin assumption.

The current distribution assumption states that the current injected into one principal cell of the isolated tubule splits equally in both directions along the tubule. The assumption is based on the reason that neighboring principal cells should be similar in their electrical properties. Indeed, in the course of our study we have found that the decay of ΔV_{bl} was quantitatively similar in both directions (data not shown). In addition, cable theory predicts that the injected current will decay to less than 5% when the distance from the injection site exceeds 3 length constants or 3.7 principal cells in view of a length constant of 0.016 cm (Table 4.2). Since we always selected principal cell 1 for voltage-clamping (and current injection) between 5 and 10 cells distal to the blind end of the tubule, we reduced, if not eliminated current asymmetries upstream as well as downstream. Furthermore, the good agreement between the measured and predicted input resistance (Table 4.1) supports the symmetrical distribution of injected current, since predicting the input resistance rests on the symmetrical circuit shown in Fig. 4.3, where no more than 7 principal cells are needed for predicting the input resistance from values of the gap-junctional and non-junctional resistances. Seven principal cells means 3.5 cells on either side of the injected cell. Between 5 and 10 cells were on either side in our experiments.

We have used the leucokinin assumption in order to simplify the double cable model of the tubule (Fig. 4.1) to a circuit that eliminates electrical coupling of cells

through the tubule lumen (Fig. 4.2). Specifically, we assumed that leucokinin reduces the paracellular shunt resistance to zero, thereby short-circuiting the epithelium. The short-circuit places the tubule lumen at the same ground potential as the peritubular bath and leaves cell-to-cell junctions as the only possibility for electrical coupling. There are two potential pitfalls in the leucokinin assumption. First, using the diuretic peptide leucokinin, we measured the gap junction resistance in tubules stimulated with leucokinin and not in control tubules. Second, although leucokinin reduces the paracellular shunt resistance nearly 6-fold and causes the transepithelial voltage to drop from 59 mV to 6 mV (22), the epithelium is not completely short-circuited as required by the leucokinin assumption. After measuring the gap junction resistance with the aid of leucokinin it was therefore prudent to test the leucokinin assumption. In particular, we evaluated the effect of the paracellular shunt resistance on the gap-junctional resistance and the non-junctional resistance using the circuit analysis software Electronics Workbench®. Table 4.4 summarizes this circuit analysis.

The Malpighian tubule was modeled as a double cable consisting of 10 principal cells in series, each cell represented by the equivalent electrical circuit shown in Fig. 4.1b. Current was injected into principal cell 5 (center tubule), mimicking the experimental design for measuring the gap junction resistance by circuit analysis. The effect of R_{sh} on R_{gj} and R_{nj} was evaluated with the software of the Electronics Workbench®, keeping constant the values of the apical membrane resistance (2.25 MΩ), the basolateral membrane resistance (2.75 MΩ), and the lumen resistance (262 kΩ), all per unit cell. The gap junction resistance at the short-circuit condition, when the shunt resistance is zero, is 431 kΩ.

Table 4.4. The effect of the shunt resistance R_{sh} on the gap junction resistance R_{gj} and the non-junctional resistance R_{nj}.

Shunt resistance R_{sh} (kΩ)	0.1	3.87	10	23.2	50
Gap junction resistance Rgj (kΩ)	430.7	427.2	424.6	422.7	422.5
Non-junctional resistance Rnj (kΩ)	1261.6	1362.9	1464.8	1592.2	1710.9

The analysis shows that as the shunt resistance increases 500-fold from 0.1 kΩ to 50 kΩ, the gap junction resistance decreases by only 8 kΩ, from 430 kΩ to 422 kΩ. The neglible effect of the shunt resistance on the measurement of the gap junction resistance stems from contrasting resistances of the apical membrane resistance (2.25 MΩ) of the single principal cell and the gap junction resistance (431 kΩ) that reduces electrical coupling through the tubule lumen, thereby minimizing the effect of the extracellular shunt resistance on the gap junction resistance.

Two shunt resistances in Table 4.4 deserve further attention: 23.2 kΩ is the shunt resistance of a single principal cell under control conditions, and 3.87 is the shunt resistance in the presence of leucokinin. The corresponding gap junction resistances are 422.7 kΩ and 427.2 kΩ. The negligible effect of leucokinin on the gap junction resistance justifies our experimental strategy for using this diuretic peptide to eliminate electrical coupling through the tubule lumen.

Revised equivalent circuit of the Aedes Malpighian tubule. In previous studies we have modeled the Malpighian tubule as a single cable that consists of a single axial resistance, i.e. the tubule lumen, and a radial resistance, the epithelial cell wall (Fig. 4.6a). The present study shows that the tubule should be modeled as a double cable with two independent axial resistances, the lumen resistance and the gap junction resistance (Fig. 4.6b). Accordingly, the electrical parameters of the tubule we previously determined on the basis of a single cable should be revised on the basis of the double cable. The new set of electrical parameters were determined by fitting previous data of membrane and transepithelial voltages summarized in our 1993 study (21) to the new equivalent circuit model that includes the gap junction resistance (Fig. 4.6). Fitting old and new data to the double cable model of the tubule was done with the software Electronics Workbench®.

Figure. 4.6. Reexamination on values of the electrical elements in Malpighian tubule cells; a) Previous estimates of R_{sh}, R_{bl}, R_a, E_{bl}, R_{core} and E_a of principal cells based on single cable model; b) Values rectified based upon double cable model.

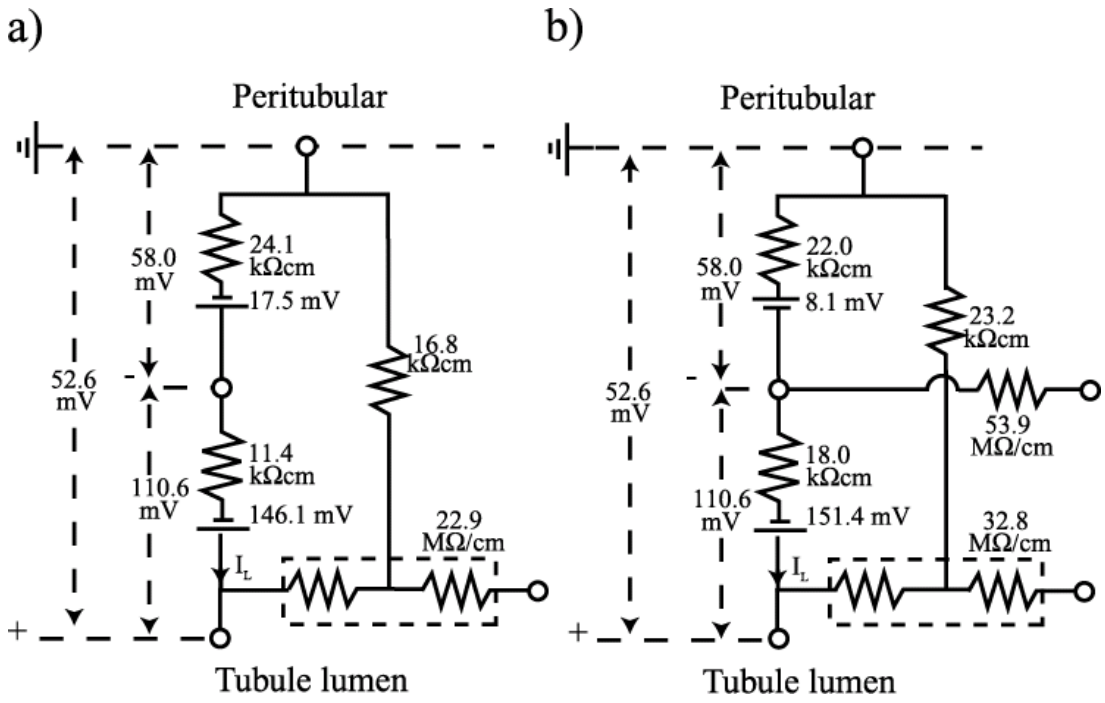
a)
Peritubular
58.0
mV
24.1
kΩcm
17.5 mV
52.6
mV
16.8
kΩcm
11.4
kΩcm
110.6
mV
146.1 mV
22.9
MΩ/cm
I_L
+
-
Tubule lumen
b)
Peritubular
58.0
mV
22.0
kΩcm
8.1 mV
23.2
kΩcm
52.6
mV
53.9
MΩ/cm
18.0
kΩcm
110.6
mV
151.4 mV
32.8
MΩ/cm
I_L
+
-
Tubule lumen

One major revision concerns the value of the fractional membrane resistance of the basolateral membrane (f_{Rbl}) which is the voltage divider ratio of the basolateral membrane voltage deflection over the transepithelial voltage deflection upon injecting current into the lumen of the isolated perfused Malpighian tubule (21). When the tubule modeled as a single cable (Fig. 4.6a) the value of f_{Rbl} is 0.62 which means that 62% of the transcellular resistance resides at the basolateral membrane and 28% at the apical membrane. When the tubule is modeled as a double cable (Fig. 4.6b), f_{Rbl} decreases to 0.55. Thus, the revised circuit model of the tubule has 55% of the transcellular resistance residing at the basolateral membrane and 45% at the apical membrane. Normalizing membrane resistances per cm tubule length, the resistance of the basolateral membrane decreases from 24.1 kΩcm in the single cable to 22.0 kΩcm in the double cable, and the apical membrane resistance increases from 11.4 kΩcm to 18.0 kΩcm (Fig. 4.6).

The second major revision concerns the value of the paracellular shunt resistance R_{sh}. In previous studies that modeled the tubule as a single cable R_{sh} was estimated as 16.8 kΩcm on the assumption that metabolic inhibition of the tubule with dinitrophenol inhibited transcellular active transport with the effect of increasing the transecellular resistance at least 4-fold (21). Modeling the tubule as a double cable we find that DNP increases the transcellular resistance only two-fold, bringing about the upward revision of the shunt resistance from 16.8 kΩcm to 23.2 kΩcm (Fig. 4.6). Other revisions of the equivalent circuit include the change of the electromotive force of the basolateral membrane from 17.5 mV to -8.1 mV, and the change of the electromotive force (emf) of the apical membrane from 146.1 mV to 151.4 mV.

The double cable model of the Malpighian tubule resolves the discrepancy we previously observed between diameter of the tubule lumen measured optically and electrically. Measured through the microscope, the lumen of the *Aedes* Malpighian

tubule has a diameter between 10 and 15 μm. But the lumen diameter calculated from core resistance (22.9 MΩ) in the single cable model is 22 μm (Fig. 4.6a). When the tubule is modeled as a double cable, the lumen resistance is 32.8 MΩ (Fig. 4.6b) which is equivalent to a lumen diameter of 16 μm (1, 15) that comes close to optical diameter of the lumen. There are two axial resistances down the tubule in the double cable model: the gap junction resistance and the lumen resistance (Fig. 4.6). In the single cable model, there is only one axial resistance, the core resistance. The core resistance includes the lumen resistance parallel with the gap junction resistance, reducing the core resistance (22.9 MΩ) below the lumen resistance (32.8 MΩ) thereby extending the 'electrical diameter' of the core beyond the lumen diameter into the epithelial cells of tubule.

Permeable to current but not to Lucifer Yellow. Lucifer Yellow injected into one principal cell did not diffuse into neighboring cells, indicating that gap junctions between principal cells or between principal cells and stellate cells do not permit the passage of this dye (Fig. 4.5). Finding evidence for electrical coupling but not chemical coupling is not unusual in the study of gap junctions. For example, gap junctions in a rat osteoblast cell line composed predominantly of the gap junction protein connexin 45 provide electrical coupling while blocking the passage of Lucifer Yellow (31).

In the present study, the arrival of Lucifer Yellow first in the tubule lumen and later at the open end of the tubule confirms the secretion of organic molecules by Malpighian tubules in insects which Ramsay observed some time ago (27) and Linton and O'Donnell more recently (17). Moreover, the secretion of Lucifer Yellow across the apical membrane of the injected principal cell confirms that the cell has not been damaged by the dye injection to the extent of closing gap junctions. The transport of

Lucifer Yellow across the apical membrane of principal cells must involve a carrier-mediated process. Consistent with such a transport system is the high expression of organic anion transporters which Wang et al. (34) found in a transcriptome analysis of *Drosophila* Malpighian tubules.

A glimpse at the regulation of gap junctions in Aedes Malpighian tubules. Although it is well known that cytoplasmic Ca^{2+} can close gap junctions, the quantitative aspects of intracellular [Ca^{2+}] that promote uncoupling are not as clear. Observations range from nanomolar to millimolar changes in the concentration Ca^{2+} (23).

If gap junctions in *Aedes* Malpighian tubules are closed by a rise in intracellular Ca^{2+} concentrations, then cytoplasmic Ca^{2+} concentrations higher than those that can be induced by treatment with the Ca^{2+} ionophore A23187 are necessary. The ionophore significantly decreased the input resistance from 215 kΩ to 194 kΩ (Table 4.3). This decrease stems from the significant decrease in the non-junctional resistance but not the gap junctional resitance. Accordingly, the ionophore induced changes at the level of basolateral and/or apical cell membranes of principal cells but not at the level of gap junctions between principal cells. We interpret these observations to indicate the relative insensitivity of gap junctions to changes in cytoplasmic Ca^{2+}concentrations in *Aedes* Malpighian tubules.

In contrast, the metabolic inhibition of the tubule with dinitrophenol had profound effects on all measured electrophysiological parameters (Table 4.3). What stands out is the effect on the gap junction resistance which increased from 0.526 MΩ to 30.7 MΩ. The 60-fold increase reflects complete uncoupling, i.e. the closure of gap junctions as evidenced by the increase in the non-junctional resistance to 1,483 kΩ which is strikingly close to the input resistance of 1,474 kΩ (Table 4.3). The non-

junctional resistance reflects largely the resistance of the basolateral and apical membrane of the principal cell. When this cell membrane resistance equals the input resistance of the cell, there may be no other conductive pathways, documenting the closure of gap junctions during metabolic inhibition.

From previous studies we know that dinitrophenol completely inhibits transepithelial electrolyte and fluid secretion in *Aedes* Malpighian tubules (21) where the uncoupler of oxidative phosphorylation causes intracellular ATP concentrations to drop from 0.9 mM to 0.08 mM within 2 min (36). In parallel with the drop in intracellular [ATP], membrane and transepithelial voltages drop towards zero (21), and the transepithelial electrical resistance and the cell input resistance rise to maximum values (21, 36) as pathways for the entry of electrolytes across the basolateral membrane and their exit across the apical membrane into the tubule lumen shut down (6). The present study shows that next to cell membranes, gap junctions also shut down in principal cells. Whether this shut-down reflects the regulation of the gap junction by intracellular ATP concentration remains to be determined. The regulation of gap junctions by intracellular ATP is known for vertebrate gap junctions (32).

Molecular evidence of gap junctions in insect Malpighian tubules. The molecular basis of gap junctions in invertebrates has been a mystery for decades. In the 1970's, connexin proteins were identified as the structural components for the gap junctions in vertebrates (13). For more than 20 years, the term "connexin" has almost become the synonym of gap junction, while at the same time all the efforts trying to find the homologous connexin in invertebrates had failed (25). It was only in 1998 that the gene family encoding invertebrate gap junction proteins, innexins, was first

confirmed in *Drosophila* (26). Up to now, 8 innexin genes have been found in the fruit fly and 25 in *C. elegans* (24).

So far, information of the tissue- or cell-specific distribution of innexin proteins in different organisms is still limited due to the lack of antibodies. In *Drosophila*, mRNA expression patterns reveal 8 innexin genes during oogenesis, and embryogenesis (30). For the Malpighian tubule of adult *Drosophila* flies, the comprehensive microarray dataset generated by Wang et al (34) shows that at least 5 innexin or innexin-like genes are present, including inx6, inx7, shakB, inx2, and gene CG7537. In particular, inx6 is significantly enriched in the Malpighian tubules. Accordingly, we shall not be surprised if we found inx6 also expressed in Malpighian tubules of *Aedes aegypti*.

6. Reference

1. **Aneshansley DJ, Marler CE, and Beyenbach KW.** Transepithelial voltage measurements in isolated Malpighian tubules of *Aedes aegypti*. *J Insect Physiol* 35: 41-52, 1988.

2. **Beyenbach KW.** Energizing epithelial transport with the vacuolar H^+-ATPase. *News Physiol Sci* 16: 145-151, 2001.

3. **Beyenbach KW.** Mechanism and regulation of electrolyte transport in Malpighian tubules. *J Insect Physiol* 41: 197-207, 1995.

4. **Beyenbach KW.** Regulation of tight junction permeability with switch like speed. *Curr Opin Nephrol Hypertens* 12: 543-550, 2003.

5. **Beyenbach KW.** Transport mechanisms of diuresis in Malpighian tubules of insects. *J Exp Biol* 206: 3845-3856, 2003.

6. **Beyenbach KW and Masia R.** Membrane conductances of principal cells in Malpighian tubules of *Aedes aegypti*. *J Insect Physiol* 48: 375-386, 2002.

7. **Beyenbach KW, Pannabecker TL, and Nagel W.** Central role of the apical membrane H^+-ATPase in electrogenesis and epithelial transport in Malpighian tubules. *J Exp Biol* 203: 1459-1468, 2000.

8. **Bukauskas F, Kempf C, and Weingart R.** Electrical coupling between cells of the insect Aedes albopictus. *J Physiol* 448: 321-337, 1992.

9. **Bukauskas FF, Kempf C, and Weingart R.** Cytoplasmic bridges and gap junctions in an insect cell line (Aedes albopictus). *Exp Physiol* 77: 903-911, 1992.

10. **Bukauskas FF, Vogel R, and Weingart R.** Biophysical properties of heterotypic gap junctions newly formed between two types of insect cells. *J Physiol* 499 (Pt 3): 701-713, 1997.

11. **Bukauskas FF and Weingart R.** Multiple conductance states of newly formed single gap junction channels between insect cells. *Pflugers Arch* 423: 152-154, 1993.

12. **Bukauskas FF and Weingart R.** Voltage-dependent gating of single gap junction channels in an insect cell line. *Biophys J* 67: 613-625, 1994.

13. **Goodenough DA.** Bulk isolation of mouse hepatocyte gap junctions. Characterization of the principal protein, connexin. *J Cell Biol* 61: 1974, 1974.

14. **Hayes TK, Pannabecker TL, Hinckley DJ, Holman GM, Nachman RJ, Petzel DH, and Beyenbach KW.** Leucokinins, a new family of ion transport stimulators and inhibitors in insect Malpighian tubules. *Life Sci* 44: 1259-1266, 1989.

15. **Helman SI.** Determination of electrical resistance of the isolated cortical collecting tubule and its possible anatomical location. *Yale J Biol Med* 45: 339-345, 1972.

16. **Karasiewicz J.** Electron microscopic studies of cytokinesis in metazoan cells. In: *Mitosis/Cytokinesis*, edited by Forer A. New York: Academic Press, 1981, p. pp. 419-436.

17. **Linton SM and O'Donnell MJ.** Novel aspects of the transport of organic anions by the Malpighian tubules of *Drosophila melanogaster*. *J Exp Biol* 203: 3575-3584, 2000.

18. **Loewenstein WR and Kanno Y.** Studies on an Epithelial (Gland) Cell Junction. I. Modifications of Surface Membrane Permeability. *J Cell Biol* 22: 565-586, 1964.

19. **Loewenstein WR, Socolar SJ, Higashino S, Kanno Y, and Davidson N.** Intercellular communication: Renal, urinary bladder, sensory, and salivary glands. *Science* 149: 295-298, 1965.

20. **Masia R, Aneshansley D, Nagel W, Nachman RJ, and Beyenbach KW.** Voltage clamping single cells in intact Malpighian tubules of mosquitoes. *Am J Physiol Renal Physiol* 279: F747-F754, 2000.

21. **Pannabecker TL, Aneshansley DJ, and Beyenbach KW.** Unique electrophysiological effects of dinitrophenol in Malpighian tubules. *Am J Physiol* 263: R609-R614, 1992.

22. **Pannabecker TL, Hayes TK, and Beyenbach KW.** Regulation of epithelial shunt conductance by the peptide leucokinin. *J Membr Biol* 132: 63-76, 1993.

23. **Peracchia C.** Chemical gating of gap junction channels; roles of calcium, pH and calmodulin. *Biochim Biophys Acta* 1662: 61-80, 2004.

24. **Phelan P.** Innexins: members of an evolutionarily conserved family of gap-junction proteins. *Biochim Biophys Acta* 1711: 225-245, 2005.

25. **Phelan P, Bacon JP, Davies JA, Stebbings LA, Todman MG, Avery L, Baines RA, Barnes TM, Ford C, Hekimi S, Lee R, Shaw JE, Starich TA, Curtin KD, Sun YA, et al.** Innexins: a family of invertebrate gap-junction proteins. *Trends Genet* 14: 348-349, 1998.

26. **Phelan P, Stebbings LA, Baines RA, Bacon JP, Davies JA, and Ford C.** Drosophila Shaking-B protein forms gap junctions in paired Xenopus oocytes. *Nature* 391: 181-184, 1998.

27. **Ramsay JA.** Excretion by the Malpighian tubules of the stick insect, *Dixippus morosus* (orthoptera, phasmidae): amino acids, sugars and urea. *Journal of Experimental Biology* 35: 871-891, 1958.

28. **Satmary WM and Bradley TJ.** The distribution of cell types in the Malpighian tubules of *Aedes taeniorhynchus* Diptera Culicidae. *Int J Insect Morphol Embryol* 13: 209-214, 1984.

29. **Scott BN, Yu M-J, Lee LW, and Beyenbach K.** Mechanisms of K^+ transport across basolateral membranes of principal cells in Malpighian tubules of the yellow fever mosquito, *Aedes aegypti*. *J Exp Biol* 207: 1655-1663, 2004.

30. **Stebbings LA, Todman MG, Phillips R, Greer CE, Tam J, Phelan P, Jacobs K, Bacon JP, and Davies JA.** Gap junctions in *Drosophila*: developmental expression of the entire innexin gene family. *Mech Dev* 113: 197-205, 2002.

31. **Steinberg TH, Civitelli R, Geist ST, Robertson AJ, Hick E, Veenstra RD, Wang HZ, Warlow PM, Westphale EM, Laing JG, and et al.** Connexin43 and connexin45 form gap junctions with different molecular permeabilities in osteoblastic cells. *Embo J* 13: 744-750, 1994.

32. **Sugiura H, Toyama J, Tsuboi N, Kamiya K, and Kodama I.** ATP directly affects junctional conductance between paired ventricular myocytes isolated from guinea pig heart. *Circ Res* 66: 1095-1102, 1990.

33. **Verselis VK, Bennett MV, and Bargiello TA.** A voltage-dependent gap junction in Drosophila melanogaster. *Biophys J* 59: 114-126, 1991.

34. **Wang J, Kean L, Yang J, Allan AK, Davies SA, Herzyk P, and Dow JA.** Function-informed transcriptome analysis of Drosophila renal tubule. *Genome Biol* 5: R69, 2004.

35. **Williams JC and Beyenbach KW.** Differential effects of secretagogues on Na and K secretion in the Malpighian tubules of *Aedes aegypti* (L.). *J Comp Physiol* 149: 511-517, 1983.

36. **Wu DS and Beyenbach KW.** The dependence of electrical transport pathways in Malpighian tubules on ATP. *J Exp Biol* 206: 233-243, 2003.

37. **Yu M and Beyenbach KW.** Leucokinin and the modulation of the shunt pathway in Malpighian tubules. *J Insect Physiol* 47: 263-276, 2001.

38. **Yu MJ and Beyenbach KW.** Leucokinin activates Ca^{2+}-dependent signal pathway in principal cells of *Aedes aegypti* Malpighian tubules. *Am J Physiol Renal Physiol* 283: F499-F508, 2002.

CHAPTER 5

PROSPECTS

From a physiologist's point of view, life is an energy-consuming process, a steady state during which the live subject continuously exchanges energy and substances with the external world and responds effectively to the always-changing environment. From this perspective, in the animal body there are no other cells like epithelial cells. While all the other cells reside in a stabilized fluid-compartment (the internal environment) throughout their whole lives, the epithelial cells have to deal with two totally different environments at the same time. That's probably the reason why epithelial cells are mostly studied in tissues as in the epithelial model systems introduced in this dissertation, since single epithelial cells (usually undifferentiated), not being able to effectively separate two different environmental compartments, will simply not perform the normal functions of this type of cells. In other words, functions of epithelial cells are behaviors of an integrative tissue instead of a simple collection of single-cell functions. Therefore, although it's still true that the primary goal of transepithelial transport research is to identify, characterize and localize the membrane transport machineries in the epithelial cells, the intercellular communications between epithelial cells, and the intercellular solutes- and fluid-transport — as it is suggested by the presence of the highly conductive gap junctions between *Aedes* Malpighian tubule cells— could be of particular importance to the future studies in this field (Fig. 5.1).

Our study showed that principal cells of the Malpighian tubules of *Aedes aegypti* were electrically coupled by highly conductive gap junctions (2.32 μS per cell contact). In epithelial cells of other insects such as the salivary gland cells of *Drosophila melanogaster*, the gap junction conductance is even higher. The role of gap junctions in these non-excitable, secretory epithelial cells is still not well

Figure. 5.1. Transport across epithelial cells in an integrative tissue. Besides transepithelial transport across the tissue, intercellular transport between epithelial cells may also contribute importantly to the whole tissue functions. Arrows show the directions of solutes and fluid movements; TJ(SJ), tight junctions (sepatate junctions); GJ, gap junctions.

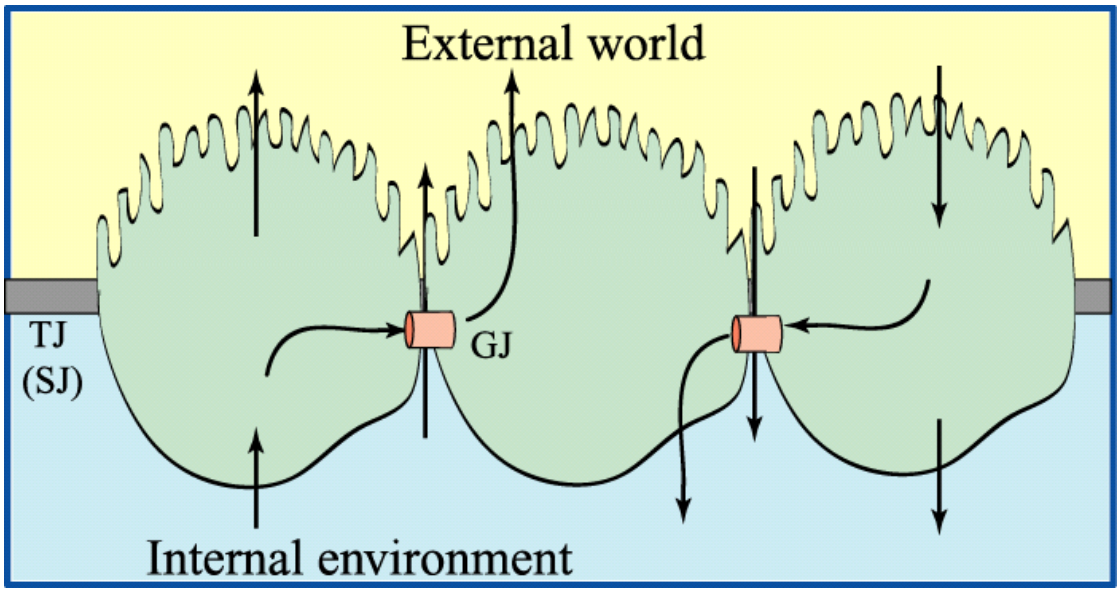
External world
TJ
(SJ)
GJ
Internal environment

understood. It has been suggested is that electrical coupling through gap junctions makes the transporting epithelium a whole unit of communicating cells, which share the same constant transmembrane voltages. This idea actually now can be tested in our *Aedes* Malpighian tubules. In 1979, Miller and Selverston invented a technique in which they injected Lucifer Yellow CH into a single neuron in a neuronal network; thereafter the dye-loaded cell could be specifically killed by blue light of high-intensity without affecting all the neighboring cells (this technique is now routinely employed in Dr. Ronald Harris-Warrick's lab in campus). Since our study has already shown that Lucifer Yellow injected into one principal cell stayed in that cell, then it would be possible to kill one or several principal cells within the tubule, consequently closing gap junctions of these cells. Therefore secretion function of the Malpighian tubules with or without gap junction disruptions could be simply tested by Ramsay assay.

The permeability of gap junctions to fluorescent dyes also deserves some further investigations. In fact, as the most commonly used fluorescent dye in gap junction research, it is quite surprising to us that Lucifer Yellow cannot pass through the gap junctions in *Aedes* Malpighian tubules. It has been reported that macromolecules with molecular weight around 1 kDa could easily pass through some vertebrate gap junctions, while insect gap junctions are supposed to have even larger pore sizes than vertebrates. Since Lucifer yellow is a negatively charged fluorescent dye with a molecular weight of 443 Dalton, it might be possible that gap junction in *Aedes* Malpighian tubules have high charge selectivity in addition to the size selectivity. Lissamine rhodamine B sulfonyl chloride, a cationic fluorescent dye with MW of 577 could be a good choice for this investigation.

Although the molecular basis of the gap junctions in *Aedes* Malpighian tubules is still unclear, with the completion of the sequencing of *Aedes* genome, this will become a quite promising direction to investigate in the coming future. The comprehensive microarray dataset of *Drosophila* Malpighian tubules reveal that at least 5 innexin or innexin-like genes are present in the Malpighian tubules, including inx6, inx7, shakB, inx2, and gene CG7537, while inx6 expression is significantly enriched. It would be of particular interest to see whether these genes are also expressed in *Aedes* Malpighian tubules. Localization of these innexin proteins would also be possible if the appropriate antibodies can be produced.

In chapter 4, our results showed that the metabolic inhibitor dinitriphenol could completely uncouple Malpighian tubule cells by closing the gap junctions. The physiological mechanism of this effect is unclear. Depletion of intracellular ATP caused by DNP could result in comprehensive changes of intracellular environment such as the $[Ca^{2+}]_i$ level, pH etc, all of which could affect gap junction conductance either directly or indirectly. ATP itself was reported to affect gap junction resistance, too. One way to test these effects is to express the identified innexins to form gap junctions in paired cells such as the *Xenopus* oocytes. Double voltage-clamp can be performed to measure the single channel conductance of the gap junctions, while by perfusing the oocyte cytosol with solutions containing the putative gap junction regulators (Ca^{2+}, H^+ and ATP etc), it would then be possible to assess their effects on the individual gap junction resistance.